IMPACT OF LAND USE/LAND COVER AND CLIMATE CHANGE ON SOIL EROSION IN SILE WATERSHED, LAKE ABAYA-CHAMO SUB-BASIN, SOUTHERN ETHIOPIA

M.Sc. THESIS

BIRHANU WOLDE GINDI

HAWASSA UNIVERSITY, HAWASSA, ETHIOPIA

MARCH, 2022

IMPACT OF LAND USE/LAND COVER AND CLIMATE CHANGE ON SOIL EROSION IN SILE WATERSHED, LAKE ABAYA-CHAMO SUB-BASIN, SOUTHERN ETHIOPIA

BY

BIRHANU WOLDE GINDI

THESIS SUBMITTED TO

HAWASSA UNIVERSITY

DEPARTMENT OF BIOSYSTEMS ENGINEERING,

FACULTY OF BIOSYSTEMS AND WATER RESOURCES ENGINEERING,

INSTITUTE OF TECHNOLOGY, SCHOOL OF

GRADUATE STUDIES, HAWASSA UNIVERSITY,

HAWASSA, ETHIOPIA

IN PARTIAL FULFILLMENT OF THE

REQUIREMENTS FOR THE

DEGREE OF MASTER OF SCIENCE IN SOIL AND WATER CONSERVATION ENGINEERING

MARCH, 2022

ADVISORS' APPROVAL SHEET

SCHOOL OF GRADUATE STUDIES

HAWASSA UNIVERSITY ADVISORS APPROVAL SHEET

This is to certify that the thesis entitled "IMPACT OF LAND USE/LAND COVER AND CLIMATE CHANGE ON SOIL EROSION IN SILE WATERSHED, LAKE ABAYA-CHAMO SUB-BASIN, SOUTHERN ETHIOPIA" submitted in partial fulfillment of the requirements for the degree of Masters' with specialization in Soil and Water Conservation Engineering, Department of Biosystems Engineering has been carried out by Birhanu Wolde Gindi ID NO; GPSWE/0004/12, under our supervision. Therefore, we recommend that the student has fulfilled the requirements and hence hereby can submit the thesis to the department.

Awdenegest Moges (Ph.D. Associate Professor)	_____	_____
Name of Major Advisor	Signature	Date
Rediet Girma (Ph.D. Candidate)	_____	_____
Name of Co-Advisor	Signature	Date

EXAMINER'S APPROVAL SHEET

SCHOOL OF GRADUATE STUDIES

HAWASSA UNIVERSITY EXAMINERS' APPROVAL SHEET

We, the undersigned, members of the board of examiners of the final open defense by Birhanu Wolde Gindi have read and evaluate his/her thesis entitled "IMPACT OF LAND USE/LAND COVER AND CLIMATE CHANGE ON SOIL EROSION IN SILE WATERSHED, LAKE ABAYA-CHAMO SUB-BASIN, SOUTHERN ETHIOPIA" and examined the candidate. This is, therefore, to certify that the thesis has been accepted in partial fulfillment of the requirements for the degree.

_____ _____ _____

Name of Major Advisor Signature Date

_____ _____ _____

Name of Internal Examiner-I Signature Date

_____ _____ _____

Name of Internal Examiner-II Signature Date

_____ _____ _____

Name of External examiner Signature Date

_____ _____ _____

Stamp of SGS Approval Signature Date

DECLARATION

I declare and confirm by my signature that this thesis entitled "IMPACT OF LAND USE/LAND COVER AND CLIMATE CHANGE ON SOIL EROSION IN SILE WATERSHED, LAKE ABAYA-CHAMO SUB-BASIN, SOUTHERN ETHIOPIA" is my original work that has not been submitted to any other institution anywhere for the award of degree, diploma or certificate. Data analysis and preparation of this paper and that all the sources that I have used or quoted have been cited and acknowledged.

Name of student: Birhanu Wolde Gindi

Signature: ……

Date: …….

Contact Address:

Cell-phone: +251-917-409-191

Email: birhanuwolde2016@gmail.com

Linkedin: https://www.linkedin.com/in/birhanu-wolde-8aa28214b/

ResearchGate: https://www.researchgate.net/profile/Birhanu-Wolde/research

ACKNOWLEDGMENT

First and above all praise to be Almighty God for unconditional love, mercy, and for holistically blessing me to complete my MSc. thesis.

I would like to express my profound gratitude to my Major Advisor Awdenegest Moges (Ph.D. Associate professor) for his valuable advice, encouragement, and critical comments during the proposal and the research periods. I would like to acknowledge my Co-Advisor, Rediet Girma (Ph.D. Candidate) for his great constructive comments and guidance.

I am very grateful to the Southern Agricultural Research Institute for allowing me to take part in the Graduate Study Program of Soil and Water Conservation Engineering with its full financial support of the study. I also like to be grateful to Hawassa University, Areka Agricultural Research Center, and the National Meteorological Agency of Ethiopia.

Last but not least, I want to express my deep gratitude to my family members, colleagues, and friends who supported and helped me in all things during the difficult times. All of you have been a source of my inspiration, encouragement, and ability, and without you, this accomplishment would not have been possible. Thank you again dear all my beloved ones.

LIST OF ABBREVIATIONS

ACSB	Abaya-Chamo Sub-Basin
ANRO	Agricultural and Natural Resource Office
ASTER	Advanced Space Boerne Thermal Emission and Radiometer
CA	Cellular Automata
CanRCM4	Canadian Regional Climate Model version 4
CCCMA	Canadian Centre for Climate Modeling and Analysis
CORDEX	Coordinated Regional Climate Downscaling Experiment
CRV	Central Rift Valley
CSA	Central Statistical Agency
DEM	Digital Elevation Model
EMA	Ethiopia Mapping Agency
ENMA	Ethiopian National Meteorological Agency
ERDAS	Earth Resources Data Analysis System
ETM+	Enhanced Thematic Mapper Plus
FAO	Food and Agriculture Organization
GHG	Green House Gas
GIS	Geographic Information System
GPS	Global Positioning System
HadGEM2-ES	Hadley Centre Global Environmental Model, Version 2 Earth System
ICHEC	Irish Centre for High-End Computing
LULC	Land use/Land Cover
LULCC	Land use/Land Covers Change
MLC	Maximum Likelihood Classification
MLP_NN	Multi-Layer Perceptron Neural Network
MoWIE	Ministry of Water, Irrigation and Electricity
MOHC	Met Office Hadley Centre
MSS	Multi-Spectral Scanner
NetCDF	Network Common Data Form
OLI	Operational Land Imager
RACMO22T	Regional Atmospheric Climate Model Version 2.2 T

RCA4	Rossby Center Regional Atmospheric Model
RCM	Regional Climate Model
RCP	Representative Concentration Pathways
RS	Remote Sensing
RUSLE	Revised Universal Soil Loss Equation
SCRP	Soil Conservation Research Project
SWC	Soil and Water Conservation
t- ha $^{-1}$ year $^{-1}$	Tons per Hectare per Year
TIRS	Thermal Infrared Sensor
TM	Thematic Mapper
TSL	Tolerable Soil Loss
USGS	United States Geological Survey
USLE	Universal Soil Loss Equation
UTM	Universal Transverse Mercator
WGS	World Geodetic System

TABLE OF CONTENTS

LIST OF TABLES

LIST OF FIGURES

LIST OF APPENDICES

ABSTRACT

*The combined impacts of land use and climate change are significantly affecting natural resources, particularly soil and water ecosystems. Thus, studying the impacts of land use/land cover (LULC) and climate changes on soil erosion in the Sile River watershed is very essential for proper natural resource management. In this study, the historical change of LULC (from 1987-2020), prediction of 2050, the impact of changing LULC & climate on soil erosion for the years of 1987, 2003, 2020, and future 2050 under two climate scenarios (RCP4.5 & RCP8.5) were evaluated. The Landsat TM for 1987, ETM+ for 2003, and Landsat-8 OLI/TIRS for 2020 were used for LULC classification. Supervised image classification method with maximum likelihood classification (MLC) was applied in the ERDAS Imagine software. Classified historical LULC map serves as a baseline to predict 2050 LULC with considering different driver variables using Multi-Layer Perceptron Neural Network and Cellular Automata-Markov Chain Model integrated with TerrSet software. Daily rainfall data from 1987-2020,102 composited soil samples, ASTER DEM with a resolution of 30*30-meter and classified LULC map was used for erosivity (R-factor) estimation, soil erodiblity (K-factor) analysis, topography (LS-factor) computation, and for both practice (P-factor) and cover (C-factor) determination respectively. In addition, the ensemble means of four regional climate models (RCMs) rainfall data under two scenarios (RCP4.5 & RCP8.5) and predicted 2050 LULC map was used to generate R-factor and both P&C factors respectively for the estimation of 2050 soil loss. A revised universal soil loss equation model (RUSLE) has been used to compute the above factors in Arc GIS software to estimate the rate of soil loss. This study revealed that, in both periods from the year 1987-2003 and 2003-2020, cultivation land, bare land, and banana land cover were expanded at the expense of shrubland, forest land, grazing land, and water body decline. Sile River watershed experienced substantial LULC alteration and will also be prolonged for the coming several years. The mean annual soil loss for the years 1987, 2003, and 2020 were 13.05, 21.04, and 41.41 t-ha^{-1}year^{-1} respectively. The lowest mean annual soil loss was observed in banana land cover and gently slope classes. While highest and severe was detected on bare land & steep slope classes correspondingly. The average soil loss under the RCP4.5 and RCP8.5 scenarios with a future 2050 LULC were predicted to be 56.48 t-ha^{-1}year^{-1} and 57.11 t-ha^{-1}year^{-1} then it will be expected to increase 36.40 % and 38.19 % respectively. LULC, climate change/variability, and the steepness of slope had been believed to be the leading factors that exacerbated soil erosion in the study area. From the finding of this study, prioritized sub-watersheds are recommended for land management intervention, and disseminating banana plantations in the other part of the watershed was suggested. Additionally, climate change will aggravate the current soil erosion problem and would need ecological sound conservation policies and strategies to mitigate the adverse impacts of climate change on soil erosion.*

Key Words: Land use/land cover, Soil Loss, RUSLE Model, Climate Change, Multi-Layer Perceptron Neural Network, Cellular Automata-Markov Chain, Sile

1. INTRODUCTION

1.1 Background of the Study

In Ethiopia, natural resources are under the influence of different interrelated factors like population pressure, agricultural expansion, migration, rapid urbanization, resettlement, climate change, and environmental pollution (Wassie, 2020). Natural vegetation in northern, central, eastern, and southern Ethiopia has also come under increasingly heavy pressure in the last century (Henricksen *et al.*, 1988). According to (Genet, 2020), there were significant LULC changes in the second half of the 20th century mainly in the highland part of the country. Particularly, in the Ethiopian Rift Valley, from 1973 to 2006, the area of cropland was increased twice at the expense of woodland and wooded grassland (Garedew*et al.*, 2009).

The adverse combined impacts of land use/land cover (LULC) and climate change are likely to significantly affect natural resources and ecosystems specifically by aggravating soil erosion (Ayele et al., 2016 ; Moges et al., 2020; Belay & Mengistu, 2021). The most visible change in soil erosion severity was due to the result of land use land cover change (LULCC) like the expansion of agricultural and bare land at the expense of forest land, grassland, and shrubland was the most detrimental factor for severe soil erosion risks (Moges & Bhat, 2017; Wassie, 2020; Moisa et al., 2021). Soil erosion caused by climate change was due to the increasing impact of future precipitation with increased rainfall erosvity factor. The impacts are also the major ecological challenges in Ethiopia (Moges et al., 2020 ;Girmay et al., 2021).

Estimation of the interaction between climate and LULC change for soil erosion is essential for the implementation of proper soil and water conservation methods (Moges & Bhat, 2017 ; Moisa et al., 2021) and to deciding on local climate adaption strategies to mitigate future

climate change impact (Belay & Mengistu, 2021). Hence, revised universal soil loss equation model (RUSLE) (Renard *et al.*, 1997with remote sensing (RS) and geographical information system (GIS) technology has been used for soil loss estimation (Kouli et al., 2009; Balabathina et al., 2020). RUSLE is an empirical-based modelling approach that predicts the effect of soil loss in the area using data layers including, rainfall erosivity (R), soil erodibilty (K), slope lemgth and steepness (LS), cover management (C),and conservation practice (P), factors (Renard *et al.*, 1997 ; Prasannakumar et al., 2012).

Abaya-Chamo sub-basin (ACSB) was under degradation due to natural and anthropogenic factors. This landscape fragmentation was related to increased soil erosion, the volume of surface runoff, and sediment transport. Accordingly, deforestation, expansion of farmlands around and highlands of the part of the lake catchments, increased siltation, intensive irrigation, invasive emboch plants (water hyacinth), and rapid population growth were the main causes for Abaya-Chamo sub-basin degradation (Yohannes et al., 2018; Gebeyehu et al., 2019; Zekarias et al., 2021). Evaluating a trend of historical LULC change and predicting future 2050 LULC with the Multi-Layer Perceptron Neural Network and Cellular Automata-Markov Chain model, estimations of the impact of LULC and climate change on soil loss was useful for implementing more efficient and effective sustainable land management practices, decision making and policy development (Yesuph & Dagnew, 2019; Belay & Mengistu, 2021). Therefore, this research was initiated to evaluate the trend of LULC change, predict the future fate of LULC, and assess both the combined impact of LULC and climate change on soil erosion of the Sile River watershed of ACSB.

1.2 Statement of the Problems

The ACSB lakes are under stress by surface runoff, sediment yield, and groundwater extraction because of LULC change through deforestation and expansion of farmlands

(Gebeyehu et al., 2019). Due to LULC change and associated problems, the risk of soil erosion was increased and consequently, it affected the levels and water quality of the lakes (WoldeYohannes et al., 2018).

In the Arba Minch Zuriya district of Gamo zone, banana production was started the early 1980s, where the then Arba Minch State farm had about 62 hectares of land covered by the Dwarf Cavendish banana variety. In that time the croplands of the smallholder farmers were covered by maize, cotton, and sweet potato (Mekonnen, 2014; Alemu, 2017). However, the ecological impact of the banana land use land cover in terms of accelerated soil erosion was not estimated and quantified yet. There was also a lack of information about the historical trend and future fate of banana land use/landcover (LULC) maps in the Sile river watershed. Therefore, this research is essential to generate the basic information to show the trend of banana and other LULC changes and their impact on water-induced soil erosion.

Climate change will lead to a boost in soil erosion velocity due to the increased erosive power of rainfall. The average annual soil loss would be increased in the future period compared with the baseline period due to the increase of rainfall projection in the future (Girmay et al., 2021; Belay & Mengistu, 2021). Soil erosion caused by climate and land-use changes is one of the main environmental challenges in Ethiopia (Moges et al., 2020). According to the suggestion of (Negese, 2021), to predict future land use/land cover and impact of soil loss is also very essential to take action of the future soil and water conservation and management interventions. So, this thesis also provides a basis for future climate change impact and land use land cover change impacts for the next three decades in the Sile River watershed of ACSB.

1.3. Objective of the Study

1.3.1 General Objective

The main objective of this research is to evaluate the impact of land use/land cover and climate change on soil erosion in Sile Watershed, Lake Abaya-Chamo sub-basin.

1.3.2 Specific Objectives

The Specific objectives of this study were:

- ❖ To identify the time series trend of land use/land cover change from the period of 1987 to 2003, and 2003 to 2020.
- ❖ To predict land use/ land cover change for the year 2050 using the MLP_NN integrating with CA-Markov model.
- ❖ To estimate the soil erosion rate under different LULC, slope classes, and sub-watershed levels using the RUSLE model
- ❖ To estimate the future soil erosion using the 2050 LULC and projected climate change scenarios.

1.4 Research Questions

1. What was the trend of land use/ land cover change in the Sile River watershed over the past three decades?
2. What would it like the future land use land cover condition of the study area in 2050?
3. To what extent do LULC and slope affect soil erosion in the Sile River watershed?
4. What are the future soil erosion rate under RCP4.5 and RCP 8.5 climate scenarios with a predicted 2050 land use?

1.5 Scope of the Study

The study was limited to the Sile River watershed which covers an area of 27,610 hectares. The time considered during the investigation of historical LULCC and its impact on the soil erosion of the study watershed was 1987, 2003 and 2020. In addition, the future 2050 LULC was predicted. Using the ensemble mean of four regional climate models (RCMs) under two climate scenarios (RCP 4.5 and RCP 8.5) a future (2050) soil loss was estimated.

ERDAS imagine 2014 software was used for image classification and Multi-Layer Perceptron Neural Network and Cellular Automata-Markov Chain Model integrated (MLP-NN_CA-MC) Model built-in TerrSet software was used for prediction of the future 2050 LULC change. Finally, Arc GIS 10.8 software and RUSLE model was used to estimate the effect of LULC, topography, soil erodibility, climate change, and conservation practice on water-induced soil erosion in the Sile River watershed.

2. LITERATURE REVIEW

2.1 Concepts of Land Use Land Cover Change

The terms land use and land cover have specific meanings in how they describe the land and should not be used interchangeably (Coffey, 2013). These terms are often incorrectly used interchangeably; however, each term has a very specific meaning. According to (Lambin et al., 2003; Ellis & Pontius, 2006) land cover is defined by the attributes of the earth's land surface and immediate subsurface, including biota, soil, topography, surface, groundwater, and human structures. Data sets used in land-use/ land cover change research represent the land surface by a set of spatial units, each associated with attributes on the other hand, and land use is defined by the purposes for which humans exploit the land cover.

Land use refers to the purpose the land serves, for example, recreation, wildlife habitat, or agriculture; it does not describe the surface cover on the ground. Land cover refers to the surface cover on the ground, whether vegetation, urban infrastructure, water, bare soil, or other; it does not describe the use of and the use of land may be different for lands with the same cover type. For instance, a land cover type of forest may be used for timber production, wildlife management, or recreation; it might be private land, a protected watershed, or a popular state park (Coffey, 2013).

Land use/ land cover change (LULCC) is the alteration of different land-use categories as the result of multiple anthropogenic and physical environment interactions. It is a major driver of global climate change and the effects on the terrestrial surface and the atmosphere (Pielke et al., 2011 ; Liping et al., 2018). Land use and land cover change (LULCC) are generally grouped into two types. Land-cover modifications and land cover conversion. Land-cover modifications are more subtle changes that affect the character of the land cover

without changing its overall classification. Land-cover conversions (i.e., the complete replacement of one cover type by another) are measured by a shift from one land-cover category to another (Lambin et al., 2003).

2.1.1 LULC Change in Rift Valley Lakes Basin of Ethiopia

In Ethiopia, as a result of population pressure, climate change, resettlement programs, and other anthropogenic and nature-induced driving forces the rapid LULC change was distinguished in the last decades (Regasa, 2021). The alarming nature of this alteration is revealed in worsening livelihood and ecological security, including the loss of woodlands, soil degradation, the loss of biological diversity, and food insecurity (Garedew et al., 2009).

The Rift Valley Lakes Basin is one of the major river basins in Ethiopia with a total area of about 52,740 km^2 (MoWIE, 2002). It constitutes nine (9) different lakes; Lake Ziway, Lake Langano, Lake Abiyata, Lake Shalla, Lake Hawassa, Lake Abaya, Lake Chamo, Lake Abbe and Lake Beseka. In the basin major LULC changes were documented, mainly arable land expansion is noticed, a decline of natural vegetation is and water resources have been shrinking in size and depth radically (Elias et al., 2019).

Different LULC studies which were conducted at different times also confirm that there was a remarkable temporal change in LULC in the landscape of the basin. For instance the year between 1985 to 2018, agricultural land and urban settlement increased by 59.8% and 28.7% respectively at the expense of forest and grassland (Belihu et al., 2020). The study which was conducted between 1985, to 2010 revealed that the LULC changes of Abaya-Chamo sub-basin (ACSB) imply a rapid reduction in shrub land (28.82%) and natural grassland (33.13%) and an increase in arable land (59.15%). The main identified driving forces of LULC changes in the basin were rapid population growth, internal migration, policy shifts, and regime change (WoldeYohannes et al., 2018).

2.1.2 The Driving Factors for LULC

LULC changes are driven by a combination of proximate and underlying drivers such as economic, demographic, biophysical, and institutional factors. Proximate driving forces are wood extraction, agricultural activities, infrastructure, settlement expansion, etc. In addition, the underlying drivers for the study watershed also demographic factors, property rights issues, and biophysical factors (Mengistu et al., 2012 ; Gessesse and Bewket, 2014).

In Ethiopia deforestation, high human and livestock population, investment (coffee, tea plantations), agricultural activities ranging from small-scale subsistence agriculture to large-scale commercial agricultural schemes, urban sprawling, charcoal production, woodland collection, poor law enforcement, land rotation searching for better grazing land, resettlement (spontaneous and planned), the prevalence of drought, were the leading drivers of land-use/cover (Muke, 2019; Dibaba et al., 2020).

According to (Wubie et al., 2016), population pressure, demand for fuel wood and construction material, agricultural expansion and policy, and tenure insecurity were the major driving forces behind the land use/cover change in the Gumara watershed of Lake Tana basin, Northwestern Ethiopia. In addition (Hassen & Assen, 2017), in the Lake Tana watershed, the major driving forces of LULC change were combinations of land reform of 1975, forest development and villagization program 1980s, civil war, frequent changes in political structure, and population pressure. Therefore, LULC change and modifications are a result of both natural and human pressure, with anthropogenic influences due to globalization as the main driver (Regasa, 2021).

2. 1.3 Prediction of LULC with MLP-NN _ CA-MC Model

Prediction of future land use land cover is the most recent research that will be very much valuable to natural resources management. LULC change modeling is growing quickly in the scientific field (Coffey, 2013). There were different LULC change modeling tools and models that are most commonly used for predicting the future LULC including Cellular Automata-Markov chain (CA-MC) (Gidey et al., 2017; Hyandye & Martz, 2017, Koko et al., 2020), Cellular Automata (CA) (Kafy et al., 2021), Markov Chain model (MC) (Khawaldah, 2016), Regression Algorithm model (Eastman, 2006b), Binary Logistic (Zekarias et al., 2021), Multi-Layer Perception Markov Chain (MLP-MC) (Gharaibeh et al., 2020; Girma et al., 2022), Artificial Neural Network (Buğday & Erkan Buğday, 2019), Markov chain and artificial neural network (Sardari et al., 2019), Similarity weighted instance-based machine learning algorithm (Eastman, 2006b), are some of the prediction models used to simulate future LULC change dynamics.

From those modeling systems like Land Change Modeler (LCM), Cellular Automata (CA), Markov Chain, CA Markov, and Multi-Layer Perception Markov Chain (MLP-MC) which are embedded in Terrset software (Eastman, 2006a). The CA model has a strong space conception, which is a strong capability of space-time dynamic advancement with complex space systems (Sang et al., 2011). The CA–Markov model, which incorporates the theories of Markov and CA is about the time series and space for the advantages of forecasting (Sang et al., 2011; Gidey et al., 2017; Hyandye & Martz, 2017. The CA–Markov module integrates the functions of cellular automaton filter and Markov processes, used to simulate complex processes such as land-use change (Eastman, 2006a). It is mainly used to study the transition probability between an initial state and a final state to determine the transition trend among different land-use states (Sang et al., 2011; Liping et al., 2018 ; Leta et al., 2021).

CA-Markov uses the contiguity rule in the simulation process (Roy et al., 2015). CA-Markov model is frequently used in monitoring, ecological modeling, simulation change trends of the LULC and to predict the amount of the land-use change and the stability of future land development in the area of interest (Hamad et al., 2018).

In the CA system, the space was represented by a grid and time by uniform steps. The states of the system were finite (i.e., integer numbers). The CA system consisted of four elements cells, states, neighborhoods, and rules. Cells are the smallest of spatial units. A neighborhood represents the cells immediately adjacent to a certain cell. The next state of each cell was determined by the states of its neighboring cells and rules were used to define the states of the cells in the next time step (Deep, 2014). In addition, the Markov chain was used to generate transition probability matrices between LULC classes and cellular automata to predict the LULC map (Leta et al., 2021).

Predicting future LULC change needs to consider different spatial, accessibility, socioeconomic, and environmental variables (elevation, slope, distance to road, and distance to rivers, population density, and other proximity factors) driving factors of LULC change (Gidey et al., 2017; Gharaibeh et al., 2020; Girma et al., 2022). Therefore, among different methodologies to advance the potential of the CA-MC model in simulation and prediction of future LULC change integrating the Multi-Layer Perceptron Neural Network (MLP-NN) into CA-MC is a successful method and accurate results depending on artificial intelligence (Gharaibeh et al., 2020; Girma et al., 2022).

2.2 Water Induced Soil Erosion

Global, 26.4 billion tons of soil is lost each year. This rate is 10 times higher than the natural rate (Lindbo et al., 2012). Soil erosion is a critical environmental problem throughout the

world's terrestrial ecosystems it is also a natural process that has been greatly accelerated by human action (Zuazo & Pleguezuelo, 2008). Water-induced soil erosion is a three-stage process: detachment, transport, and deposition of soil particles elsewhere (Lindbo et al., 2012; Lal, 2014). Detached particles are transported by flowing water and deposited when the velocity of water decreases by the effect of slope or ground cover (Lal, 2014).

Water erosion is the removal of the top layer of soil by water from irrigation, rainfall, snowmelt, runoff, and poor irrigation management and transportation of the eroded materials away from the point of removal. Water action due to rain erodes the soil and causes activities like a gully, rill, and stream erosion leading to the downstream effects of flooding and sedimentation(McIvor et al., 2014). Water erosion is caused by two detaching forces: raindrop impact and flowing water. Raindrops falling on soil surfaces may destroy soil aggregates, detach particles, and transport particles short distances. Raindrops are small, but move fast and so have a lot of energy when they strike bare soil surfaces (Lindbo et al., 2012).

Soil erosion is one of the major environmental concerns which can be influenced by natural as well as anthropogenic activities (Pal & Chakrabortty, 2019). Water erosion causes serious problems in watersheds. The movement of sediment and related agricultural pollutants into watercourses is the key impact resulting from erosion. The effects of soil erosion go beyond the loss of fertile land. It has led to increased pollution and sedimentation in the offsite downstream area. This leads to sedimentation in watercourses and dams, disruption of the ecosystems of lakes, and contamination of drinking water (Zeleňáková et al., 2019). The severity of water erosion is influenced by slope, soil type, soil water storage capacity, nature of the underlying rock, vegetation cover, and rainfall intensity and period(McIvor et al., 2014).

Some of the types of soil erosion caused by water are discussed below:

Source: Adopted by (Telkar et al., 2015)

1. **Splash erosion:**

Rain splash erosion is the removal of soil particles due to the result of water falling directly onto the ground during rainstorms or when it is intercepted by the canopy and finds its way through the ground (Telkar et al., 2015)

2. **Sheet erosion:**

Sheet erosion means removing a thin uniform covering of top productive/surface soil from large areas, often from the field, more or less, during every rain which produces a run-off. Raindrops detach the soil particles, and the detached sediment can reduce the infiltration rate by sealing the soil pores. The eroding and transporting ability of overland flow depends on the rainfall intensity, infiltration rate, slope steepness, soil.

3. **Rill erosion**:

When runoff starts, channelization begins and erosion is no longer uniform. Raindrop impact does not directly detach any particles below the flow line in rills but increases the detachment and transportation capacity of the flow. Rills are small channels, which can be removed by timely normal tillage operations.

4. **Gully erosion:**

It is a more prominent type of erosion in which heavy rainfall, rapidly running water, and transporting water may result in deeper cavities or grooves called gullies. Gullies may be „V-shaped or „U‟ shaped. Gullies cut the large fields into small fragments and, in course of time, make them unfit for cultivation uncultivable. The continuous flow of water through

gullies further deepens the grooves and may ultimately result in ravines. Ravines are 15 to 30 cm in deep and with steep vertical sides.

5. **Ravines erosion:**

It is a prolonged and advanced stage of gully erosion that leads to ravines found in deep alluvial soils. It is nothing but deep and wide gullies.

6. **Landslides or slip erosion:**

This type of soil erosion is caused by heavy rainfall and it occurs in sloppy lands, such as mountains and hilly areas with a slope is >20%. In this type of erosion when the running water percolates through the crevices of rocks great masses of soils and loose rocks lying on the steep slopes slip downward. The immediate cause of a slide may be an earthquake, or a heavy rainfall, which unduly saturates the ground or part of the road.

7. **Stream bank erosion:**

On the banks of swollen rivers, it is most active. During the rainy season when fast running water streams take a turn in some other directions, they cut the soil and make caves in the banks. As a result of this, quite often large masses of soils become detached and washed away from the banks and are deposited at places in course of streams.

2.2.1 Impact of LULC on Soil Erosion

In Ethiopia, land use and land cover (LULC) change have played a significant role in increasing the rate of soil erosion and altering the hydrological balance (Negese, 2021). Clearing of natural vegetation for different uses, cultivation of steep slopes, inappropriate farming system, and absence of soil conservation and soil fertility management methods are the reasons for soil loss (Wubie et al., 2016). Studies assured that inappropriate land

management can increase soil erosion (Moisa et al., 2021) which means soil erosion is associated with land use and a land cove (LULC) (Moges & Bhat, 2017; Sardari et al., 2019).

The test plot surface runoff rates are influenced by land use and soil degradation, and hence by population density and duration of agriculture. In effect, there is 5–40 times more surface runoff from cultivated or degraded test plots than from forested test plots (Hurni et al., 2005). The average measured annual value of soil loss from cultivation land 46t-ha^{-1} year^{-1}and 68 t-ha^{-1}year^{-1}, were reported in northeastern and southwestern Ethiopia respectively (Hurni, 1985).

In Temeji watershed, Western Ethiopia soil loss is observed when grassland and forest land were converted into cultivated land with a mean soil loss of 88.8 and 86.9 t-ha^{-1} year $^{-1}$ in 2020(Moisa et al., 2021). According to (Gezahegn & Harka, 2020), in Erer Sub-Basin, Northeast Wabi Shebelle Basin the most extensive soil loss rates were estimated in croplands and bare land cover, with a mean soil loss rate of 37.60 t-ha^{-1} year^{-1} and 15.78 t-ha^{-1} year $^{-1}$, respectively.

One of the major factors for the spatiotemporal variability of soil loss is attributed to land cover changes following the expansion of agricultural practices in high erosion-prone soil, overgrazing, and deforestation (Esa et al., 2018). In Rib watershed, north-western highland Ethiopia, expansion of agricultural land at the expense of grassland and shrub land was the most detrimental factor for severe soil erosion in the watershed. The most noticeable change in soil erosion intensity was observed from cropland with mean annual soil loss amount increased to 41.38 t ha^{-1} year^{-1} in 2016 from 26.60 in 1986 (Moges & Bhat, 2017).

2.2.2 Impact of Climate Change on Soil Erosion

Soil erosion is one of the most critical environmental issues in light of the accelerating impacts of global climate change (Jacob, 2009). Climate change can also influence susceptibility to erosion and consequently land degradation (Sardari et al., 2019). So the interaction between climate change and the land degradations process is a vicious circle (Wassie, 2020).

Global warming is expected to lead to a more dynamic hydrological cycle, including more total rainfall and more frequent high-intensity rainfall events. According to climate change models, rainfall amounts and intensities are expected to continue to increase during the 21st century. These rainfall changes, along with expected changes in temperature, solar radiation, and atmospheric CO_2 concentrations, will have significant impacts on soil erosion rates (Nearing et al., 2004).

Climate change increased total erosion volume and total sediment yield deposition at the middle and downstream of the watershed (Chen et al., 2020). According to (Chapman et al., 2021), in east Africa, future climate change led to widespread increases in rainfall erosivity, and increases in erosion risks. In Ethiopia's future, climate change studies indicated that future soil loss would be increased in the future period due to increased erosive power of precipitation (Moges et al., 2020 ; Girmay et al., 2021).

2.3 Overview of Climate Model and Climate change Scenarios

2.3.1 Climate Model

A climate model is defined as numerical equations that describe the representation of the climate system based on the biological, physical, and chemical behavior of its components

and their interactions (Gettelman & Rood, 2016). They are used to forecast and quantify the climate response to present and future human activities (Ahlonsou et al., 2018).

Climate models separate the earth's surface into a three-dimensional grid of cells. A climate model is a computer program that simulates weather patterns over time. It divides the earth's surface into a three-dimensional grid of cells and models with higher resolution have more squares in the grid which makes them more accurate and precise (Gettelman & Rood, 2016).

Climate models are known to be global climate models (GCM) or regional climate models (RCM). GCM cover the entire earth and provide information only at a relatively coarse spatial scale meaning have a resolution of hundreds of kilometers. However, RCM focus on specific areas with a better resolution of a few tens of kilometers (Jacob, 2009).

Regional climate models are much nearer to the scale of real-world clarification about soil types, topography, and land cover all of which affect the climate system. That's why, RCMs can apply more real-life data than GCMs, and their simulations are more precise and accurate (Jacob, 2009). So, RCMs are superior suitable for studying how climate change influences things essential to us, like an ecosystem, agriculture, and diseases, and for making plans to adapt to future climate change. On the other hand, global climate models help consider the consequences of anthropogenic actions across the entire globe (Randall et al., 2007).

2.3.2 Climate Change Scenarios

A climate scenario is a plausible or possible future representation of climate that has been constructed for explicit use in investigating the potential impacts of anthropogenic climate change (Mearns & Hulme, 2001; Wayne, 2003). Climate scenarios often make use of climate projections (descriptions of the modeled response of the climate system to scenarios of greenhouse gas and aerosol concentrations), by manipulating model outputs and combining them with observed climate data (Mearns & Hulme, 2001).

Scenarios are alternative images of how the future might unfold and are an appropriate tool with which to analyze how driving forces may influence future emission outcomes and to assess the associated uncertainties. They assist in climate change analysis, including climate modeling and the assessment of impacts, adaptation, and mitigation (Davidson, 2014).

Over time, different scenarios had used in climate research from SA92 used in IPCC's first assessment report to Special Report on Emission Scenarios (SRES) used in the third and fourth assessment report. Recently, the new scenarios called Representative Concentration Pathways were developed and used for preparing the fifth assessment report (AR5) of IPCC released in 2015. In addition, RCPs are time and space-dependent trajectories of concentrations of greenhouse gases and pollutants resulting from human activities, including changes in land use (Kibret et al., 2016).

The RCPs are named according to the radiative forcing target level for 2100. RCPs afford a unique set of data, mainly concerning comprehensiveness and detail, as well as the spatial scale of information for climate model projections (Wayne, 2003; Vuuren et al., 2011). Hence, four pathways were used for climate modeling and research according to the IPCC fifth Assessment Report (AR5) in 2014. The pathways describe different climate futures, all of which are considered possible depending on the volume of greenhouse gases (GHG) emitted in the years to come are labeled after a possible range of radiative forcing values in the year 2100 (Vuuren et al., 2011; Belay & Mengistu, 2021).

1. RCP 8.5 (high Emissions): - This RCP is consistent with a future with no policy changes to reduce emissions. It was developed by the International Institute for Applied System Analysis (IIASA) in Australia and is characterized by increasing greenhouse gas emissions that lead to high greenhouse gas concentrations over time. Its radiative forcing reaches 8.5 Watts per meter squared (~1370 ppm CO_2 eq) after the year 2100. Combines assumptions

about high population and relatively slow income growth with modest rates of technological change and energy intensity improvements, leading in the long term to high energy demand and GHG emissions in absence of climatic change.

2. RCP 6 (High Emissions): -This RCP is developed by the National Institute for Environmental Studies (NIES) in Japan. Radioactive forcing is stabilized shortly after the year 2100, which is consistent with the application of a range of technologies and strategies for reducing greenhouse gas emissions. Oil consumption remains high, while bio fuel and nuclear play a smaller role than in the other three scenarios. Radiative forcing reaches 6 watts per meter squared (~850 ppm CO_2 eq) after the year 2100.

3. RCP 4.5 (Intermediate emissions): - is developed by the Pacific Northwest National Laboratory in the US. Here radiative forcing is stabilized shortly after the year 2100, consistent with a future with relatively ambitious emissions reductions. Radiative forcing reaches 4.5 watts per meter squared (~650 ppm CO_2 eq) after the year 2100.

4. RCP 2.6 (Low Emissions): - is developed by PBL Netherland Environmental Assessment Policy. Here a radiative forcing reaches 3.1 watts per meter squared (W/M^2) (~490 ppm CO_2 eq) before it returns to 2.6 W/M^2 by 2100. To reach such a forcing level, ambitious greenhouse gas emissions reductions would be required over time.

2.3.3 Climate Data Downscaling and Bias Correction Techniques

In climate change projection global-scale models or general circulation models (GCMs), representing physical processes in the land surface, atmosphere, ocean, and crysphere, are the most superior tools currently accessible for simulating the response of the large-scale climate system to rising greenhouse gas concentrations(https://www.ipcc-data.org/guidelines/pages/gcm_guide.html). These global models are not capable to represent coarse atmospheric features in smaller details on local climate scale. Therefore,

dynamical downscaling is one of the techniques used as a way of bridging the gap between low spatial resolution global climate models (GCMs) and the regional catchment. Then it transfer information from coarse GCMs to finer scales by applying a higher-resolution regional climate models (RCMs) GCM (Fowler et al., 2007; Cooney, 2012).

There are two broad approaches of downscaling techniques: dynamical and statistical (Fowler et al., 2007; Trzaska & Schnarr, 2014). Dynamical downscaling means the use of high-resolution regional simulations to dynamically extrapolate the effects of large-scale climate processes to regional or local scales of interest using observational data or lower resolution climate model as a boundary condition (Fowler et al., 2007; Trzaska & Schnarr, 2014; Giorgi & Gutowski, 2015). While statistical downscaling takes in the use of the different statistics-based procedures to verify links between large-scale climate models determined by global climate models and observed local climate responses. These associations are applied to GCM products to change climate model outputs into statistically refined products, often considered to be more suitable for use as input to regional or local climate impacts studies (Trzaska & Schnarr, 2014).

Dynamical downscaling has particularly been performed in the context of the Coordinated Regional Climate Downscaling Experiment (CORDEX) of the World Climate Research Program (WCRP) (http://wcrp-cordex.ipsl.jussieu.fr/). CORDEX represents the first attempt at full worldwide coordination of regional downscaling work using a common experimental framework intended to generate the next generation of worldwide high-resolution regional climate projection through a fully coordinated experimental protocol (Giorgi & Gutowski, 2016). It also enabled a systematic comparison of different modeling initiatives and provided insights into the skills and shortcomings of the participating RCMs (Giorgi & Gutowski, 2015).

Climate models often provide significant biases including systematic model errors if compared with observed variables, especially precipitation and temperature (Tan et al., 2020). The bias correction technique is commonly used in climate impact modeling and is essential to reduce the inconsistency (under or over estimate) between observed and simulated climate variables (Teutschbein & Seibert, 2012; Rathjens et al., 2016). It also aims to correct chosen statistics of a climate model simulation to better match observed statistics over a current reference time (Maraun, 2016).

Several studies were carried out around the globe in hydrological climate-change impact using regional climate model (RCM) simulations. However, their application is challenging due to the risk of substantial biases. Therefore to deal with these biases, more than a few bias correction techniques have been developed (Teutschbein & Seibert, 2012).

All bias correction methods can correct the raw RCM simulations of rainfall and temperature to the observed rainfall and temperature values (Teutschbein & Seibert, 2012; Worku et al., 2020). Even if, the value of adjusted RCM precipitation temperature is strongly dependent on the choice of the correction algorithm, both for current and future climate conditions (Teutschbein & Seibert, 2012). These methods include linear scaling of precipitation and temperature, local intensity scaling (LOCI) of precipitation, power transformation of precipitation, variance scaling of temperature, distribution mapping of precipitation and temperature, delta-change correction of precipitation and temperature, quantile mapping, and others (Teutschbein & Seibert, 2012 ; Maraun, 2016; Worku et al., 2020).

2.4 Banana Plantation

In Queensland for horticultural soil conservation purpose banana plantation was used as tree row crops for soil conservation mound construction (Wenner, 1983). Planting bananas into a cover crop act as an effective mulch and the trash from harvested banana plants, de-suckering and de-leafing will provide additional soil protection, and increase soil organic matter (Akehurst et al., 2008).

Ethiopia has diverse climate and altitude conditions, which are appropriate for growing both tropical and temperate fruits (Yirgu, 2018). Dessert banana (*Musa spp.)* is the major fruit crop that is most widely grown and consumed in Ethiopia. It is cultivated in several parts where the growing conditions are favorable. Especially in the south and southwestern parts of the country, it is of great socioeconomic importance contributing significantly to the overall wellbeing of the rural communities including food security, income generation, and job creation (Ambisa et al., 2019).

In Ethiopia now, banana covers about 59.64% (53,956.13 hectares) of the total fruit area, about 68% (478,251.04 tons) of the total fruit produced, and about 38.3% (2,574.035) of the total fruit-producing farmers. On the other hand, about 68.72% (37,076.83 hectares) of land covered by banana, about 77.52% (370,784.17 tons) of the banana production, and 22.38% (1,504,207) of the banana producers in Ethiopia are found in the Southern Nations Nationalities and Peoples Regional State (SNNPRS) (Ambisa et al., 2019).

2.5 Soil Erosion Prediction Models

Erosion phenomena are the result of complicated natural processes. The determination of their course, their mathematical expression, and predicting erosion phenomena of certain intensities is an important hydrological problem. To obtain a solution, it is necessary to

evaluate the erosion factors in detail, which act by the origin and course of erosion processes, to analyze their influences, and to apply correct conclusions to their complex activity on this basis (Zeleňáková et al., 2019).

Efforts to mathematically predict soil loss by water began about 1940 in the Corn Belt. The soil loss estimating procedure was developed in that region between 1940 and 1956. The developments of erosion prediction technology begin with analyses such as those to identify the major variables that affect soil erosion by water (Wischmeier and Smith, 1978; Renard *et al.*, 1997). Soil erosion prediction is the most widely used and most effective tool for soil conservation planning and design. The prediction of soil erosion by water has played an important role in the use, management, and assessment of land (Laflen et al., 1991)**.** All soil erosion prediction models consider slope steepness, slope length, vegetative cover, rainfall, soil properties, and erosion control methods as parameters that influence erosion (Igwe et al., 2017).

Modelling is a useful tool for erosion scenario assessment that enables the adequate selection of erosion control measures (Igwe et al., 2017). Several erosion models such as Universal Soil Loss Equation (USLE) (Wischmeier & Smith, 1978), Revised Universal Soil Loss Equation (RUSLE) (Renard *et al.*, 1997), Coordination of information on the Environment (CORINE), Water Erosion Prediction Project (WEPP) (Laflen et al., 1991), Soil and Water Assessment Tool **(**SWAT) (Arnold et al., 2012)**,** Morgan, Morgan, and Finney model (MMF**),** Pan-European Soil Erosion Risk Assessment (PESERA), Water and Tillage Erosion Model, the Sediment Delivery Model (WaTEM/SEDEM) (Van Oost et al., 2000)**,** Modified Universal Soil Loss Equation (MUSLE), Kinematic Runoff and Erosion Model (KINEROS), Erosion Potential Model (EPM), Revised Universal Soil Loss Equation with sediment deliver ratio (SDR) (Van Oost et al., 2000 **;** Ebrahimzadeh et al., 2018)**,** Limburg Soil

Erosion Model (LISEM, etc have been developed and applied in various regions of the world.

According to (Borrelli et al., 2021), for a better understanding of the global application of soil erosion prediction models, a comprehensively reviewed relevant peer-reviewed research literature on soil-erosion modelling published between 1994 and 2017 was reviewed. Based on the finding of this review (R) USLE-type models have been extensively used and modified during the last two decades and remain the most employed modelling tool today (Table 2.1). As the result of a dominance of these model types, most of the current knowledge on the spatial distribution of soil-erosion and its temporal trends are derived through (R) USLE-type approaches. This, in turn, means that our understanding of spatial soil erosion mostly relies on empirical models dealing with water as the erosion agent and focusing on sheet and rill processes as the dominant ones.

2.1 Different soil loss estimation models

Models	Records	Percentage (%)	References
RUSLE	507	17.1	(Renard *et al.*, 1997)
USLE	412	13.9	(Wischmeier & Smith, 1978).
WEPP	191	6.4	(Laflen et al., 1991)
SWAT	185	6.2	(Arnold et al., 2012)
WaTEM/SEDEM	139	4.7	(Van Oost et al., 2000)
RUSLE-SDR	115	3.9	-
USLE-SDR	64	2.2	-
LISEM	57	1.9	**(**De Roo et al., 1996)
Customized approach	53	1.8	-
MUSLE	52	1.7	(Williams and Berndt, 1977)
Others (15 in number)	398	13.3	Different authors

Source: (Borrelli et al., 2021)

2.5. 1 RUSLE Model

The Revised Universal Soil Loss Equation (RUSLE) was first introduced in the united states department of agriculture (USDA) Soil and Water Conservation Service in 1993. RUSLE is an upgrade of USLE which is being widely implemented and used to estimate soil loss from watersheds (Renard et al., 1997). RUSLE keeps up the same empirically based equation as USLE to compute sheet and rill erosion (Renard et al., 1997; Benavidez et al., 2018).

The pioneering USLE is more accurate for soils with medium texture and slopes of less than 400 ft in length with a gradient ranging between 3% and 18 %, USLE also is an erosion model designed to predict annual soil losses from specific field areas in specified cropping and management systems and it also assumed that runoff was uniform over the catchment. (Wischmeier & Smith, 1978; Benavidez et al., 2018).

The major modifications compared to USLE are: RUSLE is to account for rock fragments on and in the soil. Rock fragments on the soil surface are treated like mulch in the C-factor, while K is adjusted for rock in the soil profile to account for rock effects on permeability and, in turn, runoff (Renard et al., 1997; Benavidez et al., 2018). One of the criticisms of the pioneering USLE method of calculating LS factor is its limited applicability to the complex topography. With using advances in GIS technology, the LS factor as a function of the upslope contributing area or flow accumulation has been determined (Renard et al., 1997; Benavidez et al., 2018). The use of DEMs to calculate the upslope contributing area and the resulting LS factor allows researchers to account for more topographically complex landscapes(Moore & Wilson, 1992). Therefore, RUSLE can handle converging and diverging terrain and considers areas and better calculations of the slope (LS) factors, as well as a more advanced computerization version of the USLE (Renard et al., 1997; Benavidez et al., 2018).

RUSLE gives more credit to the ability of surface residues to reduce erosion, as well as residues incorporated in the soil near the soil surface. The widespread field use has substantiated its usefulness and validity for this purpose. RUSLE takes better into account that some runoff is channeled into rills and gullies. RUSLE also captures better than USLE that long rains can saturate the soil, leading to reduced intake and greater erosional runoff.

Integrating RUSLE with GIS and remote sensing data are vital approaches to better estimate soil loss values, identify and delineate erosion-prone areas, and prioritize the areas for effective planning of sustainable land management based on erosion severity levels in the watersheds (Yesuph & Dagnew, 2019). In the application of RUSLE on the GIS environment, soil loss was estimated within the raster/grid GIS (Moges & Bhat, 2017). Raster models are cell-based representations of map features, which offer analytical capabilities for continuous data and allow fast processing of map layer overlay operation (Kouli et al., 2009; Fenta *et al.*, 2016).

2.5.2 RUSLE Model input Variables

RUSLE estimates the annual soil loss that is due to erosion through a factor-based approach using as input variables: rainfall erosivity (R), soil erodibility (K), length of slope and steepness (LS), cover management (C), and conservation practices (P). Therefore, the average annual soil loss was estimated from equation 2.1 below based on (Renard *et al.*, 1997).

$$\mathbf{A = R * K * L * S * C * P} \quad \ldots\ldots\ldots\ldots \quad (2.1)$$

Rainfall erosivity (R) is the ability of rainfall and runoff to detach and transport soil at a particular area and given as the product (EI_{30}) of the total energy of rainstorm (E) and the maximum 30-min intensity (I_{30}). An increase in the intensity and amount of rainfall results

in an increase in the values of R (Renard *et al.*, 1997). In the pioneering equation of RUSLE, the value of R measures the kinetic energy of the rain, and it requires measuring the rainfall intensity with autographic records continuously. Although, due to the shortage of recorded rainfall intensity data on the different parts of developing countries, the empirical equation was developed based on their conditions to estimate the R factor value (Moges & Bhat, 2017; Benavidez et al., 2018).

The soil erodibility factor (K) represents the effect of soil properties and soil profile characteristics on soil loss (Renard *et al.*, 1997; Morgan & Nearing, 2011) The K-factor is defined as the rate of soil loss per unit of R-factor on a unit plot (Renard *et al.*, 1997). Soil erodibility depends on the physical and biochemical properties of soils and ranges from 0 to 1 (Bewket & Teferi, 2009). The LS factor expresses the effect of topography, specifically hill slope length, and steepness, on soil erosion. The increase in hill slope length and steepness increases the LS factor and soil erosion (Renard *et al.*, 1997; Yesuph and Dagnew, 2019).

The cover and management factors (C) and support practice factors (P) are considered dynamic factors that vary over time (Kavian et al., 2017). The C cover-management factor is used to articulate the effect of plants and soil cover. Estimation of the C factor values in the RUSLE model requires data related to soil management status, the role of plant canopy and crop residues as soil cover, soil surface roughness, and soil moisture status. The C-factor measures the combined effect of all interrelated cover and management variables, and it is the factor that is most readily changed by human activities. The C-factor shows how different LULC types (such as cropland, forest, grassland, etc.) affect soil loss rates (Renard et al., 1997).

The P factor is the support practice factor it mainly represents how surface conditions affect flow paths and flow hydraulics. A good conservation practice will result in reduced runoff volume, velocity, and less soil erosion (Renard et al., 1997).

2.5.3 RUSLE in Ethiopia

The Revised Universal Soil Loss Equation (RUSLE) for the prediction of water-induced soil erosion has been adopted in different parts of the globe. For example, in Greece (Kouli et al., 2009), in Iran (Kavian et al., 2017), in Kenya (Angima et al., 2003), South East Asia (Chuenchum et al., 2020), in Ethiopia (Gelagay and Minale, 2016; Yesuph and Dagnew, 2019; Yadeta et al., 2020), etc.

Different scholars develop and adopt several methods and equations to estimate RUSLE input parameters in the condition of Ethiopia. For instance (Helden, 1987), suggested K factor values for use in Ethiopia based on soil color, which is believed to be a reflection of soil properties cited in (Bewket and Teferi, 2009; Yesuph and Dagnew, 2019). A similar method of determining K factor values from the color of soils has also been suggested by the Soil Conservation Research Project (SCRP, 1996) and adopted by different researchers. K values for different colors are documented for example: black, brown, red, and yellow, and their corresponding K factor values are 0.15, 0.2, 0.25, and 0.35, in order of sequence (Bewket & Teferi, 2009). The empirical equation developed by (Hurni, 1985) and (Kaltenrieder, 2007) for Ethiopian conditions was also used by several researchers to estimate the R factor value.

The geographical information system (GIS) based RUSLE model has been widely adopted and used for soil loss estimation in different parts of the country. For example, the mean annual soil loss in Wondo Genet Watershed (26 t- ha^{-1} $year^{-1}$) (Sisay, 2014), Koga watershed in the highlands of Ethiopia (42 t-ha^{-1} $year^{-1}$) (Molla & Sisheber, 2017), Upper Blue Nile River basin (27.5 t-$ha^{-1}year^{-1}$) (Haregeweyn et al., 2017), Geleda watershed (23.7 t-ha^{-1}

year^{-1}) (Gashaw et al., 2018), Beshillo Catchment (37 t-ha^{-1}year$^{-1)}$ (Yesuph & Dagnew, 2019) and Lake Tana Sub-basin (37.89 t-ha^{-1}year^{-1}) (Balabathina et al., 2020), were estimated.

2.6. RS and GIS for LULCC Detection and Estimation of Soil Erosion

To estimate soil erosion and to establish soil erosion management plans, many computer-based models have been developed and used (Devatha et al., 2015). Remote sensing (RS) and Geographical information system (GIS) are important techniques for LULC classification (Gebeyehu et al., 2019) and this technique is an area of interest that has been attracting increasing attention (Mengistu & Salami, 2007). RS is one of the tools which is very important for the production of Land use and land cover maps through a process called image classification (Rwanga & Ndambuki, 2017). Remote sensing is an effective tool for mapping natural resources at a regional level using satellite digital image processing with the aid of GIS technology in mapping and detecting LULC changes (Alawamy et al., 2020).

The application of RS and GIS in forest resource management through the identification, classification, assessment, and interpretation of different land use and land cover classes has been amply demonstrated. The remotely sensed data (imageries) are important and extremely useful in mapping and monitoring the dynamics of land use/land cover. Geographic Information System (GIS) is an information technology that has been used in public policy-making for environmental and forest planning and decision-making. Mapping of LULC and change detection using remote sensing and GIS techniques is a cost-effective method of obtaining a clear understanding of the land cover alteration processes due to land-use change and their consequences (Wang et al., 2015).

The RUSLE model required the integration of thematic factors' maps which are rainfall aggressiveness, length and steepness of the slope, vegetation cover, soil erodibility, and erosion control practices. These factors were calculated using remote sensing data and GIS (El Jazouli et al., 2017).

3. MATERIALS AND METHOD

3.1. Description of the Study Area

3.1.1 Location

Sile River watershed is located in the Gamo zone of South Nation, Nationalities and Peoples Regional State, of Ethiopia. The watershed encompasses two districts Arbaminch zuria and Bonke districts. Runoff from this watershed drains into Lake Chamo. The watershed has an area of 27610 hectare and is geographically located between 5^0 50" 30' - 6^0 4" 30' N latitude and 37^0 17" 30' '- 37^0 35" 0' ' E longitude.

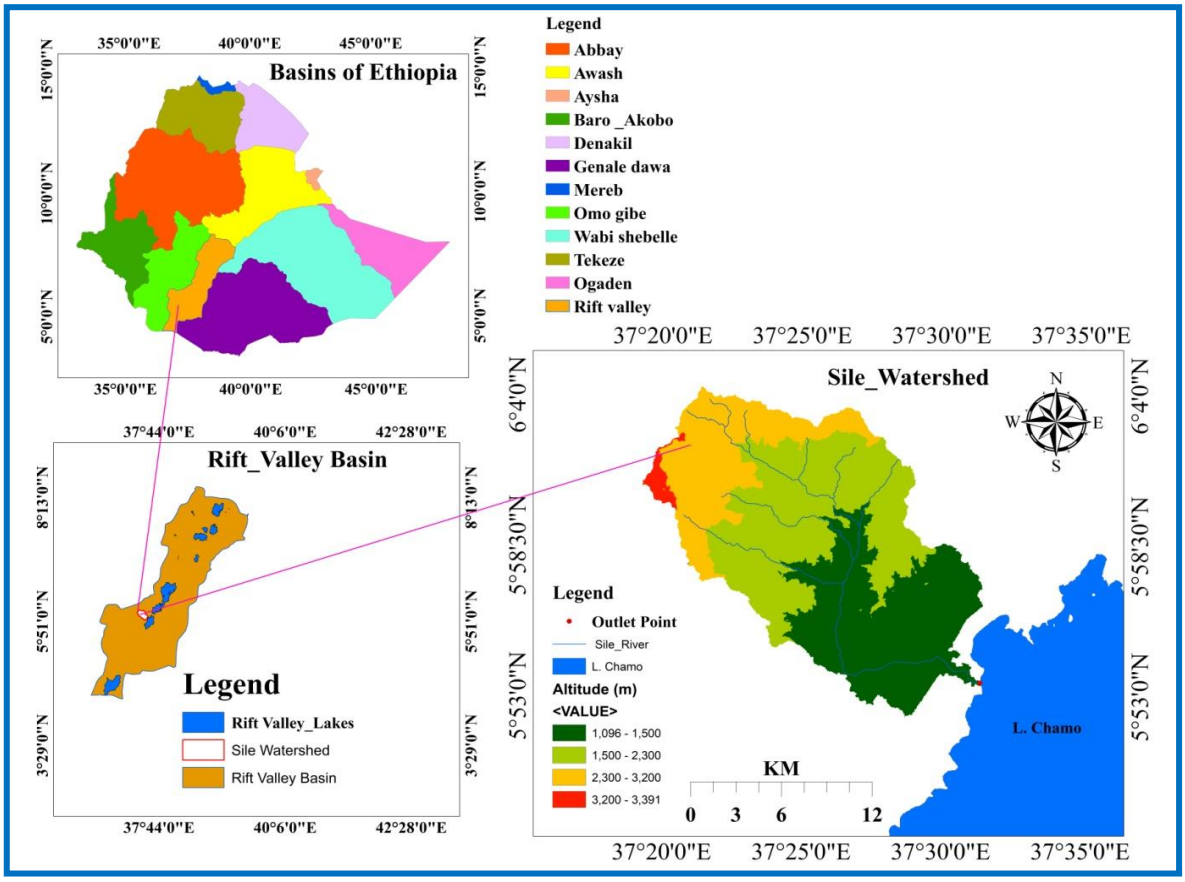

Figure 3.1 Location of the study area

3.1.2 Climate and Agro-ecology

The average annual rainfall in the Sile watershed for the thirty-four years (1987 to 2020) for Arbaminch, Mirab-Abaya, Gidole, and Gato stations was about 887.72 mm, 763.6 mm, 1256.6 mm, and 856.5 mm respectively. Source: (ENMA, 2020) Rainfall pattern is bimodal, erratic, and unreliable, depending on altitude and moisture-bearing seasonal air current. 'Belg' (long rainy season) and 'Meher' (short rainy season) are the two rainfall seasons. The main rains are from April to May, while the small rains are from September to October. Source: (Arbaminch Zuria district ANRO)

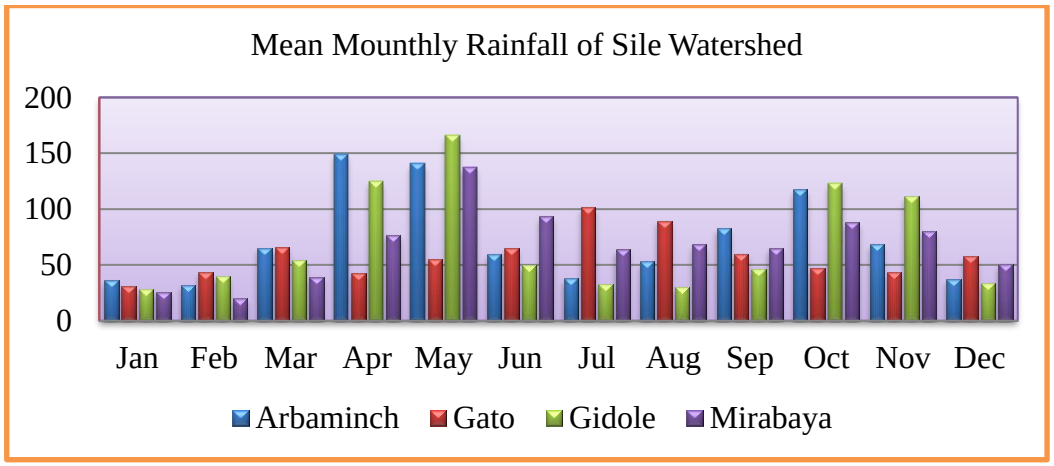

Source: ENMA, (2021)

Figure 3.2 Mean monthly rainfall of Sile Watershed from 1987-2020

The average minimum and maximum temperature of the Sile watershed were ranging from 14^0C–33.5^0C. The average maximum and minimum temperature represented in the watershed was also collected for four stations the average monthly maximum and minimum temperature of each station is shown in Figure 3.3.

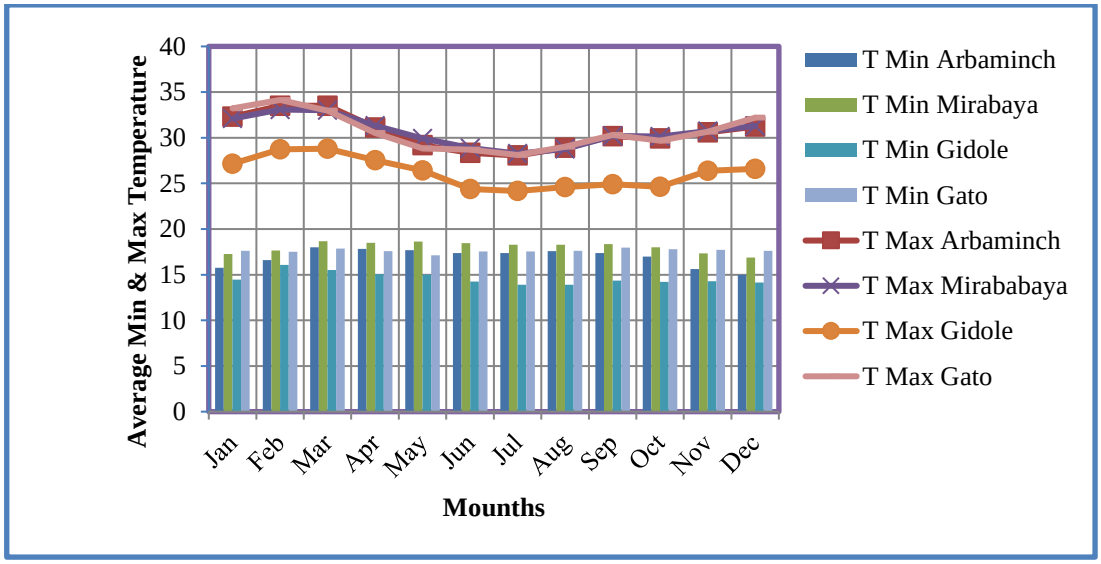

Source: ENMA, (2021)

Figure 3.3 Mean monthly Max and Min temperature of Sile watershed from the year 1987-2020

The distribution of meteorological stations around the neighbor stations nearest to the study watershed used for rainfall-runoff erosivity analysis were shown (Figure 3.4) below.

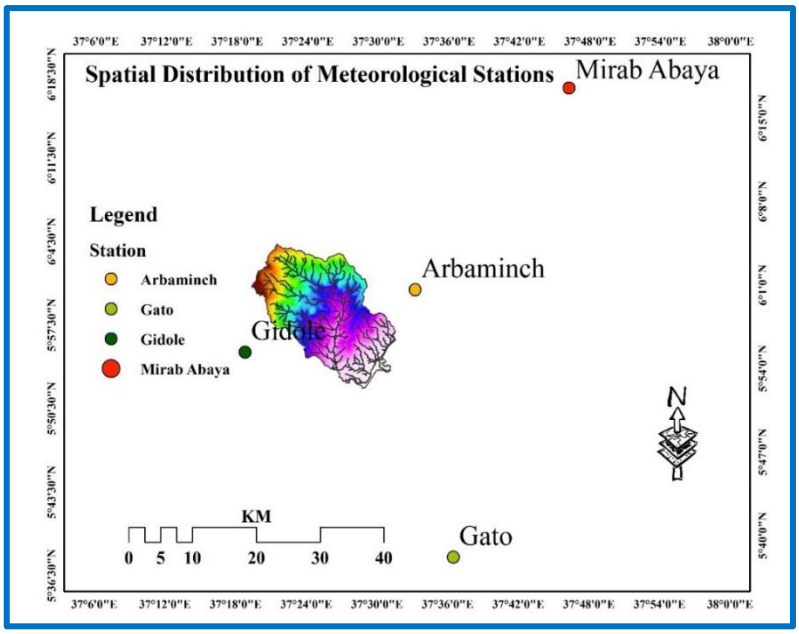

Figure 3.4 Spatial distribution of meteorological stations around the Sile Watershed

According to Ethiopia's traditional agro-ecological zone (AEZ) classification methods, in the study area, four major types of AEZ were existing. As shown in (Table: 3.1) Kolla (hot

lowlands) ranges from 500 to 1,500 m.asl, Woina Dega (mid lands) ranges from 1,500 to 2,300 m.asl, Dega (highlands) ranges from 2,300 to 3,200 m.asl, and Wurch (highlands) ranges from 3,200 to 3,700 m.asl were 36 %, 40 %, 22% and 1% shares respectively (Gorfu & Ahmed, 2011; Yohannes et al., 2018).

Table 3.1 Agro-ecological zones (AEZ) of Sile watershed

ID	Agro-Ecological Zones	Area (ha)	Area (%)
1	Kolla (Hot lowlands)	10,028	36
2	Woina Dega (Midlands)	11,185	40
3	Dega (High lands)	6,014	22
4	Wurch (High lands)	383	1
Total		27,610	100

3.1.3. Cropping Practices and LULC

Farmers in the study watershed cultivate subsistence and cash crops with rainfed agriculture and irrigation using Sile River and a mixed farming system. The major crops grown in the area are barley, maize, cotton, teff, sorghum, wheat, and in the downstream part of the watershed perennial fruits like banana, mango, and avocado are majorly produced (Gamo Zone ANRO).

The land use/land cover of the Arba Minch Zuria district (Sile River watershed existing) is dominated by intensively cultivated land with perennial and annual crops which comprises 54.7% of the land area and by bush land which comprises 33.33% of the land area, the other land use moderately cultivated with perennial and annual crops 4.7%, grass land 3.59%, State farm 1.5%, broad left forest 1.2%, and Lakes 0.95%. Source: (Arbaminch Zuria district ANRO)

3.1.4 Soil Type

According to the (FAO, 2007), soil classification the major soil types of the study area are Orthic acrisols, Calcic xerosols, Leptosols, Chromic vertisols, Orthic solonchak, Dystric nitisols, and Dystric fluvisols. The study area is mostly dominated by Orthic acrisols with 30 % and Calcic xerosols with 23 % out of the total watershed area as shown in (Table 3.2 and Figure 3.6)

Table 3.2 Major soil types and their area coverage

Soil Type	Area	
	Hectares (ha)	Percentage (%)
Calcic xerosols	6356	23
Chromic vertisols	3455	13
Dystric fluvisols	849	3
Dystric nitisols	2062	7
Leptosols	3712	13
Orthic acrisols	8232	30
Orthic solonchaks	2943	11
Total	27,610	100

Source: (FAO, 2007).

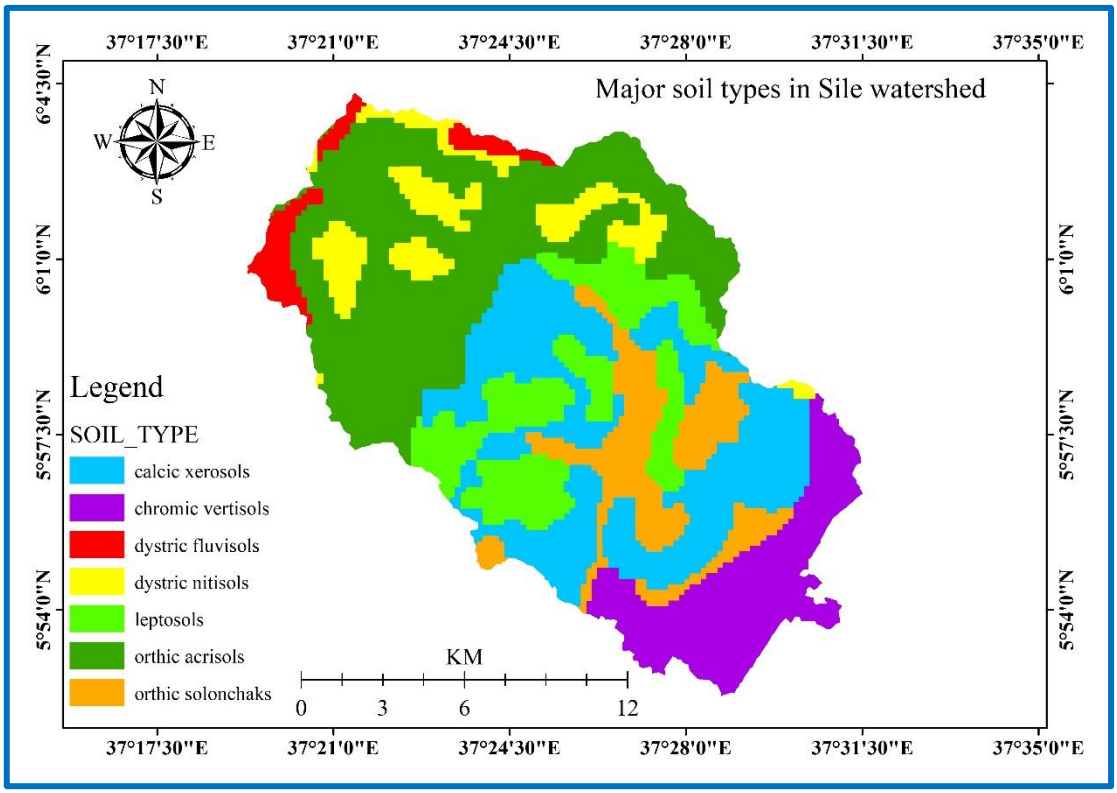

Source: (FAO, 2007)

Figure 3.5 Soil types of Sile watershed

3.1.5 Topography

The study area was highly hilly terrain and slope dissected to mountainous terrain characterizes by steep slopes in the midstream and upstream part, but the downstream part has undulating topography and relatively gentle slopes. The elevation of the study area ranges from 1098 to 3391 meters above sea level. The watershed has marked topographic variation. As shown in (Table 3.3 and Fig3.7) the dominant slope class >30% is called mountains terrain which covers 40% of the watershed area followed by 15-30 % (hilly terrain) topography with total coverage of 31%, and 10-15 % slope classes of rolling terrain cover 11% study area. The downstream of the watershed flat and gently flat topography covers only 18% of the study watershed.

Table 3.3 Slope classes and their area coverage in Sile Watershed

Slope class (%)	Slope class name	Area(ha)	Area (%)
0-2	Flat to almost flat terrain	233	1
2-10	Gently flat to undulating terrain	4,708	17
10- 15	Rolling terrain	2,988	11
15-30	Hilly terrain	8,549	31
>30	Slope dissected to mountainous terrain	11,131	40
Total		27,610	

Source: Adopted from (FAO, 1990) (https://www.fao.org/3/x0596e/X0596e02.htm/)

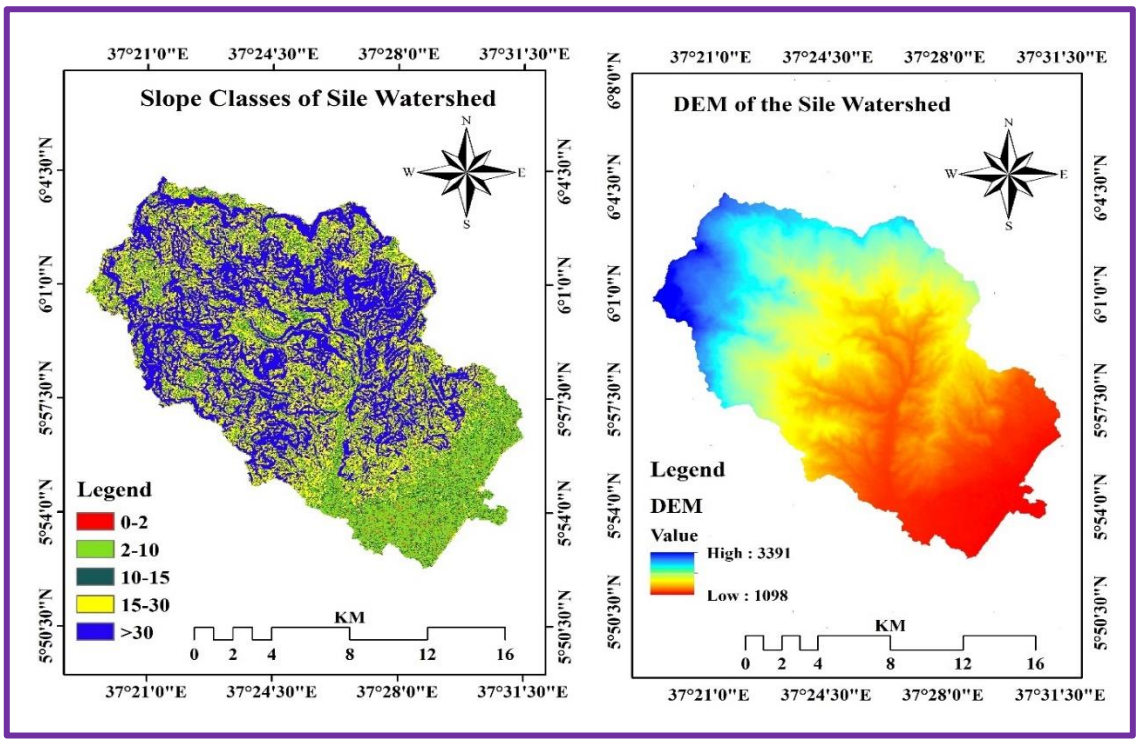

Figure 3.6 Slope class of study watershed (Left), DEM of the study area (Right)

3.2 Watershed and Sub-Watershed Delineation

The input parameter for watershed delineation was ASTER DEM 30*30-meter resolution which was downloaded from the National Aeronautics and Space Adminstration (NASA) of Earth data website (https://search.earthdata.nasa.gov/search) and projected into the same projection called UTM Zone 37N. The watershed and sub-watershed under the study area

were delineated using the automatic delineation option available in Arc Hydro Tools of ArcGIS10.8 extension (Gezahegn & Harka, 2020). For watershed delineation, the terrain processing DEM manipulation, fill sink, flow direction, flow accumulation, stream definition, stream segmentation, catchment gird delineation, catchment polygon processing, drainage line processes, and drainage point processing was followed respectively. The elevation of the area is also generated from DEM when the watershed was delineated. The highest elevation of the area is 3391 m and the lowest is 1098 meters above sea level.

3.3 Data Sources and Method of Data Collection

To achieve the objectives of this study different data sets were used. The LULC data were prepared from satellite imagery (Table 3.4) such as Land sat Thematic Mapper (TM) for the year 1987, Enhanced Thematic Mapper Plus (ETM+) for the year 2003, and Landsat-8 OLI/TIRS (Operational Land Imager/Thermal Infrared Sensor) for the year 2020 (Alawamy et al., 2020; Belay & Mengistu, 2021) were obtained from the website of the United States Geological Survey (USGS) (https://earthexplorer.usgs.gov/)

Table 3.4 Satellite images used in this study for LULC change analysis

No	Path	Row	Sensor	Date of Acquisition	Spatial Resolution	Source
1	169	056	TM	January 31, 1987	30*30	USGS
2	169	056	ETM+	February 02, 2003	30*30	USGS
3	169	056	OLI/TRS	February 27, 2020	30*30	USGS

OLI/TRS= Operational Land Imager/Thermal Infrared Sensor: TM = Thematic Mapper - sensors are Landsat 4-5 and ETM+ = Enhanced Thematic Mapper Plus

For the accuracy assessment of 2020, the LULC map total of 281 ground truth points was collected through direct field observations using the Global positioning system (GPS. While,

for the years 1987 and 2003 LULC maps Google Earth were used (Woldesenbet et al., 2020) and in each study years 504 and 485 reference points were collected respectively.

In this study, Multi-Layer Perceptron Neural Network (MLPNN) and Cellular Automata-Markov model CA-MC was used to simulate and predict future LULC of 2050 with considering different independent driving factors that highly impact LULC change (Gharaibeh et al., 2020; Leta et al., 2021; Girma et al., 2022). These variables are topography features (slope, elevation, and aspect), accessibility or proximity variables (distance from road and distance from stream), and demographic or population density. Some variables like slope, elevation, aspect, and stream network variables were generated from ASTER DEM (https://search.earthdata.nasa.gov/search). The population data were obtained from the Ethiopian Central Statistical Agency (CSA). The road network shapefile was downloaded from OpenStreetMap. (https://www.openstreetmap.org/#map=14/6.0595/37.5578) and its geometric consistency (projection to WGS 84 UTM Zone, 37 N) data conversion were done in Arc GIS 10.8 software.

To estimate potential soil loss of the watershed five RULSE model parameter data sets were considered. The soil survey was conducted throughout the watershed using a stratified random sampling technique based on consideration of land use system, slope position, and soil color. Then, a total of 102 composited soil samples 32, 18, 15, 21, 9, and 7 from cultivation land, shrub land, bare land, banana farm, grazing land, and forest were collected with a stratified random approach respectively. The collected soil samples were analyzed for soil texture and soil organic carbon content to determine soil erodibility factor (K-value).

Advanced Space Boerne Thermal Emission and Radiometer (ASTER) were used to generate the topographic factor LS map. To identify the conservation practice (P-factor) of the study watershed, data were reviewed from a need assessment report of Arbaminch agricultural

research center and field visit. Historical (1987, 2003, and 2020) and future predicted 2050 LULC maps were used to obtain cover factor (C- factor) value.

Baseline and future simulated climate data were used in this study. Daily rainfall data from 1987 to 2020 for four stations around the catchment was obtained from the Ethiopian National Meteorological Agency (ENMA). It was used to determine the rainfall-runoff erosivity factor (R), estimate the baseline (1987, 2003, and 2020) soil loss & validate the predicted 2050 climate scenarios.

Climate models were used to compute the relative change in the present and future climate, often used as an input to the soil erosion models. In this study, four different simulated regional climate models (RCMs) for two specific periods historical (2001 to 1985) and future scenarios (2006 to 2050) periods with the three driving GCM models: HadGEM2 ES, ICHEC-EC-EARTH, and CanESM2 under CORDEX AFR-44 domain (Coordinated Regional Climate Downscaling Experiment) were downloaded from (https://esgf-node.llnl.gov/search/esgf-llnl/). These models are the relatively higher spatial resolution of 0.44˚ by 0.44˚ or correspond to 50 km by 50 km and suitable based on previous research carry out in other parts of the country (Mutayoba & Kashaigili, 2017; Moges et al., 2020 ;Girmay et al., 2021; Belay & Mengistu, 2021).

Table 3.5 The CORDEX-RCM and their driving GCMs used in this study

S/N	Reginald climate model	Model Institute	Short name of RCM	Driving GCM
1	Canadian Regional Climate Model version 4 (CanRCM4**)**	Canadian Centre for Climate Modelling and Analysis (CCCMA)	CanRCM4	CCCma_can ESM2

2	Rossby Center Regional Atmospheric Model (RCA4)	The Swedish meteorological and hydrological Institute (SMHI)	RCA4	MOHC-HadGEM2-ES
3	Rossby Center Regional Atmospheric Model (RCA4)	The Swedish meteorological and hydrological Institute (SMHI)	RCA4	CCCma_can ESM2
4	Regional Atmospheric Climate Model Version 2.2 T (RACMO22T)	Koninklijk Nederlands Meteorologisch Instituut (KMNI) Royal Netherlands Meteorological Institute	RACO22T	ICHEC-EC-EARTH

In this study, two representative concentration pathways (RCPs) scenarios RCP4.5 and RCP8.5 were used to generate the RUSLE model (Moges et al., 2020 ; Belay & Mengistu, 2021). The future RCP climate data were available up to the end of the century. However, for this study, I select the event of climate data from the year 2021 to 2050 because the historical climate data that I had was three decades data (from 1987 to 2020) and policymakers usually focus on events occurring in the 2050s.

3.4 Historical LULC Classification and Analysis

3.4.1 Satellite Image Pre-Processing

In this study, to analyze and quantification of the spatiotemporal change of the LULC from 1987, 2003 to 2020 Landsat image pre-processing, classification, and post-processing were done (Lillesand et al., 2015; Zhong et al., 2015). A selection of proper satellite images is the primary task in the image data processing. The satellite image pre-processing steps were filled with the most appropriate data according to the following criterion: maximum data

quality (no missing scan lines, minimal cloud cover across the scene, pixel drop outs, saturated or missing bands), and acquisition date matched with peak greenness (Vittek et al., 2013). The satellite image collection years were intentionally preferred based on; considering events after nationwide famine and relocation during the Derg regime, following policy change of the country and finally the early green legacy initiative in 1987, 2003, and 2020 respectively. The metrological data availability in all stations around the study watershed was also considered.

The Level 1 Landsat of the U.S. Geological Survey (USGS), Earth Resources Observation and Science (EROS) center used in this study, were originally corrected for geometric and terrain distortion by the image provider using ground control points and the digital elevation model (DEM) (WoldeYohannes et al., 2018). The layer stacking of single-band into a single multi-band image layer and subset area of interest (AOI) image was carried out by ERDAS imagines 2014 software (Girma et al., 2022). Satellite imageries may have multiple spectral bands of information. Accordingly, to carry out image classification for Landsat 4-5, Enhanced Thematic Mapper Plus, and Landsat OLI/TRS the bands 1-7 were considered to layer stacking /composting. The false-color composite image made using Land sat 8 bands 5-4-3 (R-G-B), Land-sat TM bands 4-3-2 (R-G-B), and land-sat7 ETM plus 4-3-2 (R-G-B) were also used for the identification of major land cover classes in the study area.

3.4.2 Image Classification

In this study, a supervised classification method with maximum likelihood classification (MLC) algorithm was applied in the ERDAS Imagine 2014 software, and the LULC mapping was performed by Arc GIS 10.8 The maximum likelihood parametric rule is used to classify each pixel based on the known ground truth (Norovsuren et al., 2019 ; Dibaba et al., 2020 ; Alawamy et al., 2020 ; Koko et al., 2020 ; Leta et al., 2021)

In general, the image classification procedures were given as follows. The primary procedure is selecting training sites or areas of interest (AOI. The polygon sampling technique with the supervised image classification methods was used the merged signature for the land cover map production (Dibaba et al., 2020 ; Koko et al., 2020). The training data sets were used for creating signatures files and for the classification of the entire image into important information classes

Google earth data and field observation of the study area were helpful to get information about LULC during the 1987-2020 periods (Garedew et al., 2009; Leta et al., 2021). In the study area, seven land use/land cover classes were identified and their respective definitions are mentioned in (Table 3.6) below.

Table 3.6 Description of the identified LULC class

Land use/land cover classes	Description
Water body	Covered by water and it may be reservoirs, lakes, large water harvesting ponds, etc.
Forest land	Area covered by dense and tall trees both natural and plantations
Bare land	Areas that have little or no vegetation cover, mainly with classic gullies and exposed rocks.
Shrub land	Areas covered with short shrubs and thorny bushes, usually stony with a very rugged micro-relief.
Banana land	Areas covered with banana plantation
Cultivation land	Land covered by annual and perennial crops and fallow lands
Grazing land	Areas with grass cover

Source: (Zeleke & Hurni, 2001; Bewket & Teferi, 2009; Gelagay & Minale, 2016) and own observation.

3.4.3 Accuracy Assessment

In this study, a set of accuracy assessment points were chosen with a stratified random sampling strategy. Points that were used in training the classification were not be used for accuracy assessment (Congalaton & Green, 2008). The reference points for 1987 and 2003 were collected from the corresponding historic Google Earth image and the GPS point was collected for 2020. The assessment of accuracy was performed for LULC change analysis by generating a confusion/error matrix in each LULC category of 1987, 2003, and 2020 classified maps (Leta et al., 2021). Kappa statistics, overall accuracy, producer's accuracy, and user's accuracy were derived from the error matrix. Kappa coefficients typically lie between 0 and1. If the kappa value is greater than 0.8 it denotes a strong agreement, if a value between 0.4 and 0.8 it denotes a moderate agreement, and if a value below 0.4 it represents the poor agreement cited by (Mengistu et al., 2012; Dibaba et al., 2020).

$$\text{Overallaccuracy} = \frac{\text{Total number of correctly classified pixel}}{\text{Total number of reference Pixel}} * 100 \ldots\ldots\ldots (3.1)$$

$$\text{User accuracy} = \frac{\text{Number of correctly classified in each category}}{\text{Total Number of classified row Pixel in that category}} * 100 \ldots (3.2)$$

$$\text{Producer accuracy} = \frac{\text{Number of correctly classified pixcel}}{\text{Number of reference Pixel in that category}} * 100 \ldots\ldots (3.3)$$

The Kappa Statistics is computed as; (Congalton, 1991)

$$\mathbf{K} = \frac{\mathbf{N}\sum_{\mathbf{1=1}}^{\mathbf{r}} \mathbf{X_{ii}} - \sum_{\mathbf{i=1}}^{\mathbf{r}} (\mathbf{x_{i+}\, Xx_{+1}})}{\mathbf{N^2} - \sum_{\mathbf{i=1}}^{\mathbf{r}} (\mathbf{X_{ii}} + \mathbf{Xx_{+1}})} \ldots\ldots\ldots\ldots\ldots (\mathbf{3.4})$$

Where,

K = Kappa statistics

r = number of rows and columns in error matrix,

N = total number of observations (pixels)

X_{ii} = observation in row i and column i

Xi+ =marginal total of row i, and X+i= marginal total of column

3.4.4 Detection of LULC Change Analysis

The historical LULC change within the Sile watershed was examined at different time series through the satellite image classification and spatiotemporal analysis of the prepared land use/land cover maps was performed. Therefore, images with different dates (1987, 2003, and 2020) were independently classified, and compared to each other (Singh, 1989 ; Alawamy et al., 2020; Girma et al., 2022). The area of the LULC classes was calculated from the maps, and rates of changes were computed. Total LULC change between the two periods is calculated as follows Eq 3.5 and Eq 3.6: (Singh, 1989 ; Dibaba et al., 2020; Girma et al., 2022).

$$\text{Total } Gain/Loss = \text{Area of the final year} - \text{Area of the initial year} \ldots\ldots\ldots (3.5)$$

$$\text{Percent of Change} = \left(\frac{\text{Area of the final year} - \text{Area of the intial year}}{\text{Area of the initial year}} * 100\right) \ldots (3.6)$$

To compute the yearly rate of change for each land-use class, the distinction between final years to initial year which represents the extent of change between corresponding years was divided by the time interval between final and initial years. Computed as Eq 3.7 (Meshesha et al., 2016 ; Elias et al., 2019; Leta et al., 2021).

$$\textbf{Rate of change}\left(\frac{\textbf{ha}}{\textbf{year}}\right) = \frac{\textbf{Area of the final year} - \textbf{Area of the intial year}}{\textbf{Time}} \ldots (\mathbf{3.7})$$

3.5 Prediction of Future Land Use/Land Cover Change

In this study, the MLP_NN with CA-Markov chain found in the software of TerrSet18.32 (Clark Labs, Clark University, Worcester, MA, USA) with its extension of Land Change Modeler (LCM) and IDRISI GIS analysis was used to predict and model future LULC dynamics in the Sile watershed. Through the quantity of change that is projected to be generated through Markov chain analysis, principally the transition probability matrices, CA-Markov applies a contiguity kernel to grow out a land-use map to a later period through a CA function (Arsanjani et al., 2011; Leta et al., 2021). The CA-Markov model has been applied in this study for the advantages of the combination of the stochastic spatial Markov technique with the stochastic spatial CA method (Eastman, 2006; Sang et al., 2011; Hyandye & Martz, 2017; Nath et al., 2020).

The CA-MC model, used to identify the LULC change dynamics for any study area depending on the previous or current land cover condition was mathematically computed as (Eq. 3.8) (Sang et al., 2011; Koko et al., 2020 ; Leta et al., 2021; Girma et al., 2022).

$$S\,(t+1) = Pij * S(t) \quad \ldots\ldots (3.8)$$

Where, S (t), S (t +1) are the system status at the time of t or t +1; Pij is the transition probability matrix in a state which is calculated as follows (Eq 3.9).

$$Pij = \begin{bmatrix} P11 & p12 & \ldots & P1n \\ p21 & p22 & \ldots & P2n \\ \vdots & \vdots & \vdots & \vdots \\ Pn1 & Pn2 & \ldots & Pnn \end{bmatrix} \quad 0 \leq \text{Pij} < 1 \text{ and } \sum_{j=1}^{n} pij = 1, \text{ (i, j = 1, 2 . . . n)} \ldots\ldots \quad (3.9)$$

Where, P is the Markov probability matrix, and P ij stands for the probability of converting from current state i to another state j in next time period

In this study, LCM provides a spatiotemporal change of LULC category as losses and gains, net change, and contributor for each LULC category. The LCM uses the “change analysis” tab, the “transition potentials” tab, and the “change prediction” tab. The change rates were determined through the “change analysis” tab, along with the “transition potential” maps to simulate the future 2050 LULC through business as usual (BU) scenario. Using a multi-layer perceptron (MLP) neural network approach in the LCM module allows creating maps of transition potential based on the individual sub-models and associated explanatory variables. Therefore, to decide how the dependent variables (earlier image (2003) and later image (2020)) and independent variables (driving variables) influence future (2050) LULC change subsequently calculates a relative amount of transitions MLP_NN model was used (Eastman, 2006b; Gidey et al., 2017 ; Koko et al., 2020 ; Leta et al., 2021).

3.5.1 LULC Change Driver Variables

In this study environmental and anthropogenic driving factors that influence LULC changes were employed to project the future 2050 land use land change (Gharaibeh et al., 2020; Leta et al., 2021). These main possible driver variables of land use land cover change that are considered for the prediction of 2050 LULC include slope, elevation, aspect, distance to roads, distance to stream, and population density.

Topographic attributes for instance slope; elevation and aspects influence land cover distribution and modification (Birhane et al., 2019). The gentler the slope class is the simplest it is to have LULC changes than stepper land slope (Gharaibeh et al., 2020; Belay & Menstu, 2021). A slope was considered as a limitation for cultivation and banana land use areas because steep slopes are a barrier to both cultivation and banana expansion Hence, for this study the slope map, elevation, and aspect map was prepared from ASTREM_DEM using spatial analysts tools in Arc GIS 10.5 version software.

Accessibility and other anthropogenic factors have been aggravating factors of land-use change. For instance; distance from the road in this study was the major driver in enhancing more agricultural and banana farm expansion. Therefore, using vector data features from road and river network distance from roads and stream map were generated through Euclidian distance function in Arc GIS (Gharaibeh et al., 2020; Kafy et al., 2021 ; Girma et al., 2022).

Population density is the most common key factor in LULC where the higher the density more frequent land-use change (Gharaibeh et al., 2020; Girma et al., 2022). Population density map also generated in spatial analyst tools of Arc GIS. Therefore, all these drivers' variable data sets were created using ArcGIS software and then exported to TerrSet Software to run the potential transition maps using MLP_NN Model.

3.5.2 MLP-NN Performance Evaluation and Sensitivity Analysis

In this study, parameters and model performance evaluation and the MLP model sensitivity analysis was tested using the transition potentials tab in the LCM TerrSet image processing toolset. The model was trained using all the driving factor variables and 1987 LULC then the system repeat the skill tests for the relative power of driving factor variables by selectively holding the inputs from selected variables constant (Eastman, 2006b ; Girma et al., 2022).

Forcing a single independent variable to be constant; forcing all independent variables except one to be constant, and backward stepwise constant forcing mechanism are sensitivity analyses parameters that are used to run the skill measure. Any accuracy rate should be at least 80% to accept the training result (Gharaibeh et al., 2020). The skill statistic varies from -1 to 1 where the skill of 1 means perfect forecasting, while a skill of -1 means worse than chance (Eastman, 2006b; Gharaibeh et al., 2020).

$$\frac{(A - E(A))}{(1 - E(A))} \ldots \ldots (3.10)$$

Where A is measured accuracy, and E (A) is expected accuracy which is determined by using the number of transitions in the sub-model, T, and the number of persistence classes, P as Eq. (3.11).

$$E(A) = \frac{1}{(T + P)} \ldots \ldots (3.11)$$

Root mean square error (RMSE) is also used to evaluate the performance and prediction efficiency of the MLP-NN and it is a benchmark of the deviation of predicated values about the observed values (Eq 3.12). The lower the value, the more accurate is the prediction.

$$RMSE = \frac{\sqrt{\sum_{i=1}^{N}(Yi\ obs - Yi\ est)^2}}{N} \ldots \ldots (3.12)$$

Where Yi est. is the modelled for sample i, Yi obs. Is the observed data for sample i, and N is the total number of samples

3.5.3 Validation of MLP-CA- MC Process

In this study to validate the LULC prediction given by the MLP-CA-MC model, the simulated land use map of 2020 was used to compare the actual present land use map of 2020 to ensure the reliability and correctness of the MLP-CA-MC model in predicting the future 2050 LULC (Khawaldah, 2016; Gharaibeh et al., 2020).

The reference data is more accurate than the predicted LULC because no model perfectly predicts LULC dynamics (Gidey et al., 2017). The transition probabilities statistics were generated using classified LULC images of 1987 as the first (earlier) image and LULC image of 2003 as later (second) image with a driving variable by using MLP-CA-MC transition potential estimator to predict LULC of 2020. The number of time intervals (periods) between the first and second images is 16 years.

The Kappa statistic index was applied to validate the actual (2020) and predicted (2020) LULC: kappa for grid cell level location (K location), kappa for no information (Kno), kappa for stratum-level location (K location Strata), and kappa standard (Kstandard (Gidey et al., 2017; Gharaibeh et al., 2020). The values of each kappa statics were above 80%, which indicates the better performance of the model in simulating future LULC (Koko et al., 2020; Leta et al., 2021).

3.6 RCM Data Processing and Evaluation

3.6.1 RCM Data Bias Correction

In this study to remove the biases from the RCM data (Climate Model data for hydrologic modeling (CMhyd) software was used as a tool to extract and bias-correct RCM data (Rathjens et al., 2016). The software was also used to change Network Common Data Form (NetCDF) files into text format, considering the spatial references of Arbaminch, MirabAbaya, Gidole, and Gato meteorological stations.

For this study the RCM precipitation data under two emission scenarios RCP4.5 and RCP8.5 were bias-corrected. The historical RCMs and observed data were used for bias correction. Hence, RCM outputs (precipitation) are typically adjusted to eliminate any bias (Belay & Mengistu, 2021). There are various bias correction methods on precipitation of Regional Climate Model (RCM) of statistical bias correction analyzing ways (Mendez et al., 2020). Among the statically bias correction method, the distribution mapping bias correction method was preferred to adjust the simulated raw RCP rainfall data in this study. since, distribution mapping is a suitable bias correction method because, it was better in capturing the 90^{th} percentile of observed rainfall (Worku et al., 2020). It also corrects most of the statistical characteristics and has the narrowest variability ranges, combined with the greatest fit of the ensemble mean (Teutschbein & Seibert, 2012).

3.6.2 Ensemble RCM Data Performance Evaluation

In this study, the performances of the ensemble average RCM models were evaluated with time series performances by comparing the simulated rainfall data with observed data from 2006 to 2020 using three statistical measures: correlation coefficient (R^2), root-mean-square error (RMSE), and Nash–Sutcliffe measure of efficiency (NSE) (Mutayoba & Kashaigili, 2017 ; Worku et al., 2018 ; Girmay et al., 2021).

The correlation coefficient (R^2) is often used to evaluate the linear relationship between mean monthly RCM rainfall and observed rainfall. Values close to 1.0 indicate a better linear relationship between the variables and a value away from 1.0 indicates less agreement. Root Mean Square Error measures how much error there is between two data sets. An RMSE value close to zero indicates better performance (Worku et al., 2018). Nash-Sutcliffe efficiency indicates how well the observed versus simulated data fits the 1:1 line. NSE = 1, corresponds to a perfect match of the model to the observed data (Nash & Sutcliffe, 1970).

$$\mathrm{NSE} = 1 - \frac{\sum_{t=1}^{N} \left(R^{Observ} - R^{Observ}\right)^2}{\sum_{t=1}^{N} (R^{Observ} - \overline{R^{Observ}})^2} \quad \ldots\ldots\ldots\ldots\ldots\ldots\ldots\ldots\ldots\ldots\ldots\ldots\ldots\ldots (3.13)$$

$$R^2 = \frac{\sum_{t=1}^{N} \left(R^{RCM} - \overline{R^{RCM}}\right)^2 * \left(R^{Observ} - \overline{R^{Observ}}\right)}{\sum_{t=1}^{N} \left(R^{RCM} - \overline{R^{RCM}}\right) \sum_{t=1}^{N} \left(R^{Observ} - \overline{R^{Observ}}\right)} \quad \ldots\ldots\ldots\ldots\ldots\ldots\ldots\ldots\ldots (3.14)$$

$$RMSE = \sqrt{\frac{1}{N} \sum_{i=1}^{N} (R^{RCM} - R^{Observ})^2} \quad \ldots\ldots\ldots\ldots\ldots\ldots\ldots\ldots\ldots\ldots\ldots\ldots\ldots\ldots (3.15)$$

Where, R^{RCM} is a rainfall of RCMs, R^{Observ} is a rainfall of stations, the bar over the variables denotes the average throughout 2006–2020, and N represents the analysis period (15 years).

The mean mouthy rainfall data between the years 2006 to 2020 was used to check the pattern of observed stations' rainfall data and simulated RCMs with its mean ensemble data.

3. 7 RUSLE Model Input Factors

The revised universal soil loss equation (RUSLE) model was applied to map and estimate the soil erosion potential areas based on LULC, Slope class, and Subwatershed level on Sile River watershed during the three studies periods (1987, 2003, and 2020). The implementation of the RUSLE model in a raster Arc GIS 10.8 (Environmental Systems Research Institute (Esri), Inc., Redlands, CA, USA) (grid-based) and remote sensing-based approach in calculations of main factors governing soil erosion in Sile watershed namely climate factor a rainfall-runoff erosivity (R-factor), soil characteristics (K-factor), topography (LS-factor), land cover management (C-factor) and support practice (P - factor). Therefore, in the study area the average annual soil loss was estimated using the equation developed by (Renard et al., 1997) Eq 3.16:

$$\boldsymbol{A = R * K * L * S * C * P} \quad \text{……..} \quad (3.16)$$

Where;

A = is the amount of soil erosion (t-ha-^{1}year-^{1}) that is eroded within the unit area during the corresponding period of rainfall-runoff.

R=is a rainfall-runoff erosivity factor (MJ mm ha^{-1} hr $^{-1}$year $^{-1}$);

K= is a soil erodibility factor (t-hr $^{-1}$ MJ $^{-1}$ mm^{-1});

LS= is a surface characteristic factor (slope-length and steepness factor, L is the length of erosion slope, while S is the gradient of erosion slope) (dimensionless);

C= is a cover management factor (dimensionless);

P= is support practice factor (dimensionless);

3.7.1 Determination of R_ Factor

In the pioneering USLE model, the rainfall erosivity (R)-factor was determined from total storm energy and maximum 30 min rainfall intensity (Wischmeier & Smith, 1978). However, there was no record of storm energy and rainfall intensity for Sile River watershed. For areas where insufficient rainfall data is available, different empirical equations have been developed that estimate R values from mean annual precipitation.

In this study, a formula developed by Hurni (1985), point out the spatial regression analyses derived an equation from available mean annual precipitation (P) as an alternative approach to Ethiopian condition was used to estimated erosivity. This equation (Eq 3.17), was also used by several researchers in the previous study to estimate soil loss via RUSLE Model (Gelagay and Minale, 2016; Esa et al., 2018; Yiferu et al., 2018; Yesuph and Dagnew, 2019; Bewket and Teferi, 2020 ; Belay & Mengistu, 2021).

$$\boldsymbol{R = -8.12 + (0.562 * P)} \quad \text{……..……..} \quad (3.17)$$

Where,

R = rainfall erosivity factor in (MJ mm ha^{-1} h^{-1} $year^{-1}$);

P= mean annual rainfall in (mm)**;**

The historical erosivity factor maps were prepared for the three reference years (1987, 2003, and 2020). Therefore, the annual rainfall data of the year 1987 from four sations, the mean annual rainfall data from 1987-2003, and the mean annual rainfall data from 1987-2020 was used to estimate the R factor value for the years 1987, 2003, and 2020 respectively.

On other hand, to estimate the future 2050 soil loss the ensemble mean of four RCM models via three driving GCM models (CanRCM4 via CCCma_canESM2, RCA4 via MOHC-HadGEM2-ES, RCA4 via CCCma_canESM2, and RACO22T via ICHEC-EC-EARTH) was considered under both RCP 4.5 and RCP 8.5 scenarios. Therefore, the ensemble mean of all four RCM precipitation data was computed to estimate erosivity factor and used as input for the RUSLE model. The erosivity factor was interpolated using the inverse distance weighting (IDW) method for the entire watershed in spatial analyst tools of ArcGIS software version 10.8 (Environment Systems Research Institute (Esri), Inc. Redlands, CA, USA). Then equation 3.17 was applied to compute rainfall-runoff erosivity factor of the watershed in Raster Calculater-Map Algebra - Spatial Analyst Tools of ArcGIS software.

3.6.1.1 Estimation of Missed Rainfall Data

Surrounding gauges have the normal annual precipitation exceeding 10% of the considered Gauge. Therefore, the missing rainfall data for this research was computed by using the Normal Ratio method (Eq 3.18). This method is used if any surrounding gauges have the normal annual precipitation exceeding 10% of the considered gauge (Mekonnen, 2014).

$$Px = \frac{Nx}{m}\left[\frac{p1}{N1} + \frac{P2}{N2} + \frac{P3}{N3} + \frac{Pn}{Nn}\right] \ldots \quad (3.18)$$

Where, Px= Estimate for the ungagged station, Pi= Rainfall values of rain gauges used for estimation, Nx= Normal annual precipitation of X station, Ni=Normal annual precipitation of surrounding stations, m=No. of surrounding stations.

3.6.1.2 Consistency Test and Homogeneity Analysis

To detect and correct or adjust the inconsistency of the reported rainfall data a technique called the Double Mass Curve method was adopted. The principle of double mass curve analysis is to plot accumulated values of the station under investigation against the accumulated value of another station, or accumulated values of the average of other stations,

over the same period (James & Clayton, 1960). Through the double mass curve, inconsistency in the time series data (in particular jumps) was investigated. These indicated in the double mass plot, showing an inflection point in the straight line. The data series, which were inconsistent, were adjusted to consistent values by proportionality. This method helped in determining the best realistic correlation of different stations located near the watershed. If the cumulative plot of the double mass curve shows a different, gradient it should be corrected as Eq 3.19:

$$PCX = PX\frac{Mc}{Ma} \quad (3.19)$$

Where: PCX- Corrected precipitation at station x

Px - Originally recorded precipitation at station x

Mc - The corrected slope of the double mass curve

Ma - Original slope of the double mass curve

The graph of the double mass curve plot was founded linear for meteorological stations. This implies that the rainfall data was consistent over the considered period as shown in Fig (3.7) below.

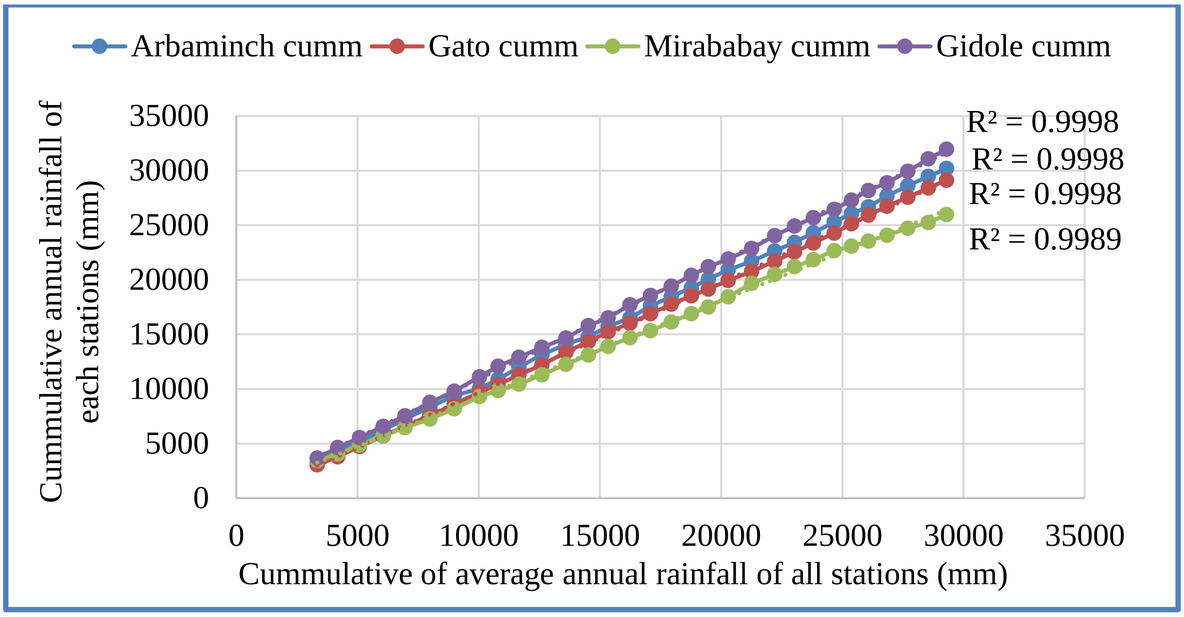

Figure 3.7 Double mass analysis representing data consistency of stations on the Sile watershed

Homogeneity analysis was used to separate a change in the statistical properties of the time-series data. To select the representative meteorological station for the analysis of areal rainfall estimation, checking the homogeneity of group stations is crucial, the homogeneity of the selected gauging stations' daily rainfall records was carried out by non-dimensional (Eq 3.20): (Alexandersson, 1986)

$$Pi = \frac{\overline{Pi}}{P} * 100 \ldots \qquad (3.20)$$

Where:

Pi - is the non-dimensional value of precipitation for the month in the station i

$\overline{Pi}$ - is over year’s average monthly precipitation for the station i

P - Over year’s average yearly precipitation of the station i

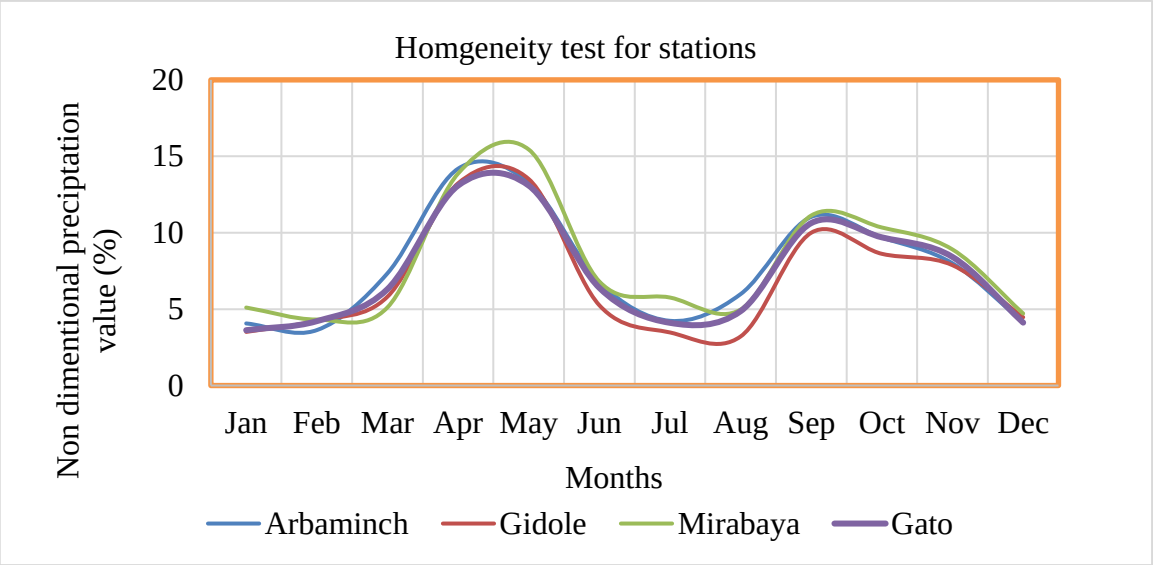

Figure 3.8 Homogeneity test for selected meteorological stations in Sile watershed

3.7.2. Determination of K_ Factor

In this study, to investigate soil erodibility factors a field survey was conducted based on different land-use systems, slope position, and soil color in Sile watershed. A total of 102 composited soil samples with a depth of 0-20 cm were collected by using the stratified random sampling technique. Then, from a total of 102 composited soil samples 32, 18, 15, 21, 9, and 7 were from cultivation land, shrubland, bare land, banana land, grazing land, and forest respectively. The collected soil samples were air-dried at room temperature and analyzed for soil texture and soil organic carbon content to determine soil erodibility factor (K-value).

Both soil texture and soil organic carbon content were analyzed in South Agricultural Research Institute (SARI), Areka Agricultural Research Center soil laboratory. The textural analysis for percent of silt, percent of sand, and percent of the clay content of the soil were conducted by the standard hydrometer method in the laboratory (Gee & Bauder, 1986: Gavlak et al., 2005).

The reagents used and procedures followed in the standard hydrometer method are: Dissolve 40 g of sodium hexametaphosphate ($NaPO_3$) and 10 g of sodium carbonate (Na_2CO_3) in distilled water in a 1-liter volumetric flask and make to volume with distilled water. Dry the chemicals in the oven at 105 ^{o}C and cool in a desiccator the day before use. Amyl alcohol ($C_5H_{12}O$) is used. Weigh 50g soil (< 2 mm) "not sandy" or 100 g of dry-soil (< 2 mm) "sandy" into a 1-liter plastic bottle with a stopper. Add 100 ml of dispersing reagent. Shake for 3 hours on an end-to-end or oscillatory shaker. Transfer the dispersed soil to a hydrometric jar. Mix with a special plunger. Makeup to the mark with distilled water. Immerse the hydrometer and read it after 45 seconds. Keep the jars undisturbed for 3 hours and take the second reading. A temperature correction factor was considered. If the temperature is greater than 20^{0}C add. If the temperature is less than 20^{0}C subtract. Subtract also the reading of the blank.

Calculation as follow (Eq: 3.21, Eq: 3.22; Eq: 3.23, & Eq: 3.24) Source: (Gee & Bauder, 1986: Gavlak et al., 2005).

$$\% \, Clay + Silt = 1^{st} \frac{R - B(\pm T) * 100}{Oven \ dry \ soil \ mass} \ldots \ldots \ldots \ldots \ldots \ldots \ldots \ldots \ldots \ldots .. \quad (3.21)$$

$$\% \, Clay = \quad 2^{\text{nd}} \frac{R - B(\pm T) * 100}{Oven \ dry \ soil \ mass} \ldots \ldots \ldots \ldots \ldots \ldots \ldots \ldots \ldots \ldots . \ldots \ldots (3.22)$$

$$\% \, Silt = (Clay + Silt) - Clay \ldots \ldots \ldots \ldots \ldots \ldots \ldots \ldots \ldots \ldots \ldots \ldots \ldots \ldots \ldots \ldots \ldots \ldots (3.23)$$

$$\% \, Sand = 100 - \% \, (Clay + Silt) \ldots \ldots \ldots \ldots \ldots \ldots \ldots \ldots .. \ldots \ldots \ldots \ldots \ldots \ldots \ldots (3.24)$$

Where: R= Hydrometric reading

B= Blank

T= Temperature

The soil organic carbon content of the analysis was determined by Walkley and Black method (Walkley & Black, 1934 ; Nelson & Sommers, 1996). Weight 1g finely ground soil sample was passed through 0.5 mm sieve without a loss was taken into 500 ml conical flask, to which add 10 ml 1 N potassium dichromate ($K_2Cr_2O_7$) solution with a pipette to both samples and blank. 20 ml conc. Sulfuric acid (H_2SO_4) was added with a measuring cylinder. The contents were shaken for a minute and allowed to stand for 30 min. Then 200 ml distilled water, add 10 ml conc. Orthophosphoric acid and just before titration, and add 0.5 ml of barium diphenylamine sulphonate indicator were added.

Titrate both samples and blanks with 0.5 N ferrous sulfate solution until the color changes to purple or blue, then add ferrous sulfate solution drop by drop until the color flashes to green then continue to a light green endpoint. The results were calculated by the following formulas (Eq: 3.25) (Walkley & Black, 1934 ; Addis & Abebaw, 2015).

$$Organic\ Carbon\ \% = Nx\left(\frac{V1-V2}{S}\right) * 0.39 * mcf \quad \text{..... (3.25)}$$

Where: N = Normality of ferrous ammonium sulfate (FAS), V1 = Volume of 0.5 N FAS required to neutralize 10 ml of 1 N $K_2Cr_2O_7$ i.e. blank reading (ml).

V2 = Volume of 0.5 N FAS needed for titration of soil sample (ml)

S = Weight of air-dry sample (g)

0.39 = 0.003 x 100% x 1.31 (0.003 is the milliequivalent weight of carbon in g)

mcf = moisture correction factor.

The K factor value was then estimated based on a formula adapted from (Williams, 1995) as follows (Eq: 3.26) in the raster calculator (Woldemariam et al., 2018; Girma & Gebre, 2020).

$$K\ RUSLE = fcsand \times fcl{-}si \times forgC \times fhisand \quad \ldots\ldots\ldots\ldots\ldots\ldots\ldots\ldots\ldots\ldots \quad (3.26)$$

Where *fcsand*, is a factor that gives low soil erodibility factors for soils with high coarse-sand contents and high values for soils with little sand,

f cl-si , is a factor that gives low soil erodibility factors for soils with high clay to silt ratios,

forgC is a factor that reduces soil erodibility for soils with high organic carbon content, and

fhisand, is a factor that reduces soil erodibility for soils with extremely high sand contents.

$$fcsand = (0.2 + 0.3 * Exp\left[-0.256 * ms * \left(1 + \frac{msilt}{100}\right)\right] \ldots\ldots\ldots\ldots\ldots\ldots\ldots\ldots \quad (3.27)$$

$$fcl - si = \left(\frac{msilt}{mc + msilt}\right)^{0.3} \ldots\ldots\ldots\ldots\ldots\ldots\ldots\ldots\ldots\ldots\ldots\ldots\ldots\ldots\ldots\ldots\ldots\ldots\ldots\ldots \quad (3.28)$$

$$\text{forgC} = \left(1 - \frac{0.256 * \text{orgC}}{\text{OrgC} + \text{Exp}[3.72 - 2.96 * \text{orgC}]}\right) \ldots\ldots\ldots\ldots\ldots\ldots\ldots\ldots\ldots\ldots\ldots \quad (3.29)$$

$$fhisand = \left(1 - \frac{0.7 * \left(1 - \frac{ms}{100}\right)}{\left(1 - \frac{ms}{100}\right) + Exp\left[5.51 + 22.9\left(1 - \frac{ms}{100}\right)\right]}\right) \ldots\ldots\ldots\ldots\ldots\ldots \quad (3.30)$$

Where ms the percent is sand content (0.05–2.00 mm diameter particles), msilt is the percent silt content (0.002- 0.05 mm diameter particles), mc is the percent clay content (< 0.002 mm diameter particles), and orgC is the percent organic carbon content of the layer (%)

Using the equation (Eq:3.26) developed by (Williams, 1995) soil erodibility factor (K-value) for each soil sample was calculated and the soil erodibility map was generated as raster data through geostatistical analysts interpolation by Ordinary 'Kriging' method. Kriging is used to estimate the value of a soil property at a location where the value is unknown by using the known values at locations about the point of interest (Carter & Gregorich, 2006).

3.7.3. Determination of LS_ Factor

Different approaches have been used to estimate the topographic (LS) factor. While field measurement and determination of slope in a complex topography is not easy, as a result, ASTER DEMs were used to compute LS factors. Hence, Digital Elevation Model (DEM) at 30 m was imported to ArcGIS and processed to obtain both slope gradient (S) and slope length (Bewket and Teferi, 2009; Wolka et al., 2015 ; Yesuph and Dagnew, 2019).

Even though lots of technique are available for the estimation of LS factor in the literature, the equations proposed by (Moore & Wilson, 1992) was adopted for this study to extract LS factor values from DEM data using map algebra expression of Arc GIS 10.8 raster calculator. The equation below (Eq: 3.31) is selected as it has been broadly used and experienced in several studies in Ethiopia circumstances (Fenta *et al.*, 2016; Yesuph and Dagnew, 2019).

$$LS = \left(\frac{\beta x}{22.13}\right)^{0.5} * \left(\frac{\sin(\theta)}{0.0896}\right)^{1.3} \ldots\ldots\ldots\ldots\ldots\ldots\ldots\ldots\ldots\ldots\ldots\ldots\ldots\ldots\ldots\ldots\ldots. (3.31)$$

Where,

β= is flow accumulation;

χ = is grid cell size (30);

22.13 is the RUSLE standard plot length;

0.5 is the exponent of slope length;

θ = is slope in degrees (i.e. Slope of DEM × 0.01745).

A step-wise procedure was followed to generate an LS factor map using the hydrology extension spatial analyst tool of the Arc GIS10.8.

3.7.4. Determination of C_ Factor

In my study area, the satellite image was classified and identified into seven land use land covers such as cultivated land, forest land, grazing land, banana land, waterbody, shrubland, and bare land. The raster map was converted to vector format to assign the corresponding C-value to assign each land-use class using the reclassified method in Arc GIS 10.8. C values as used in previous studies corresponding to the identified land covers were used see (Table 3.7).

Table 3.7 LULC classes and assigned C- values

Land Use Types	C-Values	References
Banana Land	0.089	(Angima et al., 2003)
Barren Land	1	(Yesuph & Dagnew, 2019; Girma & Gebre, 2020)
Cultivation Land	0.15	(Yesuph & Dagnew, 2019; Girma & Gebre, 2020)
Grazing Land	0.05	(Hurni,1985; (Yesuph & Dagnew, 2019); Girma & Gebre, 2020)
Forest Land	0.01	(Hurni 1985; Girma & Gebre, 2020)
Shrub Land	0.014	(Wischmeier and Smith, 1978 ;Girma & Gebre, 2020)
Water Body	0.0	(Eisenberg & Muvundja, 2020; Girma & Gebre, 2020)

3.7.5. Determination of P_ Factor

The management practices data in the watershed were gathered from Google earth, field observations. In the study area, there is only a small area that has been treated with introduced soil and water conservation through the agricultural extension programmer of the government, and these are also poorly maintained over studies of the periods. As data were lacking on records of permanent management practices and mapping of conserved areas, in study years,1987,2003, and 2020, the P-value was adopted from (Wischmeier & Smith, 1978). It was implemented in Ethiopia by different scholars (Bewket & Teferi, 2009; Gelagay & Minale, 2016; Yesuph & Dagnew, 2019; Girma & Gebre, 2020 ;Gezahegn & Harka,2020).

The slope of the area was associated with the LULC class as management activities are highly dependent on the slope of the area. The identified LULC and slope in percent of the study area has been reclassified based on the desired range of the P-values suggested by (Wischmeier & Smith, 1978). The range of P-value is from 0 to1 and the lower value indicates relatively better soil erosion control measures. The LULC was grouped into cultivated land and other land uses. The category under "other land uses" was given the P-value of 1 regardless of their slope class whereas the cultivated land was classified into six slope classes.

Spatial analyst Boolean-And operation was implemented on the reclassified cell values of the two-input raster (LULC and slope) in Arc Map. Then the outputted LULC and slope combinate raster was used to assign the corresponding p values (Table 3.8) with the help of the Arc Map editor tool and the P factor value raster map was produced (Girma & Gebre, 2020).

Table 3.8 LULC and slope classes with assigned P-values

Land-use type	Slope classes in percent (%)	P –factor
Agricultural land	0-5	0.1
	5-10	0.12
	10-20	0.14
	20-30	0.19
	30-50	0.25
	>50	0.33
Other land use	All	1

Source: Adapted from (Wischmeier & Smith, 1978).

3.7.6. Estimation of Soil Loss Using RUSLE Model

The factors of the RUSLE model were transformed into a raster format and the same coordinate system (UTM-WGS 1984-37^0 North) with a pixel size of 30×30m. Then, all layers were multiplied together using a Raster Calculator-Map Algebra-Spatial Analyst Tools–Arc Toolbox in Arc GIS 10.8. Hence, a total annual soil loss rate & mean annual soil loss was estimated for each pixel for 1987, 2003, 2020, and 2050 under both scenarios.

The estimated total soil loss map for the years 1987, 2003, and 2020 in a raster format was used to extract mean annual & total annual soil loss from different land use/land cover categories and slope classes for each year. In this procedure, Zonal Statistics-Spatial Analyst Tools–Arc Toolbox in Arc GIS was used to compute soil erosion statistics based on different land use/landcover categories, slope classes, and sub-watershed levels in Sile River watershed.

3.8 Research Conceptual Framework

The overall methodological conceptual framework for historical and future land use land change, future climate change, and its impact on soil erosion for baseline or current condition and future projection was designed.

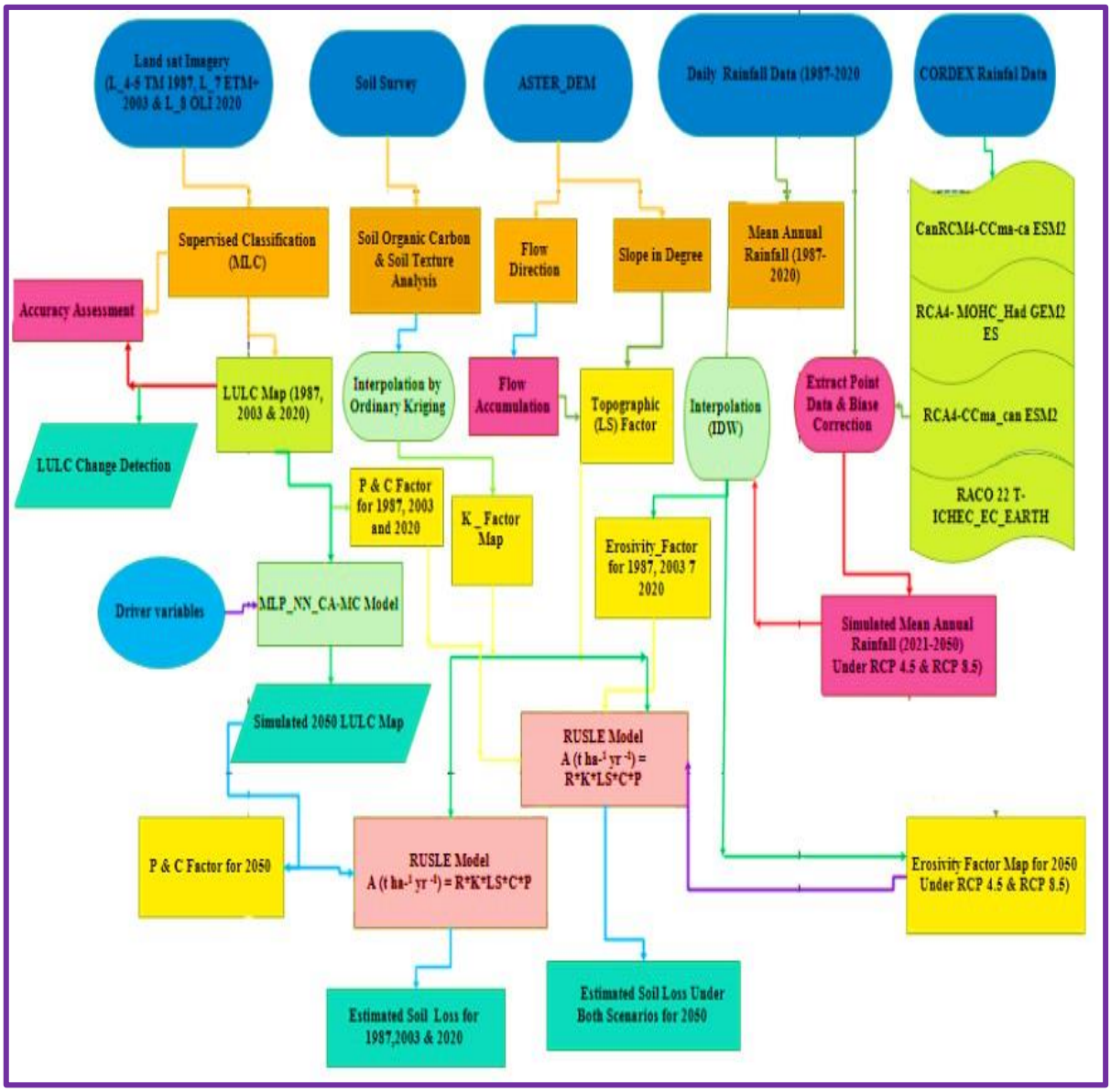

Figure 3.9 Conceptual framework flow chart for the overall study in Sile watershed

4. RESULT AND DISCUSSION

4.1 Historical Change in LULC

4.1.1 Accuracy Assessment

Before land use land cover change detection and investigation of its impact on soil erosion of the study watershed, the accuracy assessment was done for each classified image. For the seven classified LULC categories of the years 1987, 2003, and 2020 accuracy assessment was done. The diagonal values down an error matrix show reference samples that are correctly classified and off-diagonal entries are the misclassified references that correspond to individ ual LULC classes. Based on the stratified random sampling method an overall classification accuracy of 96.03%, 96.49%, and 95.73, with a kappa coefficient of 0.81, 0.80, and 0.94 were obtained for the years 1987, 2003, and 2020 respectively.

A land sat image Thematic Mapper of 1987was classified to pre-defined land-use types, then the accuracy assessment of the classified image was performed. Table 4.1: indicates the detail of the confusion matrix of 1987 and the result of accuracy assessments. The overall accuracy of 96.03% and Kappa statistics of 0.81 were achieved for the 1987 LULC map. The founded result indicated that the classification was almost perfect according to (Rwanga & Ndambuki, 2017) kappa statistics recommended range.

Table 4.1 Accuracy assessment table for the LULC map of 1987

Classified Data	Reference Data for LULC of 1987								
		WB	CL	FL	GL	BC	BL	SL	TU	UA (%)
	WB	11	0	0	0	0	0	0	11	100.00
	CL	0	165	0	3	2	2	1	173	95.38
	FL	0	0	33	0	0	0	3	36	91.67
	GL	0	3	0	38	0	0	1	42	90.48
	BC	0	0	0	0	51	0	0	51	100.00
	BL	0	0	0	1	0	89	0	90	98.89

	SL	0	1	3	0		0	97	101	96.04
	TP	11	169	36	42	53	91	102	504	OA= 96.03
	PA (%)	100	97.6	91.7	90.5	96.2	97	95	K= 0.81	

Where, WB = Water Body, CL = Cultivation Land, FL = Forest Land, GL = Grazing Land, BC = Banana Cover, BL = Bare Land, SL = Shrub Land, PA= Producers Accuracy, TU = Total users, UA = Users accuracy, OA= Overall accuracy, K, = Kappa statistics

The accuracy assessment of the 2003 land use/land cover map was performed by taking a total of 485 reference points from a Google Earth. The reference points taken concerning the LULC classes were, 12, 148, 30, 45, 67, 99, and 84 points were allocated for a water body, cultivation land, forest land, grazing land, banana land cover, bare land, and shrubland respectively to prepare confusion matrix. The accuracy assessment result shows that overall accuracy is 96.49% and Kappa statistics of 0.90 (Table 4.2). The results indicated that the classification was almost perfect according to (Rwanga & Ndambuki, 2017) kappa statistics recommended range.

Table 4.2 Accuracy assessment tables for LULC map of 2003

		Reference Data for LULC of 2003								
		WB	CL	FL	GL	BC	BL	SL	TU	UA (%)
Classified Data	WB	12	0	0	0	0	0	0	12	100
	CL	0	146	2	0	2	0	0	150	97.33
	FL	0	0	28	0	0	0	3	31	90.32
	GL	0	0	0	42	0	4	0	46	91.30
	BC	0	2	0	0	65	0	0	67	97.01
	BL	0	0	0	1	0	94	0	95	98.95
	SL	0	0	0	2	0	1	81	84	96.43
	TP	12	148	30	45	67	99	84	485	OA= 96.49
	PA (%)	100	98.6	93.3	93.3	97.0	94.9	96.4	K= 0.90	

Where, WB = Water Body, CL = Cultivation Land, FL = Forest Land, GL = Grazing Land, BC = Banana Cover, BL = Bare Land, SL = Shrub Land, PA= Producers Accuracy, TU = Total users, UA = Users accuracy, OA= Overall accuracy, K= Kappa statistics

Once the classification of Operational Land Imager/Thermal Infrared of 2020, the accuracy assessment was done to check whether the classified map was accurately classified or not. The accuracy of the 2020 classified map was done by taking a total of 281 reference points from the field using GPS. From the total collected reference, 5, 123, 13, 27, 19, 42, and 53 points were collected for the water body, cultivated land, forest land, grazing land, banana land, bare land, and shrubland respectively.

The results of user's accuracy in this study revealed (Table 4.3) that in 2020 the maximum class accuracy was achieved for the l forest land, grazing land, and banana land cover while the minimum was obtained for water body class as the result presented in the table 4.3below indicated. The overall accuracy and kappa statistics of the 2020 land use/land cover were 95.73 %, 0.94 respectively. The results of the classification were almost perfect the study is also consistent with some other studies conducted by the authors (WoldeYohannes et al., 2018) in Abaya Chamo Basin, (Leta et al., 2021) in Nashe Watershed, Upper Blue Nile Basin, Ethiopia, and (Girma et al., 2022) in Gidabo river basin, main Ethiopian rift.

Table 4.3 Accuracy assessment table for the LULC map of 2020

		Reference Data for LULC of 2020								
		WB	CL	FL	GL	BC	BL	SL	TU	UA (%)
Classified Data	WB	4	0	0	0	0	1	0	5	80
	CL	0	123	0	1	1	3	3	131	93.89
	FL	0	0	13	0	0	0	0	13	100
	GL	0	0	0	26	0	0	0	26	100
	BC	0	0	0	0	18	0	0	18	100
	BL	0	0	0	0	0	38	3	41	92.68
	SL	0	0	0	0	0	0	47	47	100
	TP	4	123	13	27	19	42	53	281	OA=95.73
	PA (%)	100	100	100	96.29	94.74	90.48	88.68	K= 0.94	

Where, WB = Water Body, CL = Cultivation Land, FL = Forest Land, GL = Grazing Land, BC = Banana Cover, BL = Bare Land, SL = Shrub Land, PA= Producers Accuracy, TU = Total users, UA = Users accuracy, OA= Overall accuracy, K= Kappa statistics.

4.1.2 Land Use/Land Cover Change Detection

Monitoring of historical land use and land cover changes in the study area was done at 2 temporal intervals: 1987 to 2003, and 2003 to 2020. The results of the post-classification comparison give an account of the quantity and type of change that has taken place for each LULC category.

In 1987, the dominant land cover type was shrubland followed by cultivation land and grazing land. In the Sile River Watershed, the spatial distribution of LULC has been observed mainly the highland and midland part of the watershed was covered with forest, shrubland grazing, and cultivation land (Figure 4.1). However, the banana land use cover was adopted only on the lower part of the outlet part of the watershed near Lake Chamo shore.

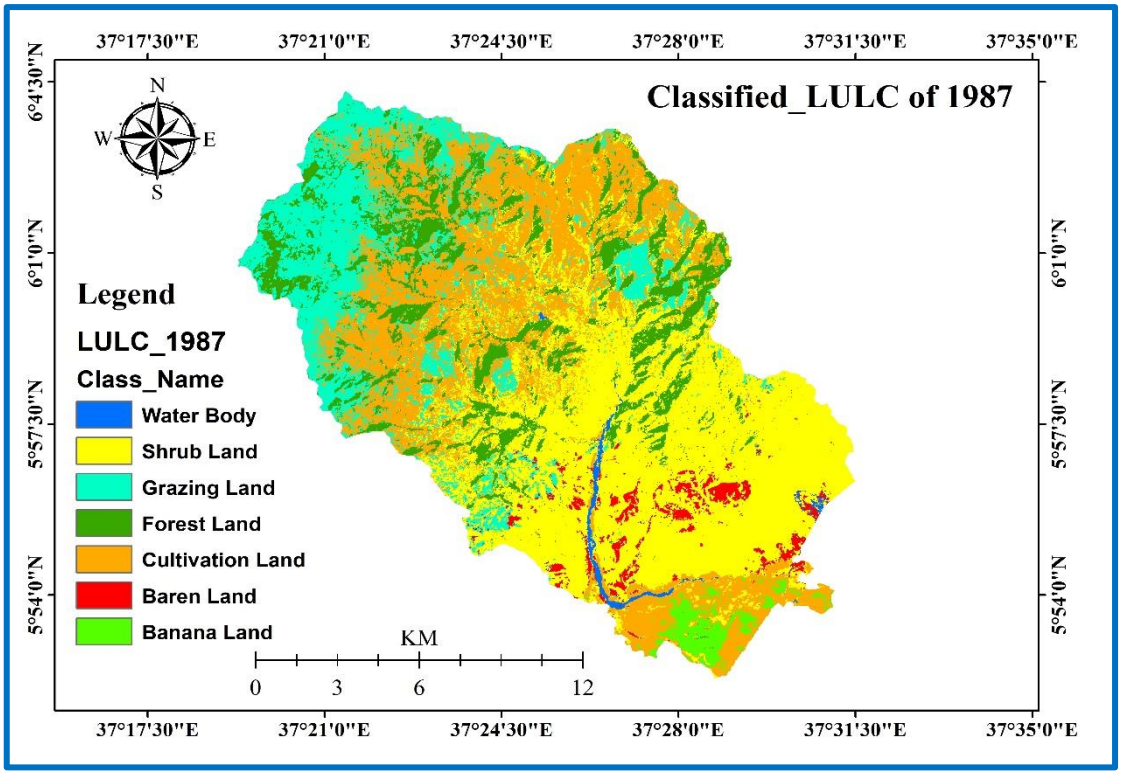

Figure 4.1 LULC map of 1987 in Sile watershed

The land use land cover types of 2003 in the study area were founded as similar to 1987 however; their coverage areas were changed within 16-year temporal variation. In 2003, cultivation land became a major LULC class followed by shrubland and l forest land Fig 4.2.

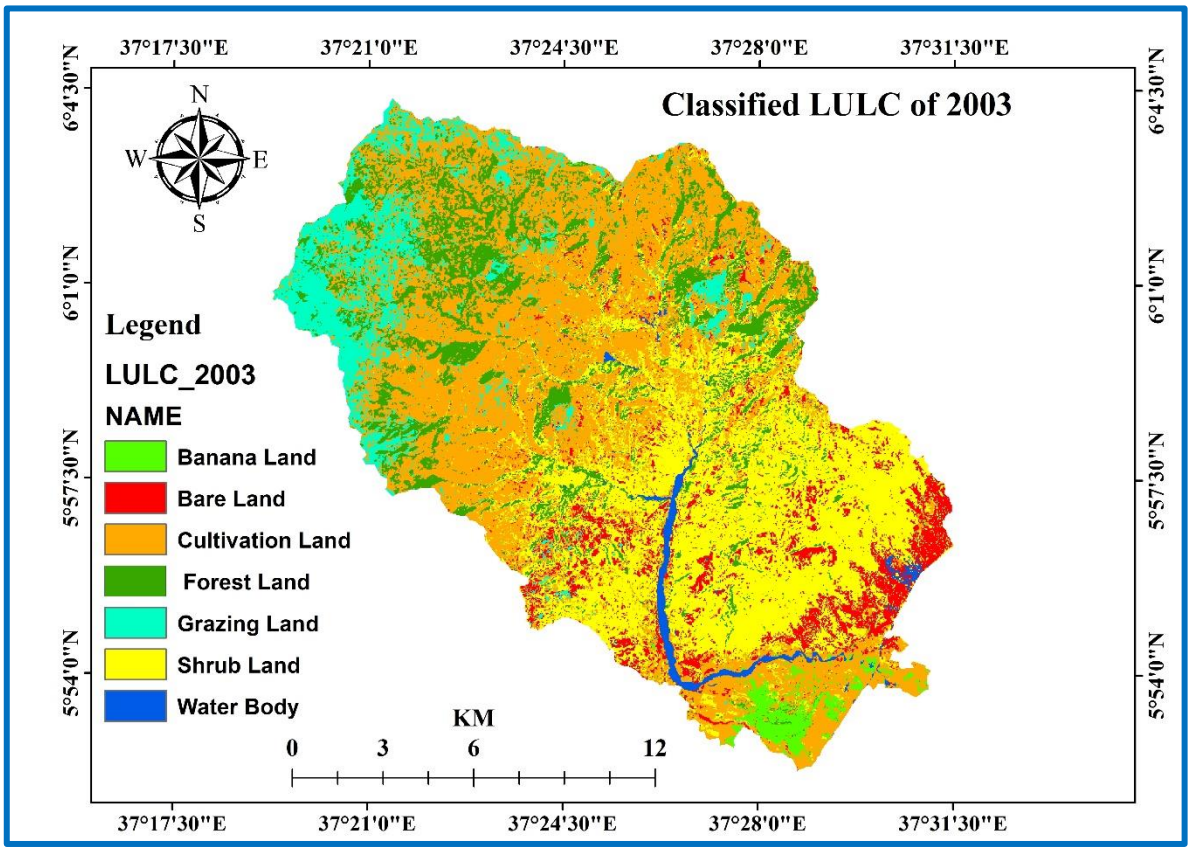

Figure 4.2 LULC map of 2003 in Sile watershed

As shown in Fig 4.3, the dominant land use class in 2020 was also cultivation land followed by shrubland. Bare land was significantly expanding in the middle part of the watershed while the banana land cover was also increased in the lower part of the watershed.

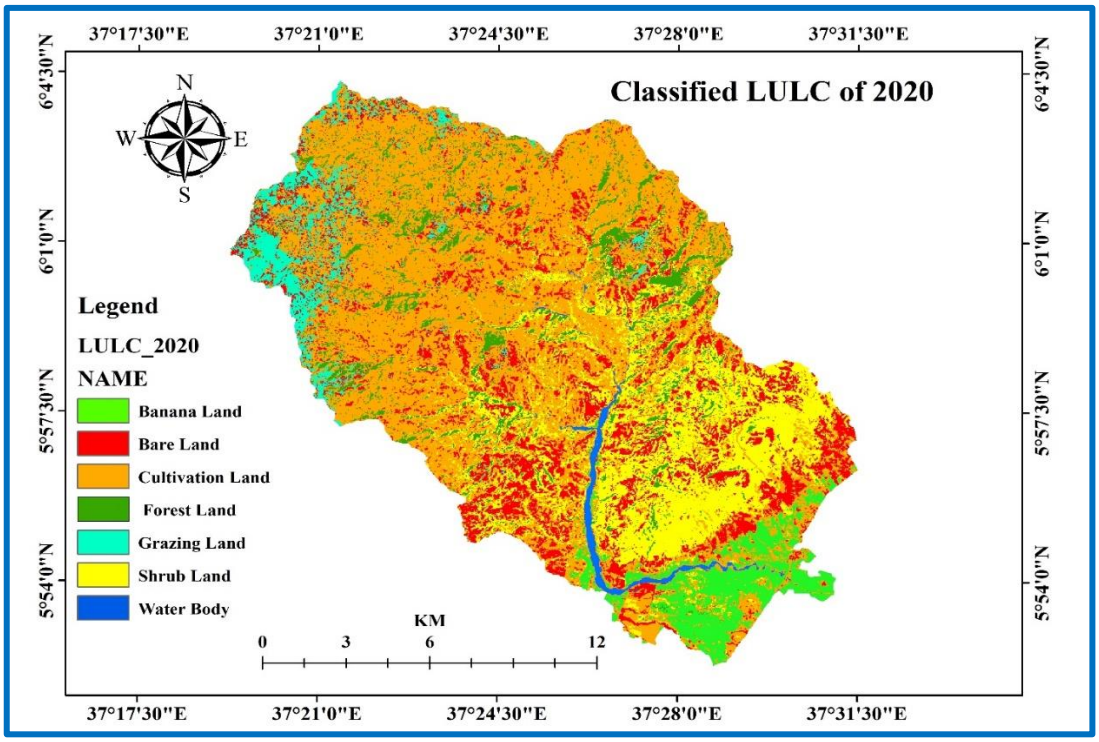

Figure 4.3 LULC map of 2020 in Sile watershed

4.1.3 LULC Change between 1987 and 2003

LULC changes between the period 1987 to 2003 are shown in Table; 4.4. In 1987 banana land cover in Sile watershed was 483 ha (2%) however, after 16 years of temporal variation the area was increased to 863 ha (3%). According to (Yirgu, 2018), in Abaya-Chamo Basin, before three to four decades small-scale traditional agriculture (mainly cotton, sweet potatoes, and sorghum) and fishery are the dominant livelihood sources. However, with the increased demands for fruit products at the national market the cereal-based subsistence farming system was transformed into a market-oriented system of irrigated banana farms and it increased by 0.21 % annually.

In the period between 1987-2003, a dramatic and significant LULC change was observed in the expansion of cultivation land from 8,375 ha to 10,465 ha (a change of 2,090 ha -25 %). On the other hand, bare land increased from 628 ha to 1,910 ha (a change of 1,282 ha -204%). On the contrary, shrubland, declined from (10,374 ha) to (8,861 ha) (a reduction of

1,513 ha- 15%), grazing land reduced from 3,795 ha to 2, 3445 ha (a decrease by 1451 ha -38 %), forest land decreased from 3,655 ha to 2,910 ha (a reduction of 746 ha- 20%) and water body was reduced from 298 ha to 257 ha or (41 ha -14% reduction) was recorded respectively.

According to (WoldeYohannes et al., 2018), during the period 1985 to 1995 in Abaya Chamo sub basin expansion of arable land, at the expense of natural grassland and shrubland was related to severe drought and famine-affected the country, and nationwide planned resettlement and villagization programs. In a study conducted by (Girma et al., 2022), in 1985 the dominant land cover type was shrubland (24.3%) followed by forest (21.8%) and agriculture (19.8%). However, in the subsequent years, 2003 agricultural land has undergone a significant expansion and overturned the dominancy by 25%. In Gumara watershed of Lake Tana basin, Northwestern Ethiopia expansion of cultivated and settlement land by 21.99 %, while forest land, shrubland, grassland, and wetland declined by 85.30, 91.39, 76.15, and 72.54 % respectively from the period of 1957 to 2005 was reported (Wubie et al., 2016).

In the last 16 years from 1987-2003 annually; bare land, cultivation land, and banana land cover, were expanded (80 ha -13 %), (131 ha -2%), and (24 ha -5 %) respectively. Whereas; grazing land, forest land, shrubland, and water body were annually declined by (91 ha -2 %), (47 ha -1 %), (95 ha -1%) and (3 ha -1%) respectively. In Abaya Chamo sub-basin barren soil and farmland had been augmented within two decades and the annual rate of change was 0.08% and 0.45% but grass and shrubland, and the woodland area have been declined by an annual rate of change of 0.48% and 0.10% respectively. Therefore, due to the expansion of cultivation and bare land and reduction of shrubland, forest land, and grazing land the sub-

basin lakes are ecological under stress by sediment yield, surface runoff, and groundwater extraction (AyeleElias et al., 2019).

A decline of shrubland, grazing land, and forest land, in those periods, was maybe related to deforestation and overgrazing which lead to an enhancement and expansion to bare land, banana land, and cultivation land. From multiple combinations of proximate and underlying driving factors of LULC change at global, regional, and local level deforestation for fuelwood or expansion of agriculture and overgrazing are the major ones and they are a vicious circle to land degradation and reduction of agricultural productivity (Gessesse & Bewket, 2014; AyeleElias et al., 2019 ; Regasa, 2021).

Table 4.4 LULC change trend between 1987 to 203

LULC Class	1987		2003		Change between 1987-2003			
	Area (ha)	%	Area (ha)	%	(ha)	(%)	Annual change	
							Ha	%
Water Body	298	1	257	1	-41	-14	-3	-1
Cultivation Land	8375	30	10465	38	2090	25	131	2
Baren Land	628	2	1910	7	1282	204	80	13
Banana Land	483	2	863	3	380	79	24	5
Shrub Land	10374	38	8861	32	-1513	-15	-95	-1
Grazing Land	3795	14	2345	8	-1451	-38	-91	-2
Forest Land	3655	13	2910	11	-746	-20	-47	-1
Total	27,610	100	27,610	100				

4.1.3. LULC Change between 2003 and 2020

Similar to the period between 1987 between 2003 Sile watershed had also experienced a significant spatiotemporal variation of LULC change over the past 17 years between 2003 and 2020. As shown in Table 4.5 bare land 116 % (2,223 ha change) banana land cover 46 % (394 ha change) and cultivation land 22 % (2,328 ha change) were increased as the expense of forest land 55%, (1615 ha reduction), grazing land 41%, (959 ha reduction),

shrubland 26%, (2322 ha reduction) and water body 19%, (49 ha of decline) for the 17 years in the study area.

The study also revealed that a period between 2003- 2020 the annual change of cultivation land 1 %, per year (137 ha increased), bare land 7% per year (131 ha increased), and banana land cover 3%, per year (23 ha increased) Table 4.5. In contrast, the annual reduction was from, shrubland 2 %, per year (137 ha decline), forest land 3% per year (96 ha reduction), grazing land 2%, per year (56 ha reduction), and water body 1%, per year (3 ha reduction) were observed.

A relatively large area of shrubland and forest was removed so, cultivation and bare land were expanded in the Sile watershed during the second period between 2003 and 2020. In the period between 1995 to 2010 west and south of Lake Chamo and Lake Abaya, the decline of shrubland was primarily due to agricultural expansion in the area, shrubland located near urban areas, and main roads were reduced due to increasing demand for wood for fuel and construction by city dwellers. The other reason may correspond to regime change, political transformation in the country, and the absence of a clear land tenure system during regime change which created free access to land located in the warm semi-arid lowlands of the basin (WoldeYohannes et al., 2018).

In Gidabo river basin, a continuous yearly deforestation of (2.4% per year) with the expense of agroforestry (1.71% per year) and agricultural land (3.23% per year) expansion by the year 2021 were reported. In addition, the annual decline in the grass (2.4%) and shrubland (2%) has been noticed for the period 1985 to 2021 (Girma et al., 2022). According to (Dibaba et al., 2020), between 1987 and 2017 agricultural land increased while rangeland, grazing lands, and swampy area decreased in Finchaa Catchment, Northwestern Ethiopia was reported.

In the early 1980s banana plantation was first time introduced to a study area during the regime of Derg in Arbaminch state farm. A frequent trial was held to introduce a banana crop to the nearby Arbaminch area, however, that effort was not successful at that time since banana was not perceived as a vital cash crop as well as a nutritional crop (Alemu, 2017). Gradually, due to the government pressure and awareness creation by agricultural development agents, the farmers in the study area were adopted this new farming system. Currently, the farmers in Sile watershed are highly fascinated with the banana farm by its profitable advantage and a household with a banana farm of more than one hectare is considered to be a "rich "household (Yirgu, 2018). The LULC change detected in the period between 1995 to 2010 confirmed the emergence of new market opportunities for cash crops like banana and cotton played the role for LULC changes. The expansion of banana and cotton production by both small-scale farmers and commercial farms was one of the main causes for the reduction of shrubland cover in Arba Minch Zuria and Mirab Abaya. In addition, a more recent expansion of infrastructure and irrigation facilities in the basin also contributed to LULC changes (WoldeYohannes et al., 2018). Hence, the result of this study is consistent with previous study findings.

The data illustrate that in Table 4.4 and Table 4.5 in both study periods (1987 to 2003) and (2003 to 2020 there was a spatiotemporal change in LULC in Sile River watershed which has undergone and experienced LULC changes in the last three decades. During the last three decades, Sile River watershed was changed from forestland, shrubland, and grazing land to cultivation land, banana land cover, and bare land. In Ethiopia, the research for the most studied basins indicated that cultivation land and bare land were increased during the last decades in a dramatic manner, while the area covered by forest, grazing land, and

shrubland decreased (Belihu et al., 2020; Dibaba et al., 2020; Regasa, 2021; Girma et al., 2022). Agricultural expansion associated with population growth, migration, shifts in government policy, and regime change is one of the major driving factors behind LULC changes in the Abaya-Chamo sub-basin and other parts of the country (Gessesse & Bewket, 2014; Genet, 2020; Dibaba et al., 2020 ; WoldeYohannes et al., 2018 ;Regasa, 2021) This study also revealed that from 1987 to 2003 and from the period of 2003 to 2020 for 33-year temporal variation, bare land, cultivation land, and banana land cover, were expanded at the expense of another land cover; shrubland, forest, grazing land, and water body were declined.

Table 4.5 LULC change between 2003 to 2020

LULC Category	2003		2020		Change between 2003-2020		Annual change	
	Area (ha)	%	Area (ha)	%	Ha	%	Ha	%
Water body	257	1	208	1	-49	-19	-3	-1
Cultivation Land	10465	38	12793	46	2328	22	137	1
Barren Land	1910	7	4133	15	2223	116	131	7
Banana Cover	863	3	1257	5	394	46	23	3
Shrub Land	8861	32	6539	24	-2322	-26	-137	-2
Grazing Land	2345	8	1386	5	-959	-41	-56	-2
Forest Land	2910	11	1295	5	-1615	-55	-95	-3
Total	27,610	100	27,610	100				

Using a Land change modeler (LCM) a loss, gain, and net change of the land use/land covers in each period (1987 to 2003 and 2003 to 2020 were analyzed. The result shows that (Fig. 4.4, 4.5 & 4.6) bare land, cultivation, and banana were gained, while shrubland, grazing, forest land, and water body were lost throughout the investigation period in the study area.

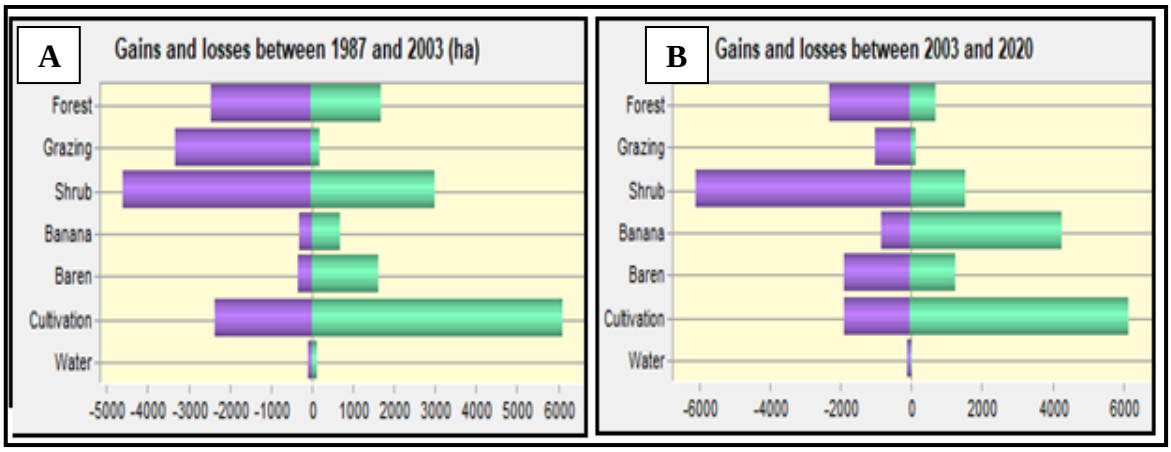

Figure 4.4 Gains and losses graph between 1987 to 2003 (A) and between 2003 to 2020 (B)

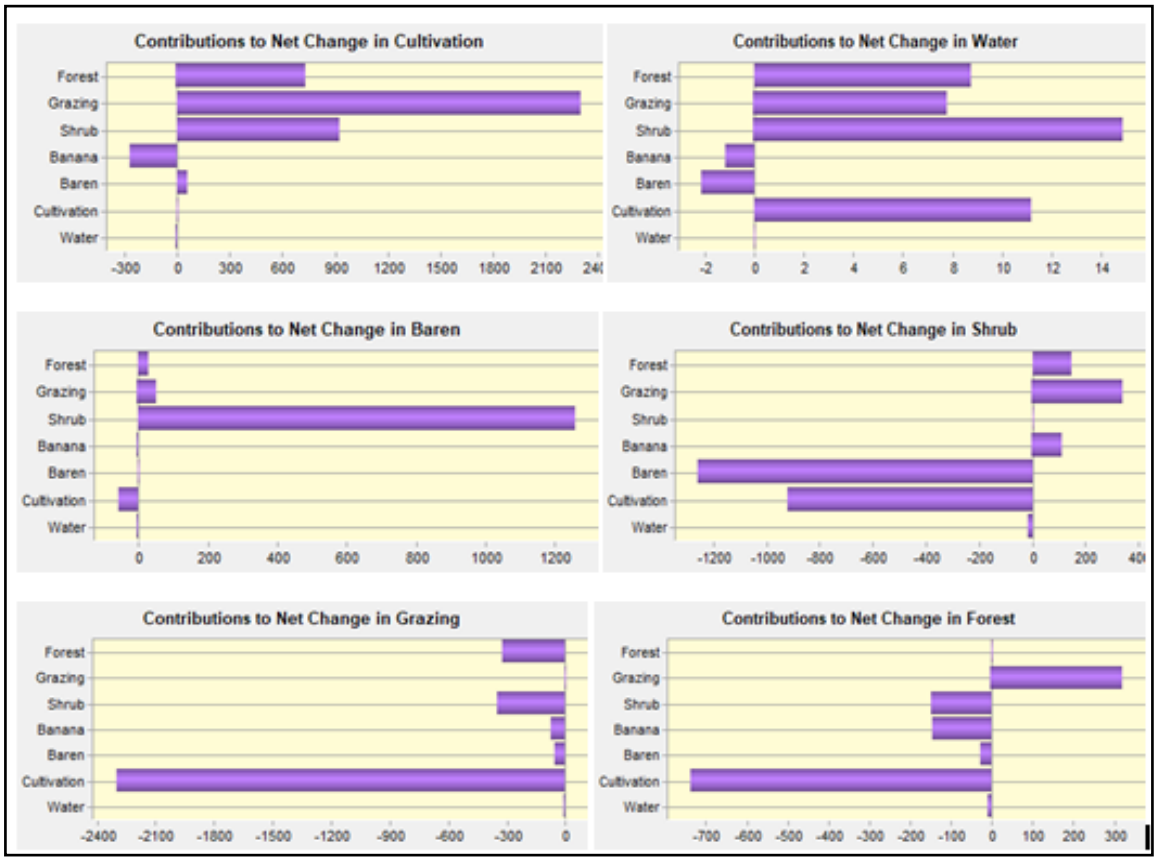

Figure 4.5 Contributions to net change LULC category between 1987 to 2003

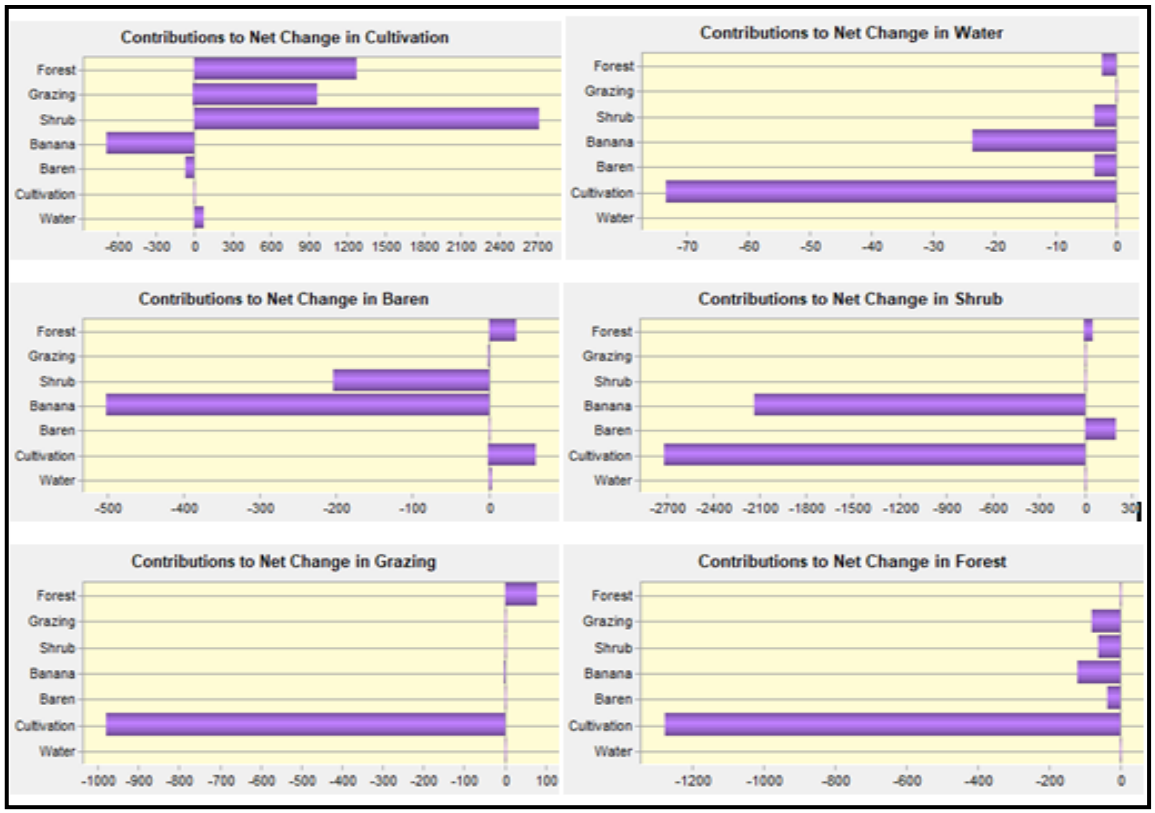

Figure 4.6 Contributions to net Change LULC category between 2003 to 2020

4.2 Prediction of the Future LULCC with MLP NN-CA- MC Model

4.2.1 Driver Variables Used in MLP NN CA_MC Model

All the driver variable data sets were prepared by ArcGIS and used as input to generate the potential transition map in (LCM) function of TerrSet software. The significance of driver variables was tested using Cramer's V and P values which are used to determine whether to consider or not a particular variable as a driving factor of LULC change (Moges et al., 2020; Leta et al., 2021). In this study, the total Cramer's V value was greater than 0.15 (Appendix Table: 4). Therefore, according to the suggestion (Leta et al., 2021), all the considered driver variables are useful to predict the future 2050 LULC change. The key driver variables (Var.) considered in this study were listed below (Fig 4:7, Fig 4.8, Fig 4:9).

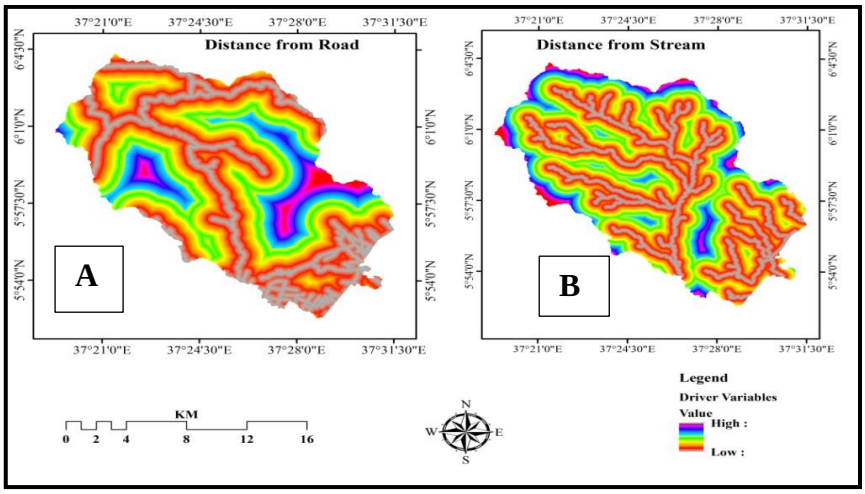

Figure 4.7 Distance from the road (A) & distance from stream (B) maps

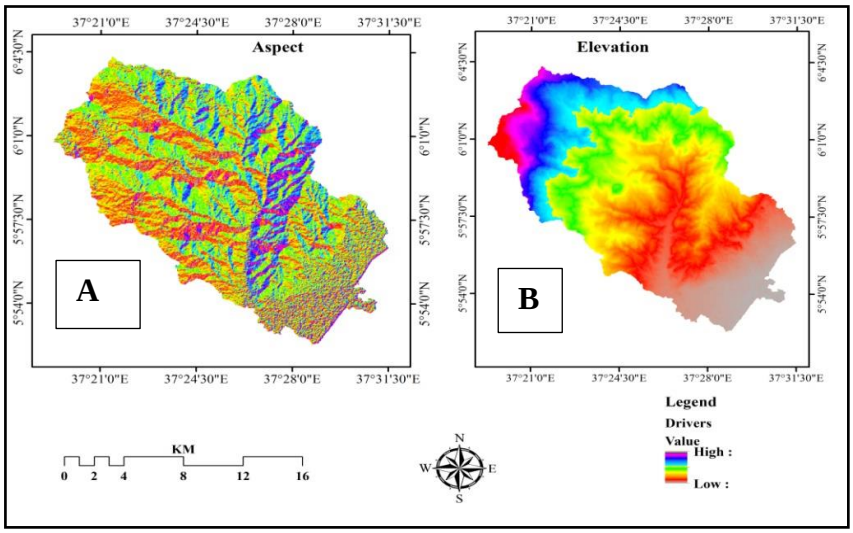

Figure 4.8 Aspect (A) & and elevation (B) maps

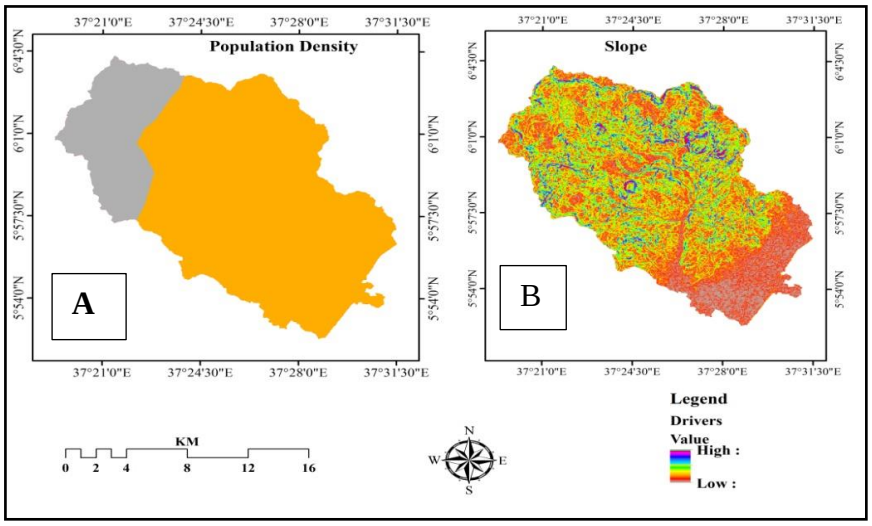

Figure 4.9 Population density (A) & Slope (B) maps

4.2.2 MLP_NN Model Performance Evaluation and Sensitivity Analysis

According to (Table:4.6) the input layer neuron had six nodes called driver variables; three nodes were created in the hidden layer and two nodes were related in the output layer. The MLP-NN skill measure of driver variable influence was statistically tested using 10,000 iterations, and 3,954 requested samples per class. The training RMS and Testing RMS were (0.3649 and 0.3787) respectively was observed. The overall (with all variables) skill (0.73) and accuracy (86.47%) of the model is well beyond the acceptable limit and the driver forces assist the model to project future LULC change more accurately (Gharaibeh et al., 2020; Girma et al., 2022).

Table 4.6 Parameters and performance

Input layer neurons	6
Hidden layer neurons	3
Output layer neurons	2
Requested samples per class	3954
Final learning rate	0.0001
Momentum factor	0.5
Sigmoid constant	1
Acceptable RMS	0.01
Iterations	10000
Training RMS	0.3649
Testing RMS	0.3787
Accuracy rate	86.47%
Skill measure	0.7294

The result in (Table:4.7), revealed that Var 6 (Elevation) constant is the most influential parameter which generates poor model accuracy (49%) and with the least skill measure of 0.0532. While Var.3 (Distance from the road) constant has determined less impact and it was measured as the least influential parameter.

Table 4.7 Forcing a single independent variable to be constant

Model	Accuracy (%)	Skill measure	Influence order
With all variables	86.47	0.7294	N/A
Var. 1 constant	86.47	0.7294	4
Var. 2 constant	86.47	0.7294	5
Var. 3 constant	86.72	0.7344	6 (least influential)
Var. 4 constant	86.47	0.7294	3
Var. 5 constant	86.47	0.7294	2
Var. 6 constant	49.97	0. 0542	1 (most influential)

Where Var. 1 is the distance from the stream; Var. 2 Aspect; Var. 3 is the distance from the road; Var. 4 is Population density; Var. 5 is the slope, and Var. 6 is Elevation.

4.2.3 Validation of Future LULCC Prediction

Validations through different kappa statistics have been done. The Kappa statistics show that Kno (0.8449), Klocation (0.8471), KlocationStrata (0.8471), and Kstandard (0.8105) respectively. A kappa statistic of 0% indicates no agreement between land cover maps and their probability, while 100% indicates a perfect agreement (Leta et al., 2021). The values of each kappa statics were above 80%, which indicates the better performance of the model in simulating future LULC (Koko et al., 2020; Leta et al., 2021). The results indicated in (Table: 4.8 & Fig: 4.10) good kappa index values, verifying the model's efficiency for future land cover simulations

Table 4.8 Result of validation index for 2020 simulated Vs actual images

Kappa index	Value	Value (%)
Kno	0.8449	84.49
Klocation	0.8471	84.71
KlocationStrata	0.8471	84.71
Kstandard	0.8105	81.05

The values of Agreement Chance, Agreement Quantity, Agreement GridCell, Disagreement Grid Cell, and Disagreement Quantity in (Table:4.9 & Fig 4:10) provide statistical agreement information between the simulated map and the reference map. The disagreement between the two maps is low and this is primarily owing to quantity errors (0.0310) rather than allocation errors (0.1048). Thus, in the study area, the model has a higher ability to forecast the LULC changes in location than in quantity (Leta et al., 2021). This shows the good capacity of the model in simulating future LULC states and an accurate specification of location

Table 4.9 The validation result analysis (agreement/disagreement) values

Agreement/disagreement	Value	Value (%)
Agreement Chance	0.1250	12.5
Agreement Quantity	0.1586	15.86
Agreement Grid cell	0.5806	58.06
Disagree Grid cell	0.1048	10.48
Disagree Quantity	0.0310	3.1

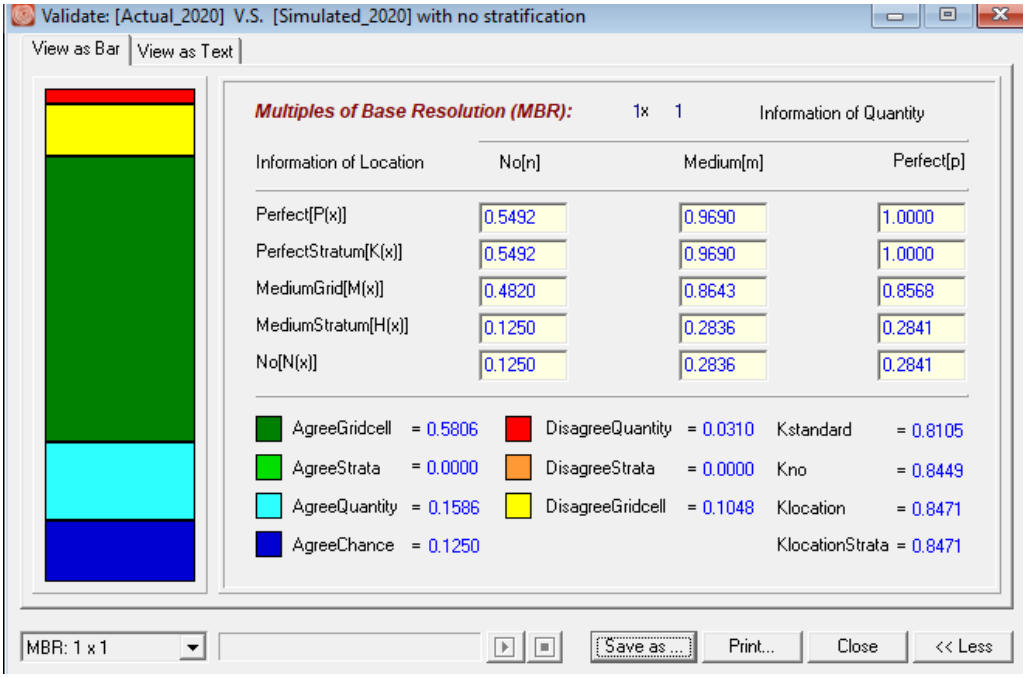

Figure 4.10 Successes and errors of the prediction

Table 4.10 Validation of LULCC prediction

LULC Category	Actual LULC_2020		Projected LULC_2020	
	Area (Ha)	Area (%)	Area (Ha)	Area (%)
Water Body	208	1	282	1
Cultivation Land	12,793	46	11,993	43
Barren Land	4,133	15	3,576	13
Banana Cover	1,257	5	1,183	4
Shrub Land	6,539	24	7,705	28
Grazing Land	1,386	5	1,165	4
Forest Land	1,295	5	1,706	6
Total	27,610	100	27,610	100

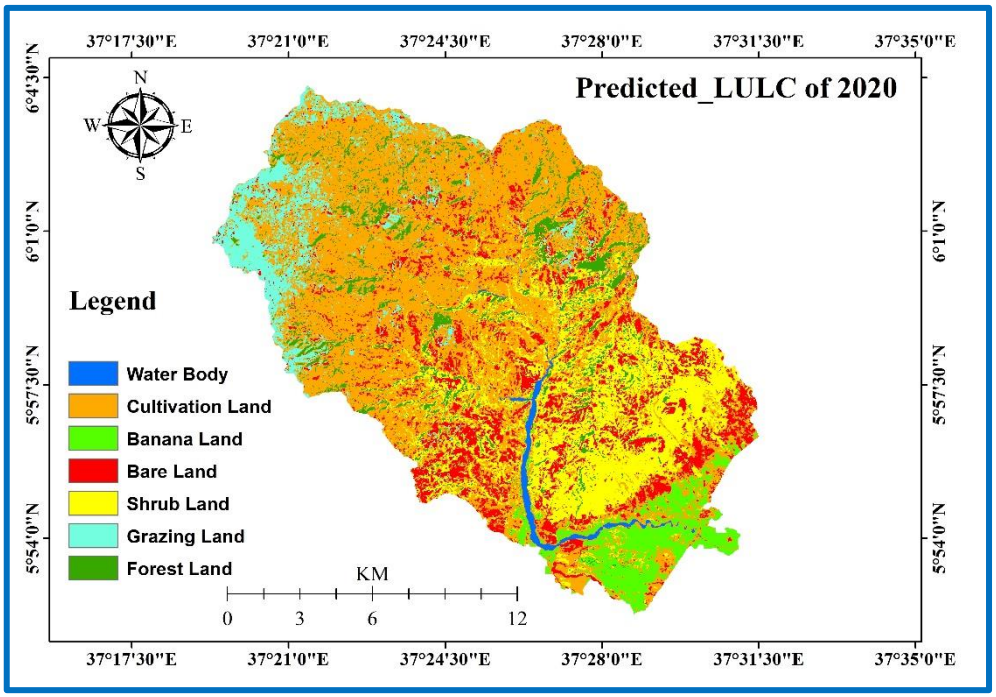

Figure 4.11 Predicted LULC of 2020

4.2.4 Predicted Future LULC Change

The future probable changes in LULC for 2050 with business as usual scenarios were analyzed. The substantial change was expected from the change analysis result in LULC change between 2020 and 2050. As shown in the (Table:4.11 and Fig:4.12) below cultivation land, barren land, and, the banana cover was increased from 12,793 ha to 14,562 ha (a change of 1,769 ha -14%), 4,133 ha to 4,791 ha (a change of 658 ha-16 %) and 1,257 ha to 1,631 (a change of 629 ha- 50 %) will be expected on the year 2050 respectively. However, shrubland, forest land, and grazing land were declined from 6,539 ha to 4,711 ha (a reduction of 1,953 ha-30%), 1,295 ha to 728 ha (a decline of 697 ha-54%), and 1,386 ha to 990 ha (a reduction of 397 ha-29%) on the period of 2020 to 2050 will be predicted respectively. In addition, the projected yearly rate of change from cultivation land, barren land, and banana land were 59 ha, 22 ha, 21 expansion while, in shrubland, grazing land, and forest 65 ha, 13, and 23 ha

decline will be expected correspondingly. The result shows land-use change trend from historical to future was probable to continue in the future.

According to (Girma et al., 2022) in Gidabo river basin, the main Ethiopian rift, a continuous expansion of agricultural land by 55%, and a water body of 2.5% will be predicted in 2050. Though, grassland 3%, forest 2.6%, and shrubland 2.8% will decrease radically while barren land will show a positive growth till 2035 by 6.82% and decreased by 2050. The historical land use land cover change analysis in Ethiopia indicates that Ethiopian lands were changed from forest land, grazing land, shrubland to bare land and agricultural land covers (Regasa, 2021). This trend of modification will also be expected for the coming 30 years (2050). However, if the different natural resource management and intervention activities like afforestation or reforestation are conducted by the government (i.e. Green Legacy Initiatives) or by other stakeholders the alteration will not be continued as predicted.

Table 4.11 Expected change of future LULC (2050) study area

LULC Category	LULC_2020		LULC_2050		Change (2020-2050)		Annual change	
	Area (ha)	%	Area (ha)	(%)	Area (ha)	%	Area	%
Water Body	208	1	198	1	-10	-5	-0.35	-0.17
Cultivation	12,793	46	14,562	53	1,769	14	59	0.46
Barren Land	4,133	15	4,791	17	658	16	22	0.53
Banana Land	1,257	5	1,631	6	629	50	21	1.67
Shrub Land	6,539	24	4,711	17	-1,953	-30	-65	-1.00
Grazing Land	1,386	5	990	4	-397	-29	-13	-0.95
Forest Land	1,295	5	728	3	-697	-54	-23	-1.79
Total	27,610		27,610					

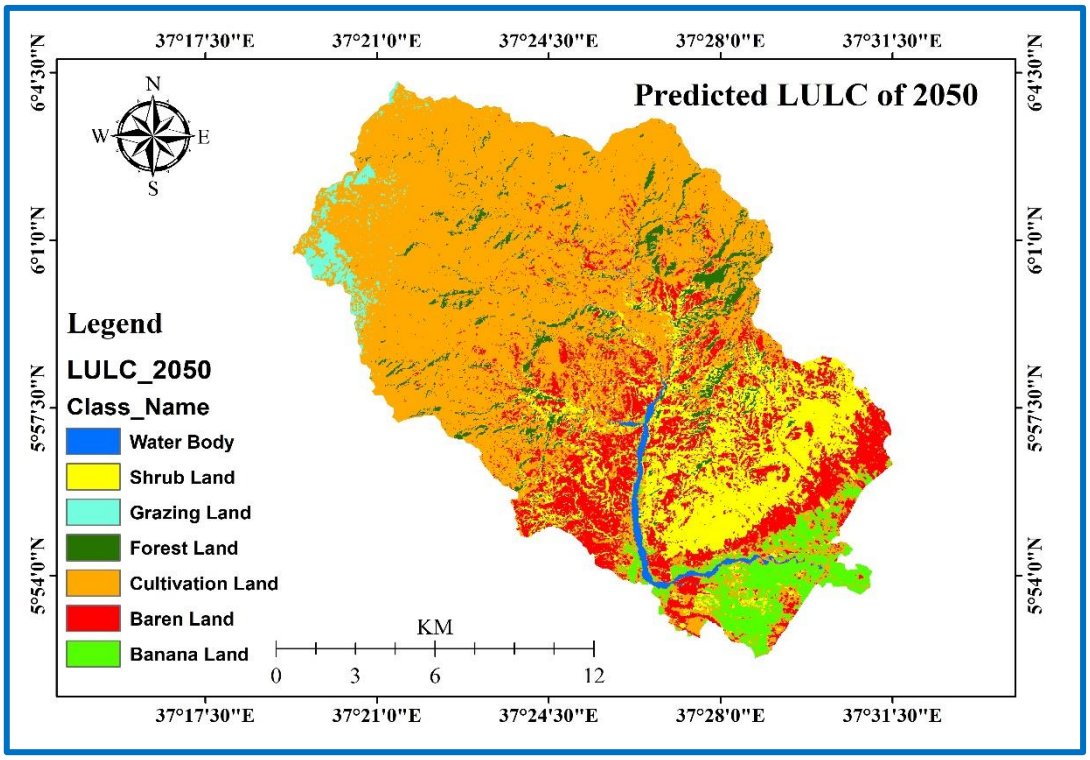

Figure 4.12 Predicted 2050 LULC map of Sile watershed

4.3 Ensemble RCM Performance Evaluation

Statistical metrics (Correlation coefficient (R^2), Nash-Sutcliffe efficiency (NSE), and Root mean square error (RMSE) between the mean monthly observed and ensemble average RCMs rainfall was to be evaluated (Table 4:12). The correlation of RCP 4.5 and RCP 8.5 ensemble average rainfall data with observed rainfall data was ranged from 0.699 to 0.794 and 0.50 to 0.802 from different stations respectively. In both the scenarios (RCP 4.5 and RCP 8.5) the ensemble mean of rainfall data was better correlated with observed station dates. The result of Nash-Sutcliffe efficiency (NSE) and Root mean square error (RMSE) value in both scenarios also confirmed that there was a better relationship performance between the observed and simulated rainfall.

According to (Worku et al., 2018) in Jemma sub-basin, Upper Blue Nile Basin, Ethiopia the ensemble mean of all 10 RCMs simulations was better in capturing the seasonal pattern of the rainfall and had a superior correlation with observed annual (R^2 =0.6) was reported. In addition, the study conducted in the Mbarali River catchment, Rufiji Basin Tanzania also confirmed that the ensemble average RCMs were performed better than individual models in representing rainfall with a correlation of 0.98 (Mutayoba & Kashaigili, 2017). The ensemble average performed better than individual simulated RCM models (Mutayoba & Kashaigili, 2017; Worku et al., 2018; Belay & Mengistu, 2021). Therefore, in this study four RCM models' ensemble mean under two scenarios was computed and used as input for the RUSLE model.

Table 4.12 Ensemble RCM performance evaluation

Stations	NSE		RMSE		R^2		RCM Name
	RCP4.5	RCP8.5	RCP4.5	RCP8.5	RCP4.5	RCP8.5	
Arbaminch	0.686	0.589	20.684	26.382	0.794	0.50	Ensemble
M/Abaya	0.627	0.756	12.647	12.271	0.723	0.802	Ensemble
Gidole	0.691	0.576	14.245	23.333	0.699	0.646	Ensemble
Gato	0.599	0.745	16.961	14.804	0.764	0.777	Ensemble

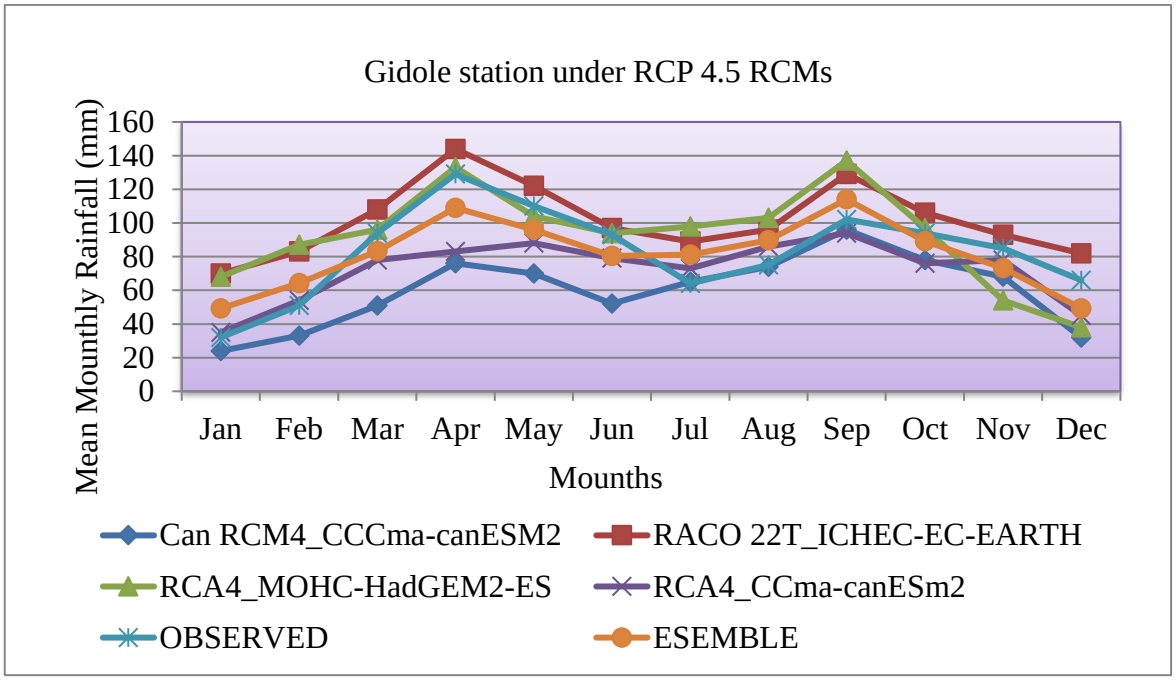

Figure 4.13 Mean monthly rainfall from observations and RCMs under RCP 4.5 in Gidole station from the year 2006-2020

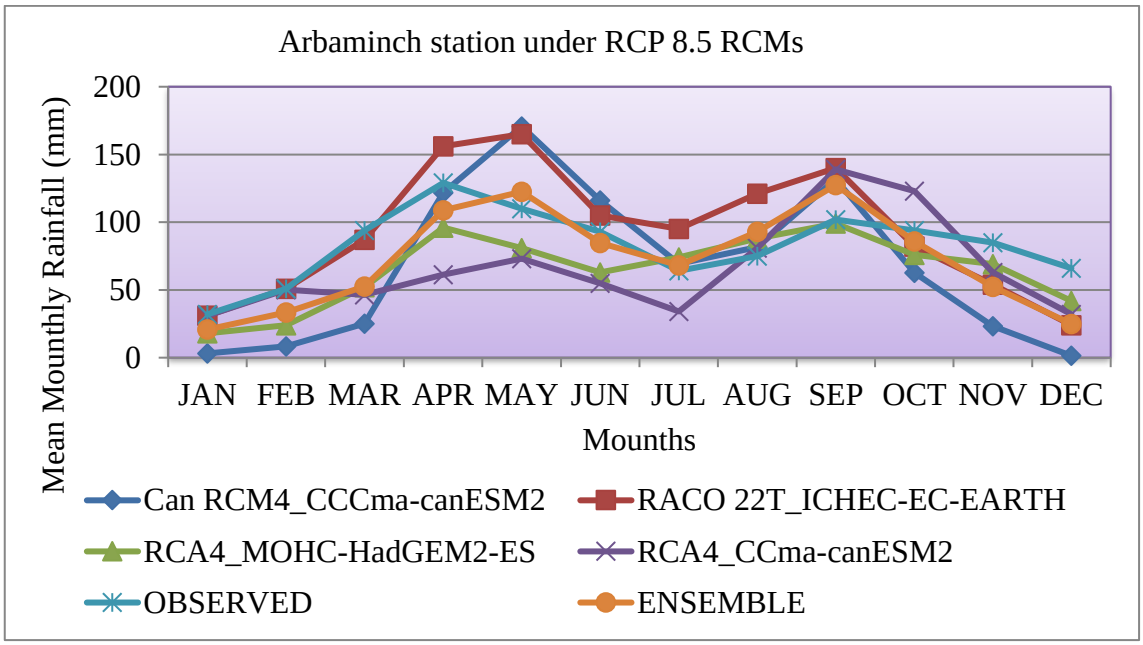

Figure 4.14 Mean monthly rainfall from observations and RCMs under RCP 8.5 in Arbaminch station from the year 2006- 2020

4.4 Estimated RUSLE Model Parameters

4.4.1 Rainfall-Runoff Erosivity (R) Factor

The mean annual rainfall data of 34 years (1987-2020) was derived from four rainfall stations (Arbamich, Mirab-Abay, Gidole, and Gato) were considered to estimate the R factor for three different periods. The R-factor analyzed using Equation:3.17 indicated that (Fig: 4.15 & Fig: 4.16) the value ranges from 401 to 475 MJ mm ha^{-1} $h^{-1}$$year^{-1}$ with a mean of 434 MJ mm ha^{-1} h^{-1} $year^{-1}$, 471 to 500 MJ mm ha^{-1} h^{-1} $year^{-1}$ with a mean of 485 MJ mm ha^{-1} h^{-1} $year^{-1}$ and 504 to 683 MJ mm ha^{-1} h^{-1} $year^{-1}$ with a mean of 590 MJ mm ha^{-1} h^{-1} $year^{-1}$ for the period 1987, 2003 and 2020 years respectively. For the future, the mean annual rainfall (2021 to 2050), the ensemble means of all four RCM rainfall data under two scenarios (RCP 4.5 & RCP 8.5) were used to generate the map of R values. The erosivity value ranges from 702 to 673 with its mean value of 686.04 MJ mm ha^{-1} h^{-1} $year^{-1}$, and 707 to 682 with a mean value of 693.4 MJ mm ha^{-1} $h^{-1}$$year^{-1}$ under both scenarios were observed (Fig 4.7). The rainfall erosivity showed an increasing trend by 14%, and 15% for 2050 respectively, under the RCP 4.5 and RCP 8.5 scenarios correspondingly (Fig:4.15).

According to the IDW result, it was observed that the highest rainfall and R-value were recorded in the upper part and eastern aspect of the watershed and lowest at the middle and down part of the watershed. Rainfall-runoff erosivity factor values have resulted highest to lowest Gidole Arbaminch, Gato Mirba Abaya station respectively on the baseline and future periods. The results also indicated that (Fig:4.15) the rainfall-runoff erosivity values were increased from the period of 1987 to 2020 and simulated future scenarios (2021 to 2050), which imply that the impact of climate change which alters soil erosion in the Sile Watershed was increasing due to the increased influence of rainfall-runoff erosivity. This result agrees with previous studies (Moges et al., 2020 ; Girmay et al., 2021; Belay & Mengistu, 2021).

The R-value is lower indicates that low erosivity of rainfall erodes the soil and low the rainfall intensity in the study area. (Asmamaw & Mohammed, 2019; Girmay et al., 2020) that predicted increasing precipitation in other parts of Ethiopia.

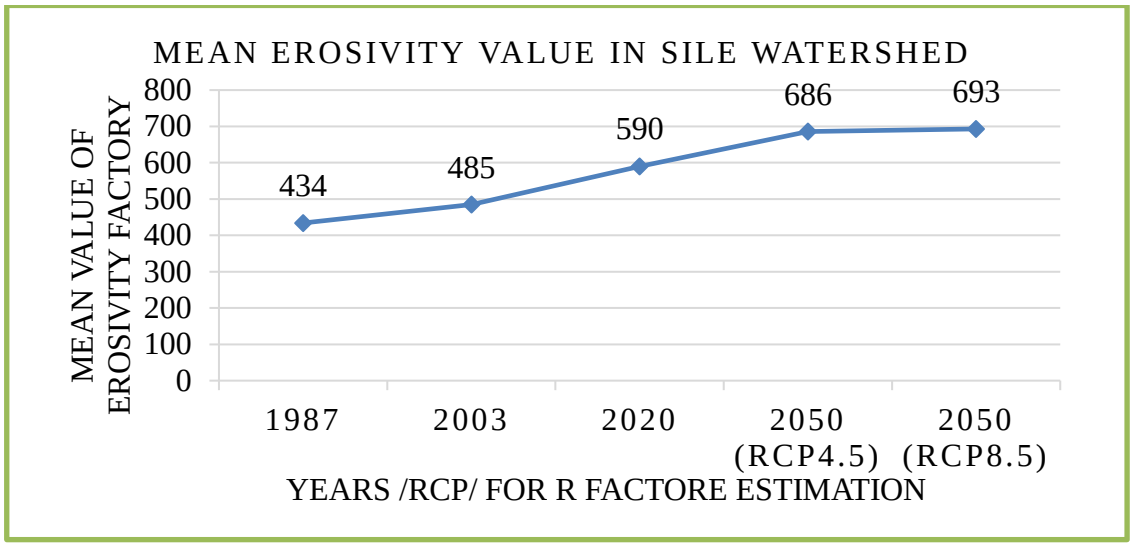

Figure 4.15 Mean erosivity value under different periods & scenarios in Sile watershed

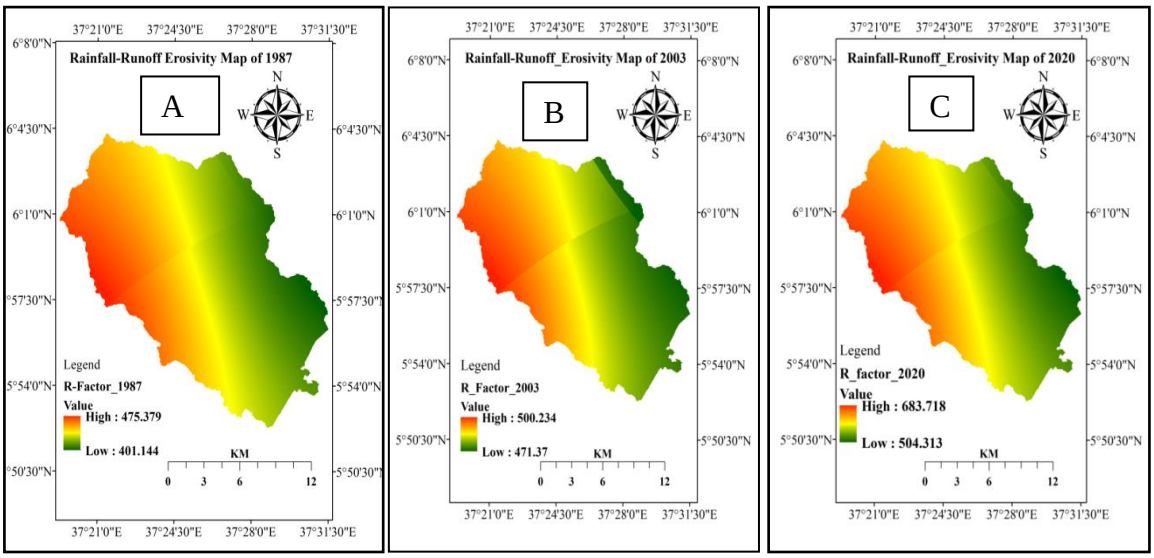

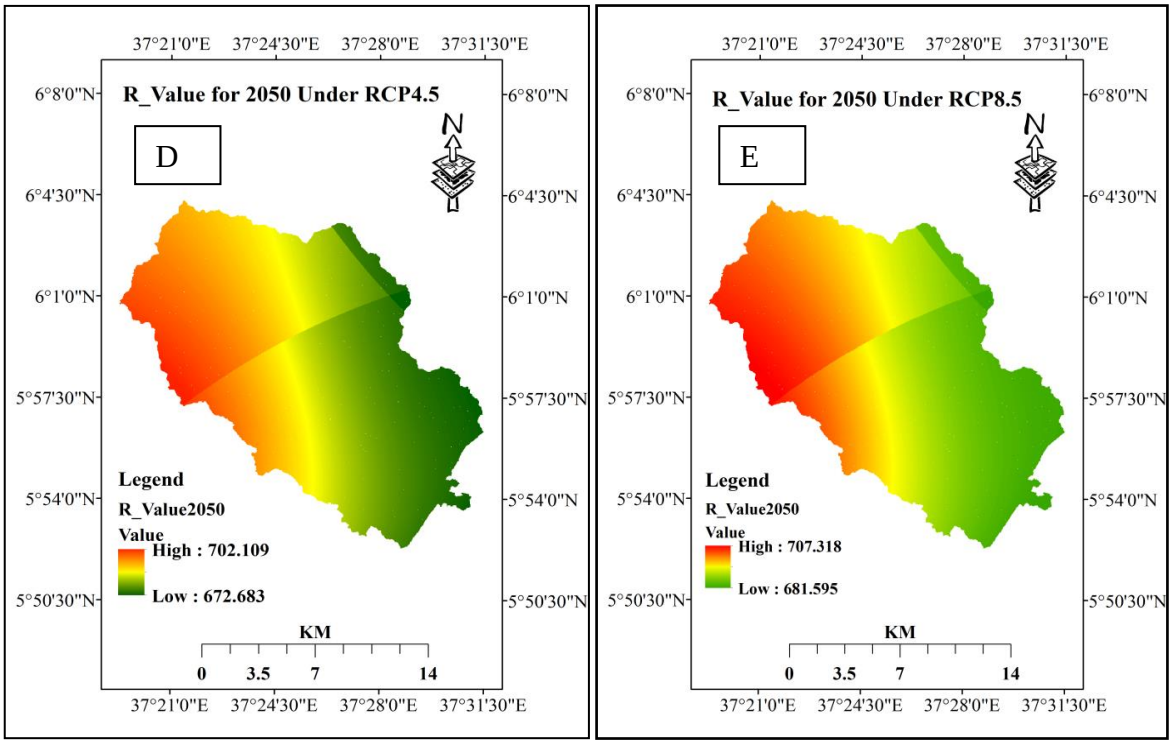

Figure 4.16 Erosivity (R) factor map for 1987 (A), for 2003 (B), for 2020 (C) for 2050 under RCP 4.5 (D) & for 2050 under RCP 8.5 (E)

4.4.2 Soil Erodibility (K) Factor

The laboratory analysis presented in (Appendix Table:3) revealed that the soil textural classes of my study area in the lower and middle part of the watershed were silty clay loam, clay loam, and sandy clay loam, which are dominant whereas, in the upper part of the watershed clay, clay loam and sandy textural class dominated. Similarly, a study conducted by (Zebire et al., 2019) in Sile watershed concluded that the lower part of the watershed was dominated by silty clay loam soil.

The soil organic carbon (SOC) content of the study area was ranged from 0.128 % to 3.9 % with an average value of 2.167%. The mean SOC in the lower Sile -Sego watershed with a soil depth from 0-35 cm was 2.16 was recorded (Zebire et al., 2019). In another hand, the

study finds from North West Ethiopia in Koga watershed, SOC ranged from 1.5 % to 3.9 %, and with a mean value of 1.5 % were reported (Gebeyehu & Soromessa, 2018).

According to the result of (Fig:4.17A), geostatistical analyst's interpolation by Ordinary 'Kriging' method, K value in the study area ranged from 0.0987604 to 0.181381 t-ha^{-1} MJ^{-1} mm^{-1} and mean of 0.12874 t-ha^{-1} MJ^{-1} mm^{-1}. In the Sile watershed, the soil erodibility factors (K) were relatively high and moderate in the upper part of the watershed as a result of its topography of a long slope length and steep slope. In the area where long slope length or steep slope, eroded soil, less organic matter content and less % clay fractions the erodibility K-factor values were high (Manyiwa & Dikinya, 2013). In contrarily, low K value was observed in the area where; shrubland, forest, and banana are black colored, and clay or silty clay loam or clay or sandy textural classes. The nature of soil erodibility induced by runoff was governed by mainly; soil textural class and organic matter content of the soil. Thus, the above-mentioned soil biophysical properties were directly or indirectly influenced the value of soil erodibility in the study area.

Clays have low K values because they are not as easily detached, sandy soils also have low K values because they are difficult to transport via runoff. Silt loam soils have medium K values and soils high in silt have high K values. The soil property (soil texture, soil structure, organic matter, water content, and density) of the soil affects infiltration capacity and the extent to which the soil particles can be detached and transported (Woldesenbet et al., 2020).

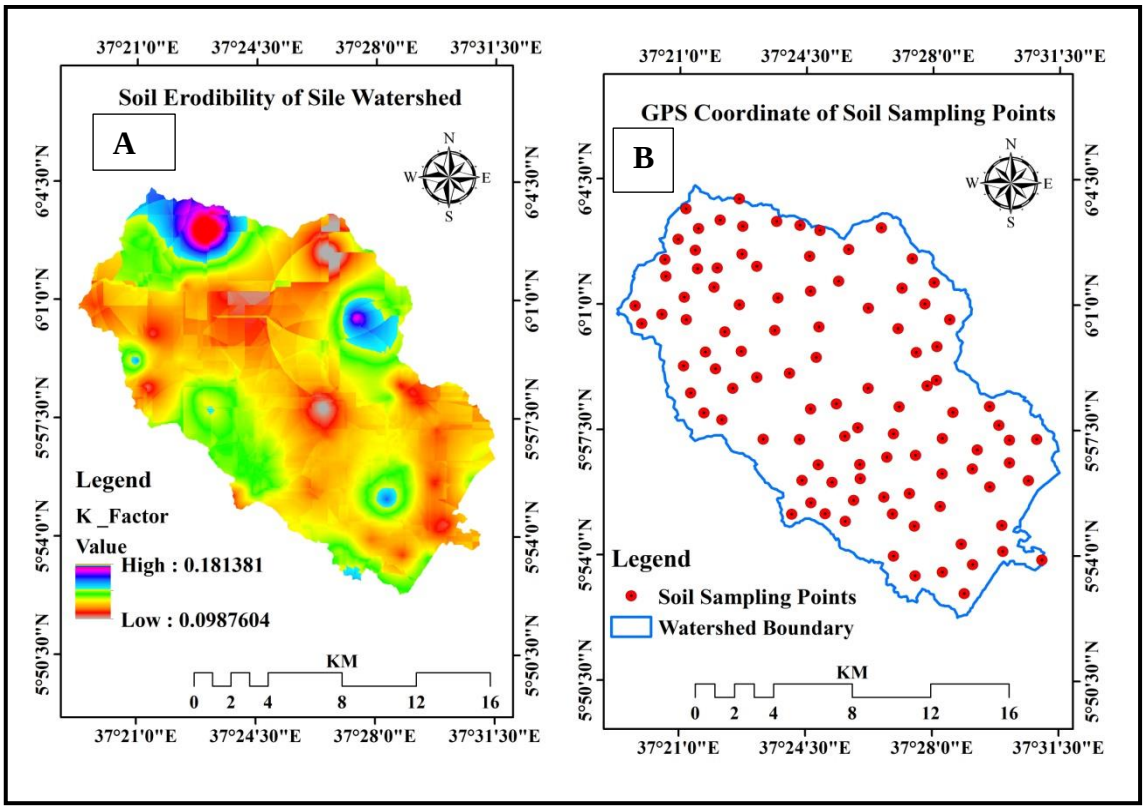

Figure 4.17 Soil erodibilty (K) factor map (A) and soil sampling points in the study area (B)

4.4.3 Topographic (LS) Factor

According to the analysis, the average value of the LS factor was 3.42 with a standard deviation of 4.53 and it varies from 0 in the lower part of the watershed to 54 in the steepest and upper part of the watershed. Topographic characteristics have a significant impact on the spatial distribution of erosion and deposition (Girmay et al., 2020). As observed in Figure: 4.17, the highest value of LS was distributed in the steep mountainous terrain and the lowest value of LS was distributed in gently flat to undulating terrain. The lowest LS value of the watershed indicates that less vulnerable to erosion and the higher value which was found in the midstream and upstream part of the study area showing a high LS factor and therefore, high sensitivity to soil erosion (Gelagay & Minale, 2016).

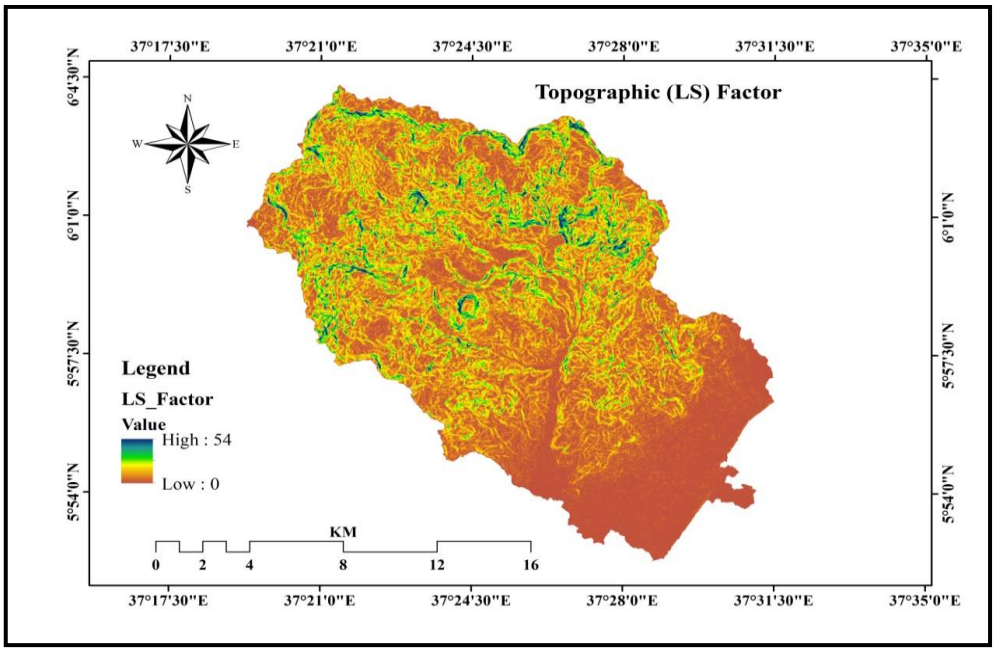

Figure 4.17 Topographic (LS) factor map of Sile watershed

4.4.4. Cover (C) Factor

The cover and management factors (C) are considered as dynamic factors that vary through time (Kavian et al., 2017 ; Woldesenbet et al., 2020) so, four different C- factor maps were generated for the period 1987, 2003, 2020, and for the future predicted 2050 (Fig: 4.18). The value of C-factors was ranging from 0–1 which was estimated from different works of literature. Based on the analysis the larger value shows more vulnerable land use to soil erosion and on the other hand, the lower value shows less vulnerable land use for erosion

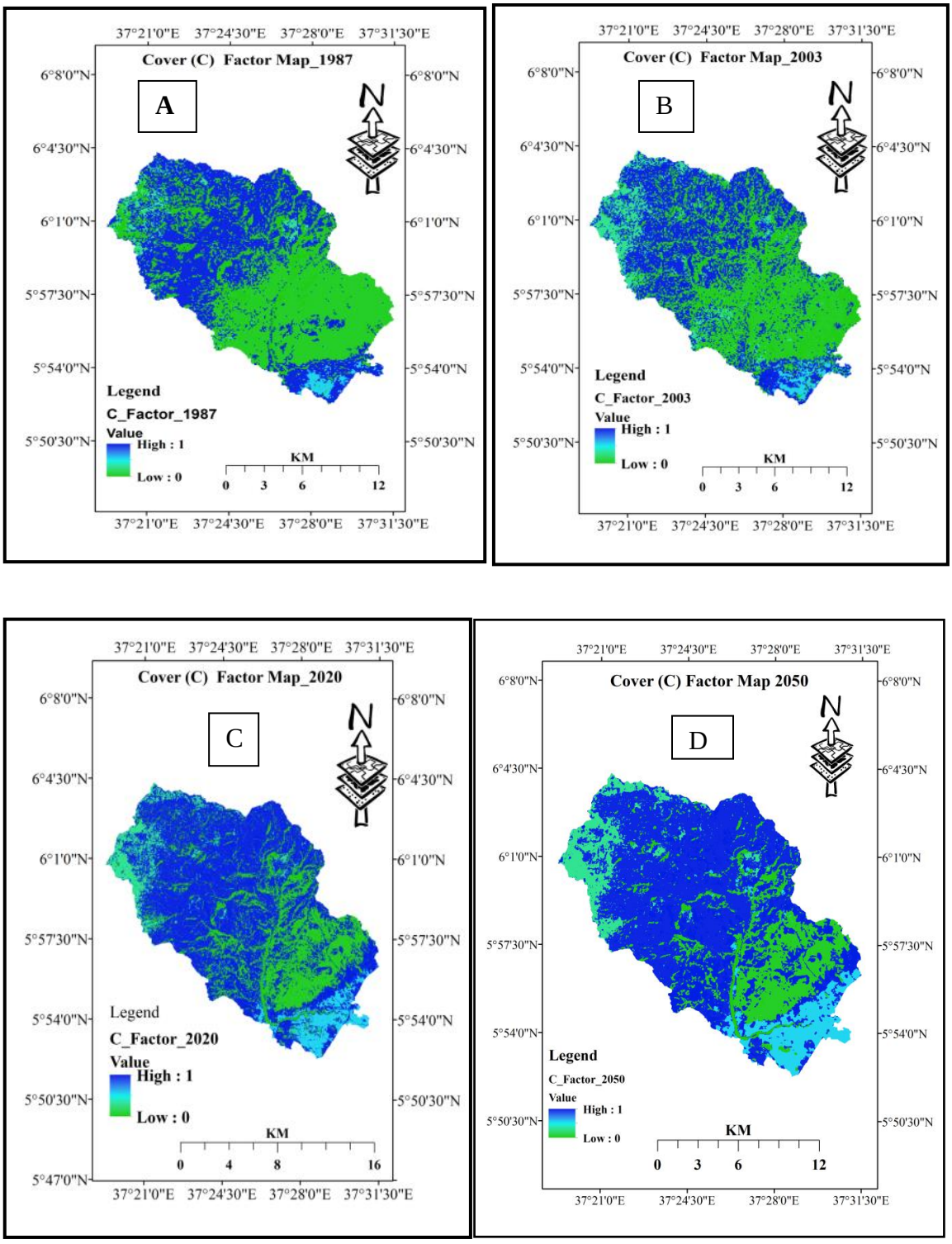

Figure 4.18 Cover (C) factor map for 1987(A), for 2003 (B), for 2020 (C) and for 2050 (D)

4.4.5. Management practice (P) Factor

For land management factors (P) four different P- factor maps were also prepared based on the value assigned according to its slope classes and LULC for the period 1987, 2003, 2020 and simulated 2050 (Fig:4.19). The results indicated that the distribution of the P-factor ranges from 0.1 to 1 in the cultivated land based on its corresponding slope class and 1 for other land use. The highest P-value of the watershed was found in the upstream part of the study area, but the smallest value was indicated in the downstream and midstream part of the watershed. The lower P value indicates relatively better soil erosion control measures.

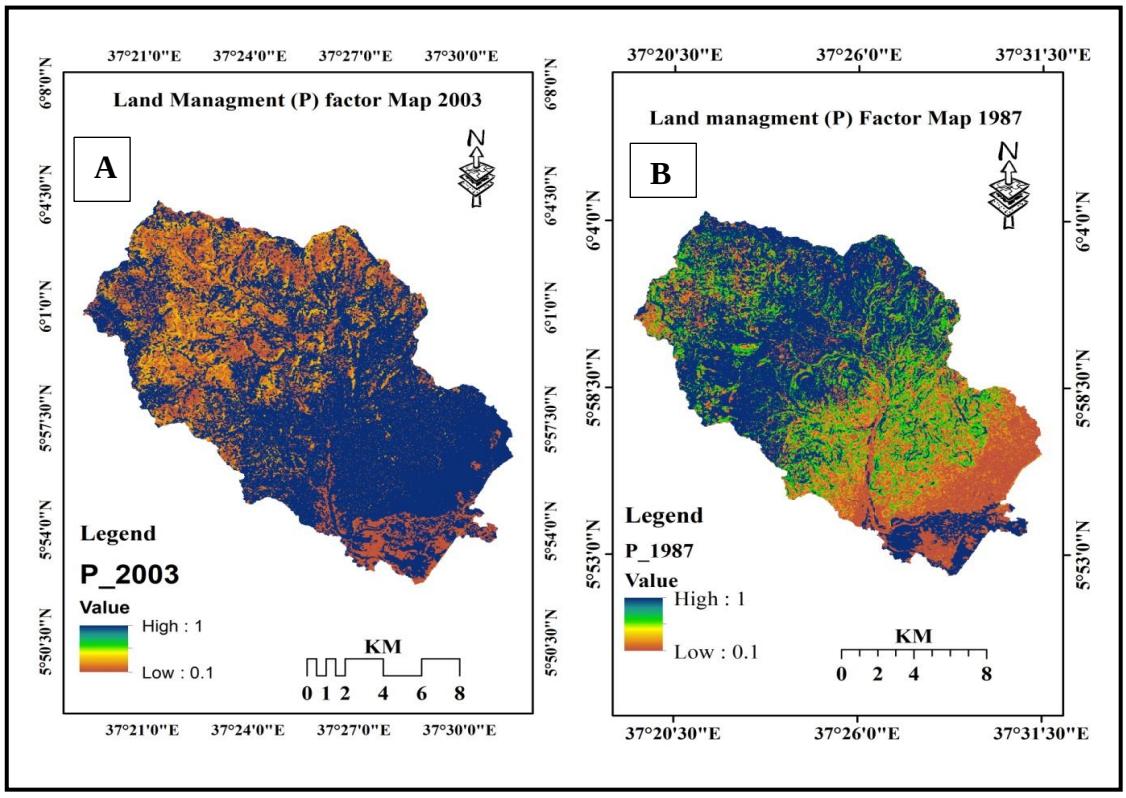

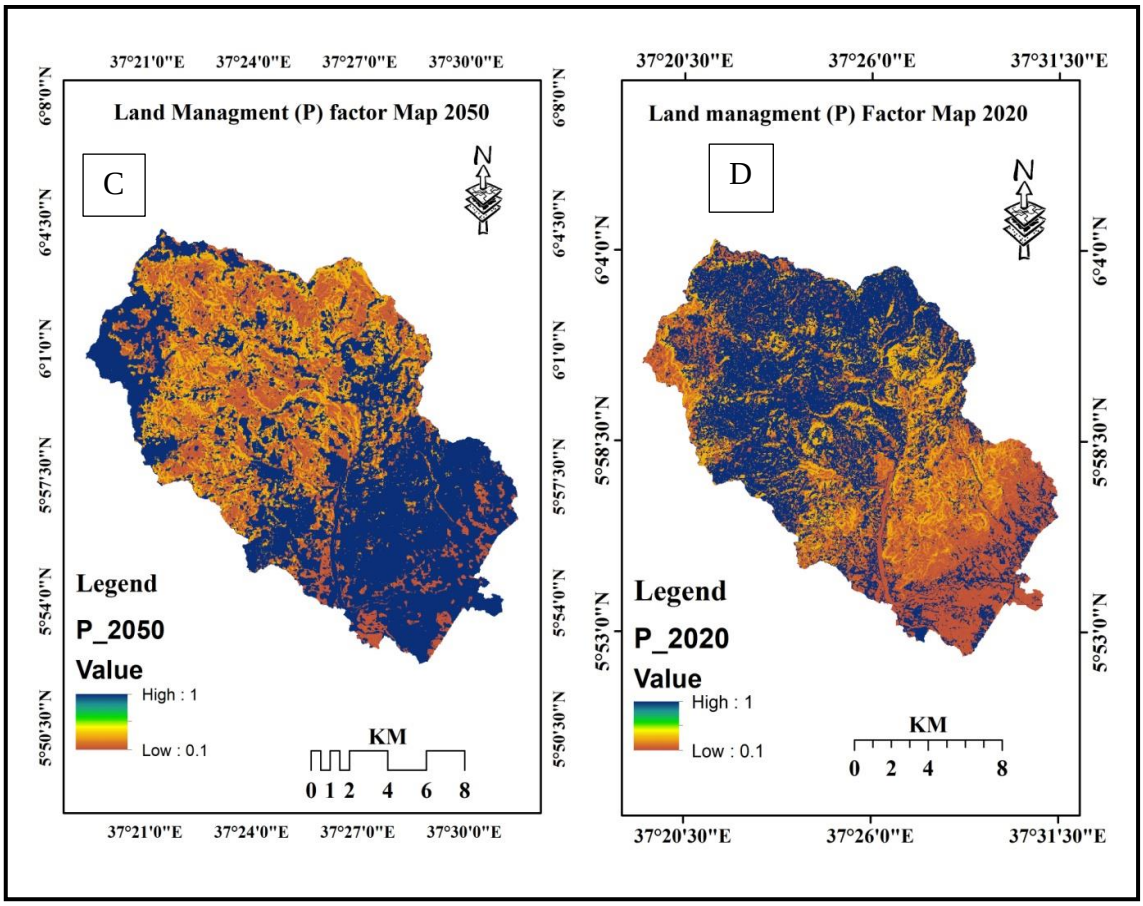

Figure 4.19 Practice (P) factor map for 1987 (A), for 2003 (B), for 2020 (C) and for 2050 (D)

4.5 Estimated Annual Soil Loss

4.5.1 Soil Erosion Rate in Sile Watershed

The factors of RUSLE have been analyzed in Arc GIS 10.8 spatial analyst tools to calculate the spatiotemporal annual soil erosion rate for the three study periods. The result in (Table: 4.14) indicates that the mean annual soil loss for the years 1987, 2003, and 2020 were 13.05 t-ha^{-1} year^{-1}, 21.04 t-ha^{-1} year$^{-1,}$ and 41.41 t-ha^{-1} year^{-1} respectively. In three different study years, the mean annual soil loss in Sile River watershed was above the tolerable limit of 11 t-ha^{-1} year^{-1} (Gashaw et al., 2018). The total annual soil loss potential of the study area was 389,456 t year^{-1}, 616,669 t year$^{-1,}$ and 1,184,920 t-year^{-1} for the year 1987, 2003, and 2020 respectively from the area of 27,610 hectares.

According to (Table: 4.13), the estimated mean annual soil loss rate in this study is a comparable range with the reported mean annual soil loss rates in the different parts of the country. In Medego Watershed, Northern Ethiopia with 9.63 t-ha^{-1}year^{-1} (Brhane & Mekonen, 2009) and in Erer Sub-Basin, Northeast Wabi Shebelle Basin, Ethiopia 107.07 t-ha^{-1}year^{-1} (Gezahegn & Harka, 2020) was reported. Therefore, the estimated soil loss for three study periods using the RUSLE model in this study also coincided with previous findings of different researchers (Table: 4.14).

Table 4.13 Comparison of estimated mean annual soil loss with different scholars' findings

No	Study period	Study area	Mean annual soil loss (t-ha^{-1} year^{-1})	References	Model used
01	2018	Lake Tana Sub-basin, Ethiopia Upper Blue Nile Basin, Northwest Ethiopia	37.89	(Balabathina et al., 2020)	GIS-based RUSLE
02	2019	Agewmariayam Watershed, Northern Ethiopia	25	(Girmay et al., 2020)	GIS-based RUSLE
03	2017	Beshillo Catchment of the Blue Nile Basin, Ethiopia	37	(Yesuph & Dagnew, 2019)	GIS-based RUSLE
04	2000	Erer Sub-Basin, Northeast Wabi Shebelle Basin, Ethiopia	75.85	(Gezahegn & Harka, 2020)	GIS-based RUSLE
05	2018	Erer Sub-Basin, Northeast Wabi Shebelle Basin, Ethiopia	107.07	(Gezahegn & Harka, 2020)	GIS-based RUSLE
06	2016	Upper Blue Nile River, Ethiopia	27.5	(Haregeweyn et al., 2017)	GIS-based RUSLE
07	2016	Welmel Watershed of the Genale Dawa Basin, Ethiopia	31	(Yadeta et al., 2020)	GIS-based RUSLE

08	2013	Eastern Escarpment of Wondo Genet Watershed, Ethiopia	26	(Sisay, 2014)	GIS-based RUSLE
09	2016	Koga watershed in the highlands of Ethiopia	42	(Molla & Sisheber, 2017)	GIS-based RUSLE
10	2008	Medego Watershed, Northern Ethiopia	9.63	(Brhane & Mekonen, 2009)	USLE
11	2016	Geleda watershed, Blue Nile basin, Ethiopia	23.7	(Gashaw et al., 2018)	GIS-based RUSLE

As shown in (Table: 4.14) the potential soil loss and vulnerability to erosion was observed to increase tremendously for the last three and half decades (1987-2020). LULC and climate variability/ and climate change are the most important factors which govern the temporal variability of soil erosion rate and extent in the study area. The mean annual soil loss from 1987 to 2003 was augmented by 61.23% and from 2003 to 2020 the increment of 96.81 % was estimated. These results may be related to the temporal variation of climate variables (i.e. increased R_ Factor) and detrimental change of LULC. For instance, the mean value of the R factor from 1987 to 2003 was increased by 10%, and from 2003 to 2020 by 21.65 % was increased (Figure:4.15 & Fig:4.16). In the same manner, LULC from 1987 to 2003, cultivation land, and bare land was increased by 25 % and 204 % at the expense of shrubland, grazing land, and forest land by 15 %, 38 %, and 20 % decreased respectively (Table: 4.4). The change of LULC from the year 2003 to 2020 was also drastically observed and may have also a significant influence on soil loss. In (Table: 4.5), indicated that cultivation land was 22 % and bare land was 116 % increased at the expense of shrubland, grazing land, and forest land by 26 %, 41%, and 55 % decline for the year 2003 to 2020 in that order.

Land use/land cover (LULC) alteration and climate change influence a susceptibility to soil erosion (Moges & Bhat, 2017; Sardari et al., 2019) and have also played a significant role in the spatiotemporal variability of the soil erosion rate (Esa et al., 2018 ; Negese, 2021). Removal of vegetation covers, cultivation of steep slopes, inappropriate farming systems, and absence of soil conservation measures are the major factors for soil loss (Wubie et al., 2016; Moisa et al., 2021). The increase in rainfall amounts and intensities have an essential impact on soil erosion rates (Nearing et al., 2004; Chen et al., 2020) as a result of the increased erosive power of precipitation (Moges et al., 2020 ; Girmay et al., 2021). Therefore, the chronological increment of soil loss was mainly as the result of a temporal variation of runoff- rainfall erosivity and the expansion of cultivation land and bare land at the expense of the decline of shrubland, grazing land, and forest in the study area.

Table 4.14 The rate of soil loss in the study area

Study years	Total soil loss (t yr^{-1})	Mean annual soil loss, (t ha^{-1} yr^{-1})	Relative changes between two periods (%)
1987	389,456	13.05	-
2003	616,669	21.04	61.23
2020	1, 184,920	41.41	96.81

Where, (t yr^{-1}) = tone/year, (t ha^{-1} yr^{-1}) tone per hectare per year

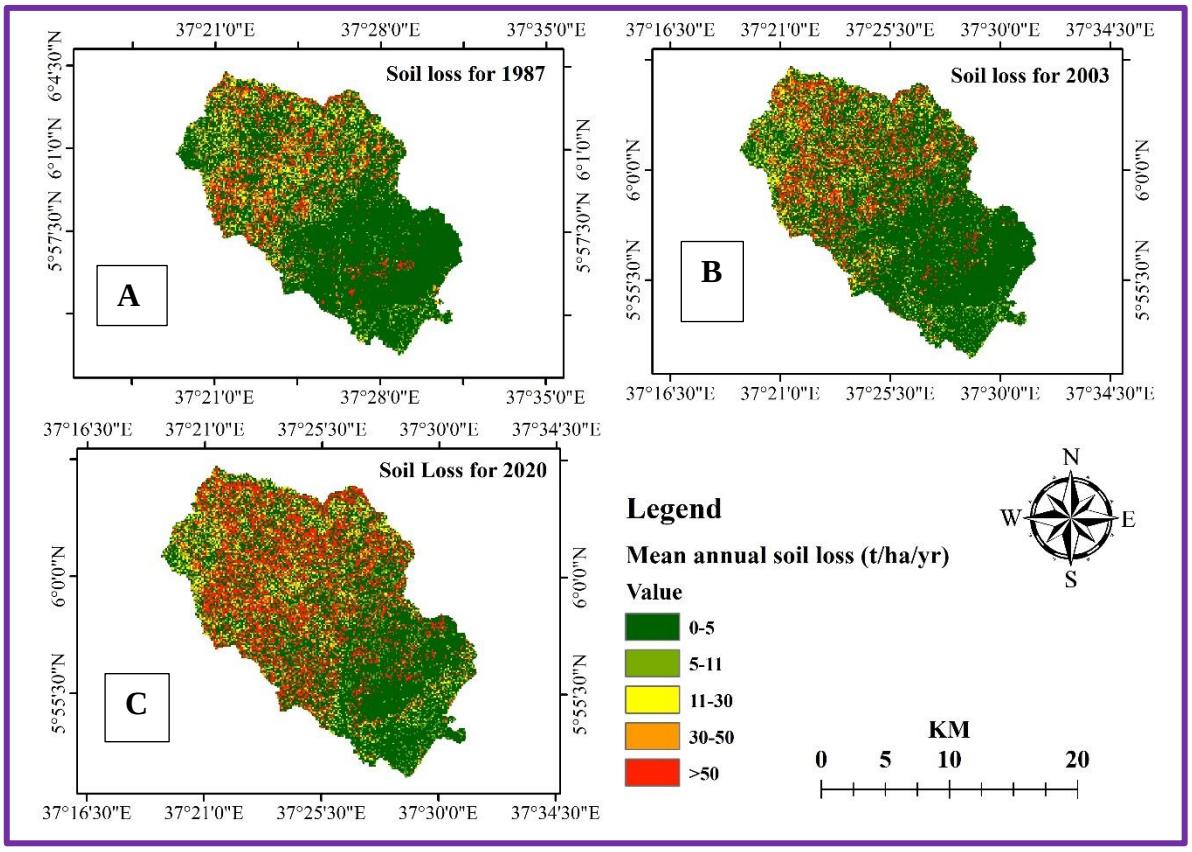

Figure 4.20 Estimated soil loss map for the year 1987(A), for the year 2003 (B), for the year 2020 (D) in the Sile watershed

4.5.2 Soil Erosion Under Different LULC Category

This study revealed that the estimated soil loss from each LULC category was increased during the period between 1987 to 2020 and each LULC have their detrimental impacts on soil loss by water erosion (Table 4:15). The most very severe soil loss rates were estimated in bare land and cultivation land, with a mean soil loss rate of (27.9 t-ha^{-1} year^{-1} & 23.3 t-ha^{-1} year^{-1}), (35.5 t-ha^{-1} year^{-1}, & 29.5 t-ha^{-1} year^{-1}) and (45.6 t-ha^{-1} year^{-1} and 41.7t- ha^{-1} year^{-1}) in 1987, 2003 and 2020 respectively. On other hand, the moderate mean annual soil loss was estimated from grazing land in which 15.4 t-ha^{-1} year^{-1}, 15.2 t-ha^{-1} year^{-1}, and 20 t-ha^{-1} year^{-1} in 1987, 2003, and 2020 respectively. For all three study years lowest, average annual soil loss was observed from banana land cover. In the year 1987 (2 t-ha^{-1} year^{-1})

mean annual soil loss, in the year 2003 (3.5 t-ha^{-1} year^{-1}) and in the year 2020 (1.9 t-ha^{-1} year^{-1}) mean annual soil was estimated from banana land cover of the study watershed. Following banana land cover, forest and shrubland also show good performance to resist soil erosion. In 1987, (8.6 t-ha^{-1} year^{-1}) and (5.1 t-ha^{-1}year^{-1}) mean annual soil loss, in 2003 (4.7 t-ha^{-1} year^{-1}) and (7.9 t-ha^{-1} year^{-1}) mean annual loss and currently in the year 2020 (8.1 t-ha^{-1} year^{-1} and (9.3 t-ha^{-1} year$^{-1)}$ mean annual soil loss was observed from forest land and shrubland respectively. Accordingly, the mean annual soil erosion rate of three land use land cover categories (banana land cover, forest, and shrubland) in the watershed were below the Tolerable Soil Loss (TSL) limit of 11 t-ha^{-1} year^{-1}) (Gashaw et al., 2020).

The average measured annual value of soil loss from cultivation land 46 t-ha^{-1} year^{-1} and 68 t-ha^{-1} year^{-1}, were reported in northeastern and southwestern Ethiopia respectively (Hurni, 1985). Hence, in this study, the result of predicted mean soil loss from cultivation land was agreed with the measured value of mean annual soil loss from cultivation land. According to (Gezahegn & Harka, 2020), in Erer Sub-Basin, Northeast Wabi Shebelle Basin, Ethiopia the estimated mean annual soil loss from bare land, cropland, shrub, and the forest was 15.78, 37.60, 11.62, and 2.47 t- ha^{-1} year^{-1} respectively. In Temeji watershed, Western Ethiopia high soil loss was observed when grassland and forest land were converted into cultivated land with a mean soil loss of 88.8 and 86.9 t- ha^{-1} year^{-1} in 2020 (Moisa et al., 2021).

In Ethiopia, the expansion of cultivated land at the expense of forest land, shrubland, and grassland has increased the mean rate of soil erosion, sediment yield, surface runoff (Negese, 2021). In addition, cultivation of steep lands, overgrazing, and deforestation has been believed to be the driving force to soil erosion and the conversions of marginal areas and forests to cultivated land have contributed to the existing high rate of soil erosion and land degradation in the highlands of Ethiopia (Bewket & Teferi, 2009).

In the Abaya-Chamo sub-basin, LULC changes increased soil erosion, sediment transport the volume of surface runoff which subsequently, affected the levels and water quality of the lakes (WoldeYohannes et al., 2018). However, based on the results of this study besides its economic feasibility (Yirgu, 2018), the banana land cover had an ecological sound, environmentally friendly farm, and specifically, it plays a vital role to mitigate the soil erosion risk in the study watershed and the whole Abaya-Chamo sub-basin.

Table 4.15 Soil erosion under different LULC classes in the study watershed

	Soil loss 1987		Soil loss 2003		Soil loss 2020	
LULC	Annual soil loss (t yr^{-1})	Mean (t ha^{-1} yr^{-1})	Annual loss (t yr^{-1})	Mean (t ha^{-1} yr^{-1})	Annual loss (t yr^{-1})	Mean (t ha^{-1} yr^{-1})
BC	1,028	2	2,626	3.5	2,639	1.9
GL	14,698	15.4	38,067	15.2	38,153	20
BL	31,571	27.9	214,178	35.5	534,664	45.6
CL	257,224	23.3	270,126	29.3	545,637	41.7
SL	51,556	5.1	73,559	7.9	48,466	9.3
FL	33,375	8.6	18,110	4.7	15,361	8.1
Total	389,456		616,669		1,184,920	

Where, CL = Cultivation Land, NF = Forest Land, GL = Grazing Land, BC = Banana Cover, BL = Bare Land, SL = Shrub Land, (t yr^{-1}) = tone/year, (t ha^{-1} yr^{-1}) tone per hectare per year

4.5.3 Soil Erosion Under Different Slope Classes

The results revealed that low soil loss was estimated in the gentle flat slope while, high soil erosion was estimated on the steep slope areas of the study watershed for the three different study periods (Table: 4.16) The estimated mean annual soil loss on 1987, 2003, and 2020 were 5 t-ha^{-1} $year^{-1}$, 4 t-ha^{-1} $year^{-1,}$ and 10.3 t-ha^{-1} $year^{-1}$ in slopes class less than 2 percent respectively. In slopes of (2–10) % the mean annual soil loss was 7.1 t-ha^{-1} $year^{-1}$, 8.7 t-ha^{-1} $year^{-1,}$ and 17.6 t- ha^{-1} $year^{-1}$ in 1987, 2003, and 2020 in that order. For the slope class of (10-15) %, the mean annual soil erosion rate in the study area was 13.1 t- ha^{-1} $year^{-1}$, 16.2 t-ha^{-1} $year^{-1}$, and 33 t-ha^{-1} $year^{-1}$ in 1987, 2003, and 2020 correspondingly. As well, 18.8 t-

ha^{-1} $year^{-1}$ in 1987, 32.4 t- ha^{-1} $year^{-1}$ in 2003, and 60.3 t- ha^{-1} $year^{-1}$ in 2020 were estimated for the slope class of (15-30) %. Finally, the slope class above (30) % were 27 t-ha^{-1} $year^{-1}$, 50.9 t-ha^{-1} $year^{-1,}$ and 97.5 t- ha^{-1} $year^{-1}$ change was estimated for the years 1987, 2003, and 2020.

In Table 4:16 the extent of soil loss within the same slope class at three different study periods (1987, 2003, and 2020) shows an increasing trend. This alteration may be due to the influence of temporal variation of a cover factor of the study area. The conversion of forest, grazing land, and shrubland into cultivation land and bare land at different slope classes has increased the susceptibility of soil erosion in the study area.

Both slope and land use/land cover are associated factors of soil erosion. According to (Girmay et al., 2020), the severity of soil erosion occurred in steep slope cultivation. Therefore, both topography and human-induced land use/land cover change like cultivation on steep slopes were played a significant role in accelerating soil erosion rates (Bewket & Teferi, 2009; Yesuph & Dagnew, 2019).

In 2020 the soil loss from flat terrain was 9,197 t-$year^{-1}$ with a mean annual loss of 10.3 t-ha^{-1} $year^{-1}$ from undulating terrain 152,726 t-$year^{-1}$ with a mean annual soil loss of 17.6 t-ha^{-1} $year^{-1}$ and from rolling terrain 174,131 t-$year^{-1}$ with a mean annual soil loss of 33 t-ha^{-1} $year^{-1}$ change was observed. The hilly terrain and mountainous terrain of the study area 611,135 t-$year^{-1}$ & 237,731 t-$year^{-1}$ annual soil loss and 60.2 t-ha^{-1} $year^{-1}$ & 97.5 t-ha^{-1} $year^{-1}$ mean annual soil loss which has very severe erosion extent was recorded respectively. According to (Gashaw et al., 2018), soil erosion is a key problem in the steep areas of the Geleda watershed, Blue Nile basin of Ethiopia which extends up to 237 t ha^{-1} $year^{-1}$. The study finding of (Kogo et al., 2020) also agrees with this study while the steepness of the slope increased the soil loss would be increased. Topography had the strongest influence on soil erosion rates (Balabathina et al., 2020). Therefore, in the Sile River watershed, the slope classes above 2 % experienced soil losses above the tolerable limit of 11 t ha^{-1} $year^{-1}$ (Gashaw et al., 2018).

Table 4.16 Effect of different slope class for soil loss in study watershed

Slope classes (%)	Soil loss 1987		Soil loss 2003		Soil loss 2020	
	Annual soil loss (t-yr^{-1})	Mean (t-ha $^{-1}$ yr^{-1})	Annual soil Loss (t-yr^{-1})	Mean (t-ha $^{-1}$ yr^{-1})	Annual soil Loss (t-yr^{-1})	Mean (t-ha $^{-1}$ yr^{-1})
0-2	4,463	5	3,541.82	4	9,197	10.3
2-10	61,815	7.1	75,680.27	8.7	152,726	17.6
10-15	68,508	13.1	85,425.50	16.2	174,131	33
15-30	189,080	18.8	328,223.64	32.4	611,135	60.3
30-62	65,589	27	123,797.83	50.9	237,731	97.5
Total	389,456		616,669		1,184,920	

Where, (t -yr^{-1}) = tone/year, (t- ha^{-1} yr^{-1}) = tone per hectare per year

Source: Adapted from (FAO, 1990) (https://www.fao.org/3/x0596e/X0596e02.htm/)

4.5.4 Soil Loss Severity Class Based on Sub Watershed Level

To identify the spatial variation, extent of soil loss, and prioritize for intervention planning, the study watershed was subdivided into ten main sub-watersheds and additional categorized into five erosion severity classes. The soil loss amount, severity, and extents varied for the different parts of the subwatershed. As shown in (Table: 4.17) and (Fig: 4.21): about 15,897 ha (58 %) and 1,414 ha (5%) of the area were categorized under very slight and slight erosion risk which extends from 0–5 t-ha^{-1} year^{-1} and 5- 11 t-ha^{-1} year^{-1}; mainly along the flat to gentle slopes of the downstream area with a banana cover were dominated by low soil loss values.

In the Sile watershed, 2,143 ha (8%) is characterized in moderate class ranging between 11–30 t-ha^{-1} year^{-1} and 1,846 ha (7%) of the area is found in the severe erosion risk class (30–50 t-ha^{-1} year^{-1}); 6,310 ha 22% of the entire area which was categorized under very severe erosion risk (>50 t-ha^{-1} year^{-1}). About (29%) of the watershed area is experiencing severe and very severe soil losses. Several factors that influence soil erosion from that factors high LS (topographic) factor (Girma & Gebre, 2020) and low C-factor or less vegetation cover (Wolka et al., 2015) contribute high to extreme severe soil erosion in the study area. This threatens the agricultural productivity and livelihood of the local farmers (Wolka et al.,

2015). The erosion from the Sile watershed may also have off-site consequences for the degradation of the Lake Abaya-Chamo sub-basin. The sedimentation from the catchment and application of chemical fertilizer and herbicides or pesticides in the cultivation land may have the possibility of cause's invasive plants (water hyacinth) in the basin (Dersseh et al., 2019; Zekarias et al., 2021).

According to Table: 4.17, out of the total soil loss 258,282 t-year^{-1} (22%) highest quantity was contributed from sub-watershed five with its 2,127 ha (8 %) area coverage. Next to subwatershed five, subwatershed 4 also contributed (247,264 t-year^{-1}) 21 % and the second priority area for proper soil and water conservation practices in the Sile watershed. As a result, the main concern should be given to those erosion-prone areas for watershed management planning and implementation.

Table 4.17 Soil erosion severity in sub-watershed level and conservation priority class

Sub WS	Severity class (t-ha $^{-1}$ yr^{-1}) and its area coverage (ha)						Total soil loss(t/yr^{-1})	%	Priority
	0-5(very slight)	5-11 (Slight)	11-30 (Moderate)	30-50 (Severe)	>50 (very Severe)	Sub WS area (ha)			
Sub_1	1,252	103	322	279	976	2,932	126,591	11	4
Sub_2	776	53	198	184	508	1,719	84,656	7	7
Sub_3	1020	120	189	188	721	2,238	123,159	10	5
Sub_4	1817	270	500	358	941	3,886	247,264	21	2
Sub_5	833	92	213	196	793	2,127	258,282	22	1
Sub_6	647	62	78	93	437	1,317	75,450	6	8
Sub_7	3005	176	139	87	323	3,730	47,300	4	9
Sub_8	2634	187	251	253	908	4,233	126,988	11	3
Sub_9	2481	196	110	38	109	2,934	9,364	1	10
Sub_10	1432	156	142	170	594	2,494	85,866	7	6
Tt(ha)	15,897	1,414	2,143	1,846	6,310	27,610	1,184,920	-	-
Tt (%)	58	5	8	7	22		-	-	-

Source: (Gashaw et al., 2020)

Where, SW= Sub watershed, (t yr^{-1}) = tone/year, (t ha^{-1} yr^{-1}) = tone per hectare per year,

Tt =Total

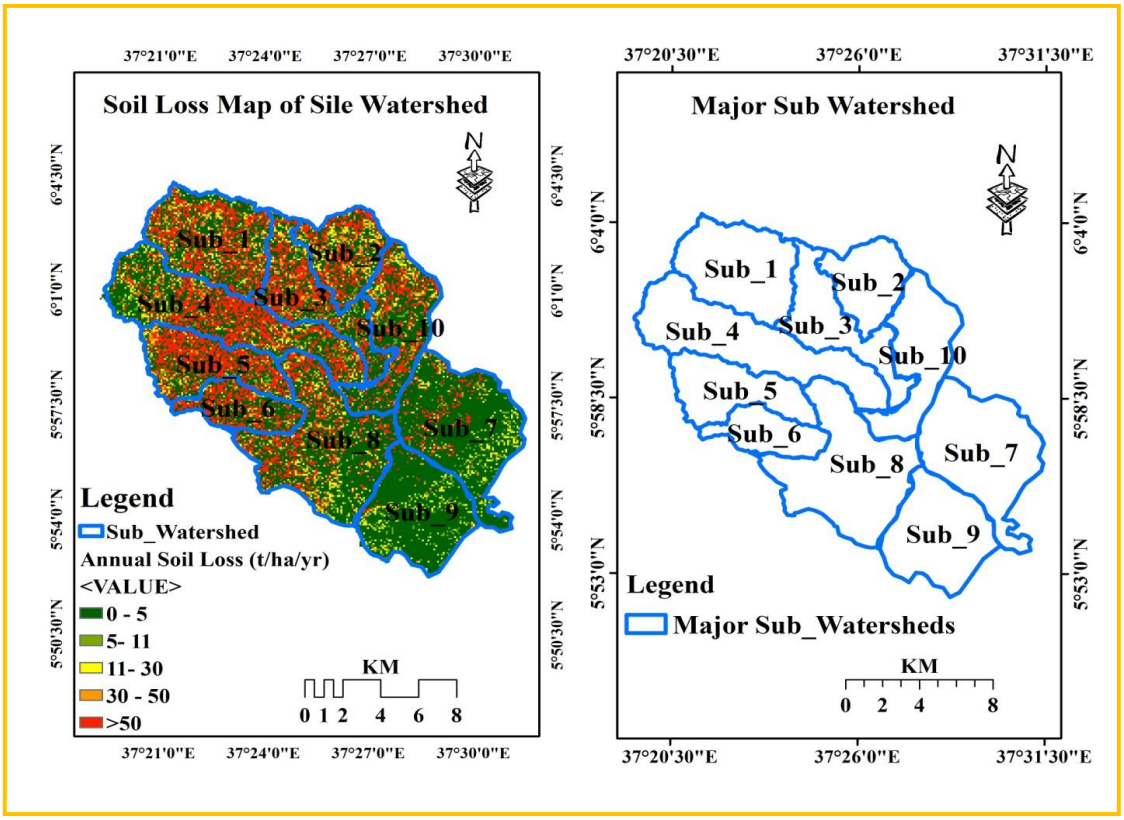

Figure 4.21 Estimated soil erosion severity classes based on sub-watershed level in Sile watershed

4.6 Effect of Future LULC and Climate on Soil Erosion

In this study, to assess the future combined impact of LULC and climate change on soil erosion, the values of C, P, and R factors were changed, while the other factors (i.e soil erodibility (K), and slope length and slope steepness (LS) kept constant. According to the RUSLE modeling, the total annual soil loss potential in both scenarios RCP4.5 (Intermediate) and RCP8.5 (Extreme) with the predicted LULC of 2050 the 1,469,375 t-year^{-1} and 1,485,810 t-year^{-1} were estimated respectively. Therefore, the soil loss rate is expected to increase under both scenarios (RCP4.5 and RCP8.5) with a predicted future LULC due to the higher erosive power of the future intense rainfall and conversion of vegetation cover to agricultural land and bare land.

The study also assured that under the RCP 4.5 and RCP 8.5 scenarios (Table: 4.18) the average soil loss was 56.48 t-ha^{-1}year^{-1}, and 57.11 t-ha^{-1} year^{-1} respectively for the year of 2050 was predicted. When we compare the mean annual soil loss of baseline time (2020) 41.41 t-ha^{-1} year^{-1} with 2050 predicted under both scenarios (RCP 4.5 and RCP 8.5) soil loss has been increased by 15.07 t-ha^{-1}year^{-1} (36.40 %) and 15.7 t-ha^{-1}year^{-1} (38.19%) respectively.

The study finding of (Belay & Mengistu, 2021) in the Muga watershed upper blue Nile Basin Ethiopia, when both LULC and climate changes act together, the mean annual soil loss rate shows a rise of 13.2% and 15.7% in 2050 under RCP 4.5 and RCP 8.5 of ensemble RCMs, respectively was estimated. However, my study result was more than twice higher than (Belay & Mengistu's, 2021) conclusions. This disparity maybe is from the variation of selected RCM model types /and the difference of future predicted LULC change of the study area. On another hand, the result of (Girmay et al., 2021), showed that under the RCP 4.5 and RCP 8.5 scenario, for the year 2050 predicted average annual soil loss was increased by 1.18 t-ha^{-1} year^{-1} (4.7%) and 2.38 t-ha^{-1}year^{-1} (9.5%) respectively. In the Rib watershed using the predicted LULC of 2050 under RCP 4.5 scenarios mean annual soil loss was projected from 69.4 t-ha^{-1}year^{-1} in 2017 to 78 t-ha^{-1}year^{-1} for the year 2050. This represents an increase of 12% compared with the baseline period (2017) (Moges et al., 2020)

In the study of (Girmay et al., 2021), the impact of future LULC was not considered but only the impact GCM models under RCP 4.5 and RCP 8.5 was used to predict 2050 soil erosion in Agewmariam watershed in northern Ethiopia.

The average annual soil loss would be increased in the future period compared with the base period. Climate changes, particularly due to the changed precipitation trend, can have a severe impact on future soil erosion (Gupta & Kumar, 2017). In the catchment of Saxony/Germany the impact of the expected increase of precipitation intensities leads to a significant increase of soil loss by 64% by 2050 (Routschek et al., 2014).

In general, the results are shown in (Table: 4.18 and Fig: 4.12) the total area of Sile river watershed 4,224 ha (15%) and 4,283 ha (16%) under RCP 4.5 and RCP 8.5 in that order were expected to be very severe soil loss for the year 2050. In Sile River watershed rift valley lake basin Ethiopia from the period 2021 to 2050, the increasing soil erosion rates caused by LULC and climate change will adversely threaten the sustainability of agricultural production and downstream Lake Abaya-Chamo aquatic ecosystem. Soil erosion endangers the sustainability of agriculture and water quality (Haregeweyn et al., 2017; Issaka & Ashraf, 2017).

Table 4.18 Soil loss under RCP 4.5 and RCP 8.5 with 2050 LULC

Scenarios	Current (2020) (t-ha^{-1} year $^{-1}$)	Future (2050) (t ha^{-1} year $^{-1}$)	Relative change (%)
RCP 4.5	41.41	56.48	36.40
RCP8.5	41.41	57.11	38.19

Table 4.19 Annual soil erosion risk class and area coverage under RCP 4.5 and RCP 8.5

Mean annual soil loss (t-ha $^{-1}$ year $^{-1}$)	Soil Loss Severity class	2050 (RCP 4.5)		2050 (RCP 8.5)	
		Area(ha)	%	Area(ha)	%
0-5	very slight	14,859	54	14,830	54
5-10	Slight	3,369	12	3,342	12
10- 30	Moderate	3,655	13	3,649	13
30-50	Severe	1,504	5	1,506	5
>50	very severe	4,224	15	4,283	16
Total area	Total area	27,610	100	27,610	

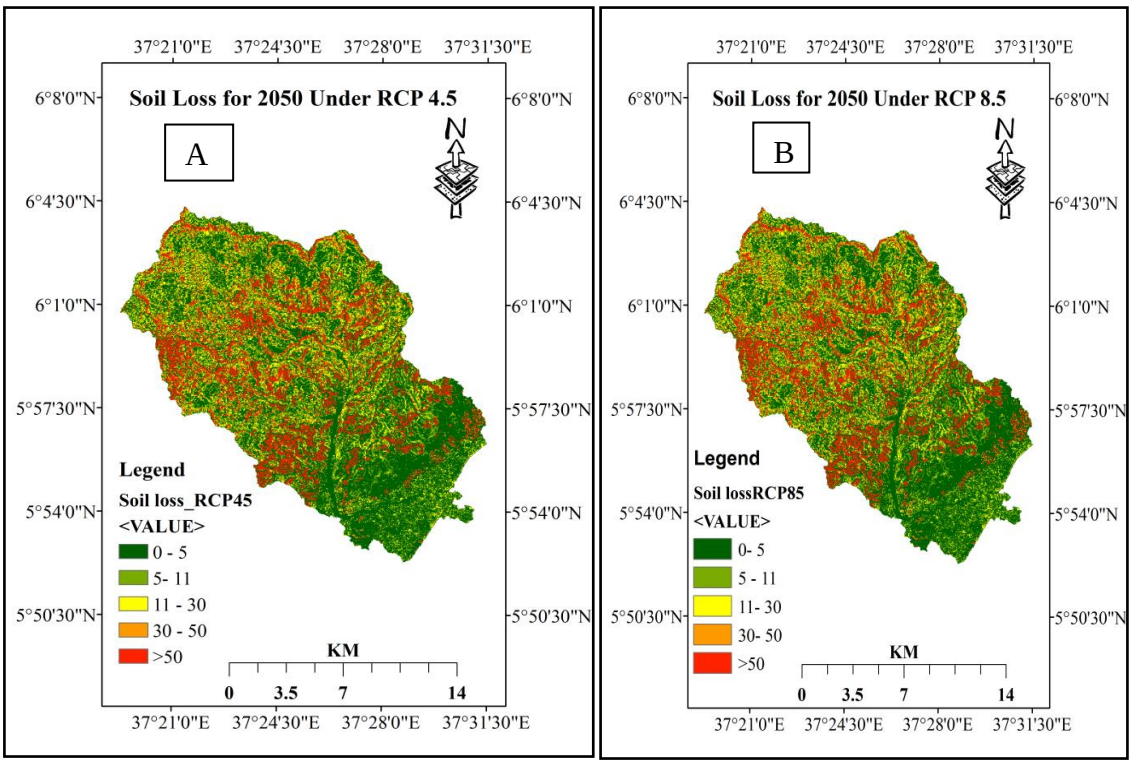

Figure 4.22 Estimated soil losses for the year 2050 under RCP 4.5 (A) and under RCP 8.5 (B) in Sile watershed

5. SUMMARY AND CONCLUSION

5.1. Summary

This study investigates the impact of land use land cover and climate change on soil erosion in the Sile River watershed Abaya-Chamo sub-basin-southern Ethiopia. To meet the objectives of this graduation thesis primary and secondary datasets were used.

This study first detects a time-series change of 1987, 2003, and 2020 LULC using the supervised image classification method with maximum likelihood classification (MLC) algorithm. Secondly, 2050 LULC dynamics was predicted with a model Multi-Layer Perceptron Neural Network and Cellular Automata-Markov Chain model (MLP NN-CA-MC) found in the software of TerrSet18.32 (Clark Labs, Clark University, Worcester, MA, USA) via its extension IDRISI GIS analysis. Both anthropogenic and environmental deriver variables were considered in this study to predict 2050 LULC. Thirdly, to estimate the future impact of climate change on soil erosion the ensemble models of RCM precipitation data which were bias-corrected by distribution mapping method was used under two emission scenarios (RCP4.5 and RCP8.5). Finally, to evaluate the annual soil loss rate for the baseline periods 1987, 2003, and 2020 based on LULC category, slope classes, and sub-watershed level and for the future period (2050) under both scenarios with a predicted 2050 LULC, the RUSLE model was used. Using the RUSLE model, the main factors which govern soil erosion: rainfall-runoff erosivity (R_factor), soil erodibilty characteristics (K-factor), topography (LS-factor), land cover management (C-factor), and support practice (P-factor) were computed in Arc GIS 10.8 (Environmental Systems Research Institute (Esri), Inc., Redlands, CA, USA).

According to this study, seven different LULC types were identified in the Sile river watershed. This LULC includes; cultivation land, forest land, bare land, grazing land, shrubland, banana land cover, and water body. Historically, in both periods from the year 1987 to 2003 and 2003 to 2020, cultivation land, bare land, and banana land cover were expanded at the expense of shrubland, forest land, grazing land, and water body decline. The study revealed, the Sile River watershed experienced substantial LULC alteration and will also be prolonged for the coming several years. Cultivation land, barren land, and banana land were expected to increase from 12,793 ha to 14,562 ha a change of (14%), 4133 ha to 4,791 ha a change of (17%), and 1,257 ha to 1,631 ha (50%) on the year of 2020 to 2050 respectively. Whereas, shrubland, forest, and grazing land were predicted to decline from 6,539 ha to 4,711 ha a reduction of (30%), 1295 ha to 728 ha a decline of (54%), and 1,386 ha to 990 ha a decline (29%) on the period of 2020 to 2050 respectively. Based on the RS-GIS-based RUSLE modeling analysis, the mean annual soil loss for the years 1987, 2003, and 2020 were 13.05 t-ha^{-1} year^{-1}, 21.04 t-ha^{-1} year$^{-1,}$ and 41.41 t-ha^{-1} year $^{-1}$ respectively. The total annual soil loss potential of the study area was 389,456 t-year^{-1}, 616,669 t-year$^{-1,}$ and 1,184,920 t-year^{-1} for the years 1987, 2003, and 2020 respectively from the area of 27,610 hectares. From all other LULC categories, the lowest average annual soil loss was observed from banana land cover. While highest and severe soil loss was detected on bare land and cultivation land respectively. The topography of the watershed was recognized as the major factor which influences soil erosion. In the study area, while the steepness of the slope increases soil erosion also increased. The risky and very severe soil loss is also estimated in sub-watersheds five and four. Finally, the results revealed in the Sile river watershed of Abaya- Chamo sub-basin Ethiopia, under RCP 4.5 and RCP 8.5 scenarios the average soil loss was 56.48 t-ha^{-1}year$^{-1,}$ and 57.11 t-ha^{-1} year^{-1} respectively for the year of 2050 was predicted. When we compare this result from a baseline period (2020) under both

scenarios (RCP 4.5 and RCP 8.5) soil loss has been expected to increase 36.40% and 38.19% respectively.

5.2 Conclusion

This study concluded that from 1987 to 2020 for 33-year temporal variation; cultivation land, bare land, and banana cover were expanded at the expense of other land covers; shrubland, forest land, grazing land, and water body were declined. The expansion of bare land at the expense of forest land, shrubland, and grazing land was found to be the major cause that is contributing to high soil loss rates in the study area. The predicted LULC of 2050 result also shows the trend from historical to future land use/ land cover change will be expected to be ongoing in the future. However, if the different natural resource conservation and intervention actions will carry out with a concerned body it will be not continued as predicted.

As a result of the study cultivation of steep lands, overgrazing, removal of vegetation cover and the temporal variation of rainfall-runoff (R) factor from 1987 to 2020 had been believed to be the leading factors that aggravated soil erosion in the study area. In addition, the future LULC and climate change will adversely affect the future soil erosion in the Sile River watershed of Abaya- Chamo sub-basin. Therefore, historically and for projected future periods due to the LULCC, climate variability, /and climate change the rate and magnitude of soil erosion in the study area were increased and expected to increase from time to time.

Recommendation

Based on the results and conclusions of this study, the following recommendations are recommended.

- Accordingly, to reduce the impacts of changing land use/land cover there should be appropriate & ecologically sound natural resource management interventions must be implemented.
- In the Sile river watershed of the Abaya-Chamo sub-basin, the combined impact of LULC and climate change is expected to have a considerable critical issue and it must need soil & water conservation policies, strategies, and intervention activities to mitigate the adverse impacts of climate change on soil erosion.
- Disseminating and boosting banana plantations in the remaining area of the watershed with the same agroecology should be highly recommended.
- It is recommended that the LULC category and slope class with having the mean annual soil above the Tolerable Soil Loss (TSL) limit of (11 t-ha^{-1} year^{-1}) should be considered for land management intervention planning.
- Priority should be given to those erosion-prone sub-watersheds to implement soil and water conservation measures.
- Since gully erosion is not considered in this study, further studies should be done to estimate soil loss from gully erosion .

6. REFERENCES

Addis, W., & Abebaw, A. (2015). Analysis of Selected Physicochemical Parameters of Soils Used for Cultivation of Garlic (*Allium sativum* L.). *Science, Technology and Arts Research Journal*, *3*(4), 29. https://doi.org/10.4314/star.v3i4.4

Ahlonsou, E., Ding, Y., & Schimel, D. (2018). *The Climate System : an Overview*.

Akehurst, A., Newley, P., & Hickey, M. (2008). Soil & Water Best Management Practices for NSW Banana Growers. In *NSW Department of Primary Industries*.

Alawamy, J. S., Balasundram, S. K., Husni, A., & Hanif, M. (2020). Detecting and Analyzing Land Use and Land Cover Changes in the Region of Al-Jabal Al-Akhdar, Libya Using Time-Series Landsat Data from 1985 to 2017. *Sustainability*, *12*, 1–24.

Alemu, M. M. (2017). Banana as a Cash Crop and Its Food Security and Socioeconomic Contribution: The Case of Southern Ethiopia, Arba Minch. *Journal of Environmental Protection*, *08*(03), 319–329. https://doi.org/10.4236/jep.2017.83024

Alexandersson, H. (1986). A homogeneity test was applied to precipitation data. *Journal of Climatology*, *6*(6), 661–675. https://doi.org/10.1002/joc.3370060607

Ambisa, Z., Tesfa, B., Olani, T., & Abdeta, D. (2019). Review on the Production and Marketing of Banana in Ethiopia. *World Journal of Agriculture and Soil Science*, *2*(1), 1–9. https://doi.org/10.33552/wjass.2019.02.000529

Angima, S. D., Stott, D. E., O'Neill, M. K., Ong, C. K., & Weesies, G. A. (2003). Soil erosion prediction using RUSLE for central Kenyan highland conditions. *Agriculture, Ecosystems and Environment*, *97*(1–3), 295–308. https://doi.org/10.1016/S0167-8809(03)00011-2

Arnold, J. G., Srinivasan, R., Muttiah, R. S., & Williams, J. R. (2012). Large area hydrologic modeling and assessment part I: Model development. In *Journal of the American Water Resources Association* (Vol. 34, Issue 1, pp. 73–89). https://doi.org/10.1111/j.1752-1688.1998.tb05961.x

Arsanjani, J. J., Kainz, W., & Mousivand, A. J. (2011). Tracking dynamic land-use change using spatially explicit Markov chain based on cellular automata: The case of Tehran. *International Journal of Image and Data Fusion*, *2*(4), 329–345. https://doi.org/10.1080/19479832.2011.605397

Asmamaw, L. B., & Mohammed, A. A. (2019). Remote Sensing Applications : Society and Environment Identi fi cation of soil erosion hotspot areas for sustainable land management in the Gerado catchment , North-eastern Ethiopia. *Remote Sensing Applications: Society and Environment*, *13*(February 2018), 306–317. https://doi.org/10.1016/j.rsase.2018.11.010

Ayele, G. T., Demessie, S. S., Mengistu, K. T., Tilahun, S. A., & Melesse, A. M. (2016). Landscape Dynamics, Soils and Hydrological Processes in Varied Climates. In *Springer International Publishing Switzerland* (pp. 1–839). https://doi.org/https://doi.org/10.1007/978-3-319-18787-7_4 Copyright

AyeleElias, G., Chunju, Z., & Yihong, Z. (2019). Assessment and Mapping of Land Use Change by Remote Sensing and GIS : A Case Study of Abaya Chamo Sub-basin, Ethiopia. *Nature Environment and Pollution Technology An International Quarterly Scientific Journal*, *18*(2), 549–554.

Balabathina, V. N., Raju, R. P., Mulualem, W., & Tadele, G. (2020). Estimation of soil loss using remote sensing and GIS-based universal soil loss equation in the northern catchment of Lake Tana Sub-basin, Upper Blue Nile Basin, Northwest Ethiopia. *Environmental Systems Research*, *9*(1). https://doi.org/10.1186/s40068-020-00203-3

Belay, T., & Mengistu, D. A. (2021). Impacts of land use/land cover and climate changes on soil erosion in Muga watershed , Upper Blue Nile basin (Abay), Ethiopia. *Ecological Processes*. https://doi.org/10.1186/s13717-021-00339-9

Belihu, M., Tekleab, S., Abate, B., & Bewket, W. (2020). Hydrologic response to land use land cover change in the Upper Gidabo Watershed, Rift Valley Lakes Basin, Ethiopia. *HydroResearch*, *3*, 85–94. https://doi.org/10.1016/j.hydres.2020.07.001

Benavidez, R., Jackson, B., Maxwell, D., & Norton, K. (2018). A review of the (Revised) Universal Soil Loss Equation ((R)USLE): With a view to increasing its global applicability and improving soil loss estimates. *Hydrology and Earth System Sciences*, *22*(11), 6059–6086. https://doi.org/10.5194/hess-22-6059-2018

Bewket, W., & Teferi, E. (2009). Assessment of Soil Erosion Hazard and Prioritization for Treatment at the Watershed Level: Case study in the Chemoga watershed, Blue Nile basin, Ethiopia. *Land Degradation & Development*, *20*, 609–622. https://doi.org/10.1002/ldr.944

Birhane, E., Ashfare, H., Fenta, A. A., Hishe, H., Gebremedhin, M. A., G. wahed, H., & Solomon, N. (2019). Land use land cover changes along topographic gradients in Hugumburda national forest priority area, Northern Ethiopia. *Remote Sensing Applications: Society and Environment*, *13*(November), 61–68.

https://doi.org/10.1016/j.rsase.2018.10.017

Borrelli, P., Alewell, C., Alvarez, P., Anache, J. A. A., Baartman, J., Ballabio, C., Bezak, N., Biddoccu, M., Cerdà, A., Chalise, D., Chen, S., Chen, W., De Girolamo, A. M., Gessesse, G. D., Deumlich, D., Diodato, N., Efthimiou, N., Erpul, G., Fiener, P., … Panagos, P. (2021). Soil erosion modelling: A global review and statistical analysis. *Science of the Total Environment*, *780*. https://doi.org/10.1016/j.scitotenv.2021.146494

Brhane, G., & Mekonen, K. (2009). Estimating soil loss using Universal Soil Loss Equation (USLE) for soil conservation planning at Medego Watershed, Northern Ethiopia. *Journal of American Science*, *5*(1), 58–69. https://doi.org/doi:10.7537/marsjas050109.10

Buğday, E., & Erkan Buğday, S. (2019). Modeling and simulating land use/cover change using artificial neural network from remotely sensing data. *Cerne*, *25*(2), 246–254. https://doi.org/10.1590/01047760201925022634

Carter, M. R., & Gregorich, E. G. (Eds.). (2006). *Soil Sampling and Methods of Analysis* (Second Edi). Canadian Society of Soil Science.

Chapman, S., Birch, C. E., Chapman, S., Birch, C. E., Galdos, M. V, Pope, E., Davie, J., Bradshaw, C., Eze, S., & Marsham, J. H. (2021). Assessing the impact of climate change on soil erosion in East Africa using a convection- permitting climate model Assessing the impact of climate change on soil erosion in East Africa using a convection-permitting climate model. *Environmental Reaserchserch Letters*.

Chen, C., Tfwala, S. S., & Tsai, C. (2020). Climate Change Impacts on Soil Erosion and Sediment Yield in a Watershed. *Water*, *12*. https://doi.org/10.3390/w12082247

Chuenchum, P., Xu, M., & Tang, W. (2020). Estimation of soil erosion and sediment yield in the lancang-mekong river using the modified revised universal soil loss equation and GIS techniques. *Water (Switzerland)*, *12*(1), 1–12. https://doi.org/10.3390/w12010135

Coffey, R. (2013). *The difference between "land use" and "land cover."* Michigan State University Extension.

Congalaton, R. G., & Green, K. (2008). Assessing the Accuracy of Remotely Sensed Data: Principles and Practices. In *The Photogrammetric Record* (Second Edi, Vol. 25, Issue 130). Taylor & Francis Group. https://doi.org/10.1111/j.1477-9730.2010.00574_2.x

Congalton, R. G. (1991). A review of assessing the accuracy of classifications of remotely sensed data. *Remote Sensing of Environment*, *37*(1), 35–46. https://doi.org/10.1016/0034-4257(91)90048-B

Cooney, C. M. (2012). Downscaling Climate Models:Sharpening the Focus on Local-Level Changes. In *Environmental Health Perspectives* (Vol. 120, Issue 1). https://doi.org/https://doi.org/10.1289/ehp.120-a22

Davidson, O. (2014). Summary for Policymakers Emissions Scenarios. In *International Panel on Climate Change* (Issue April 2007). http://ebooks.cambridge.org/ref/id/CBO9781107415416A011

Deep, S. (2014). Urban sprawl modeling using cellular automata. *The Egyptian Journal of Remote Sensing and Space Sciences*, *17*(2), 179–187. https://doi.org/10.1016/j.ejrs.2014.07.001

Dersseh, M. G., Kibret, A. A., Tilahun, S. A., Worqlul, A. W., Moges, M. A., Dagnew, D. C., Abebe, W. B., & Melesse, A. M. (2019). Potential of Water Hyacinth Infestation on Lake Tana ,. *Water 2019*, *11*(9), 1921.

Devatha, C. P., Deshpande, V., & Renukaprasad, M. S. (2015). Estimation of Soil loss Using USLE Model for Kulhan Watershed, Chattisgarh- A Case Study. *Aquatic Procedia*, *4*(Icwrcoe), 1429–1436. https://doi.org/10.1016/j.aqpro.2015.02.185

Dibaba, W. T., Demissie, T. A., & Miegel, K. (2020). Drivers and Implications of Land Use/Land Cover Dynamics in Finchaa Catchment, Northwestern Ethiopia. *Land*, *9*(113), 1–20. https://doi.org/10.3390/land9040113

Eastman, J. R. (2006a). *IDRISI Andes Guide to GIS and Image Processing* (Issue April).

Eastman, J. R. (2006b). *TerrSet Manual, Geospatial Monitoring and Modeling Sys- tem. Clark University, Worcester, USA. Clark University, Worcester, USA* . http://www.clarklabs.org/

Ebrahimzadeh, S., Motagh, M., Mahboub, V., & Mirdar Harijani, F. (2018). An improved RUSLE/SDR model for the evaluation of soil erosion. *Environmental Earth Sciences*, *77*(12), 0. https://doi.org/10.1007/s12665-018-7635-8

Eisenberg, J., & Muvundja, F. A. (2020). Quantification of Erosion in Selected Catchment Areas of the Ruzizi River (DRC) Using the (R)USLE Model. *Land*, *9*(4). https://doi.org/10.3390/LAND9040125

El Jazouli, A., Barakat, A., Ghafiri, A., El Moutaki, S., Ettaqy, A., & Khellouk, R. (2017). Soil erosion modeled with USLE, GIS, and remote sensing: a case study of Ikkour watershed in Middle Atlas (Morocco). *Geoscience Letters*, *4*(1). https://doi.org/10.1186/s40562-017-0091-6

Elias, E., Seifu, W., Tesfaye, B., & Girmay, W. (2019). Impact of land use / cover changes on lake ecosystem of Ethiopia central rift valley. *Cogent Food & Agriculture*, *5*(1). https://doi.org/10.1080/23311932.2019.1595876

Ellis, E., & Pontius, R. (2006). Land-use and land-cover change Local Processes and Global Impacts. In *Encyclopedia of Earth*.

Esa, E., Assen, M., & Legass, A. (2018). Implications of land use / cover dynamics on soil erosion potential of agricultural watershed , northwestern highlands of Ethiopia. *Environmental Systems Research*, *7*(21), 1–14. https://doi.org/10.1186/s40068-018-0122-0

Fenta, A. A., Yasuda, H., Shimizu, K., Haregeweyn, N., & Negussie, A. (2016). Dynamics of Soil Erosion as Influenced by Watershed Management Practices: A Case Study of the Agula Watershed in the Semi-Arid Highlands of Northern Ethiopia. *Environmental Management*, *58*(5), 889–905. https://doi.org/10.1007/s00267-016-0757-4

Fowler, H. J., Blenkinsop, S., & Tebaldi, C. (2007). Linking climate change modelling to impacts studies: Recent advances in downscaling techniques for hydrological modelling. *International Journal of Climatology*, *27*(12), 1547–1578. https://doi.org/10.1002/joc.1556

Garedew, E., Sandewall, M., Soderberg, U., & Campbell, B. M. (2009). Land-Use and Land-Cover Dynamics in the Central Rift Valley of Ethiopia. *Environmental Management*, *44*, 683–694. https://doi.org/10.1007/s00267-009-9355-z

Gashaw, T., Tulu, T., & Argaw, M. (2018). Erosion risk assessment for prioritization of conservation measures in Geleda watershed, Blue Nile basin, Ethiopia. *Environmental Systems Research*, *6*(1), 1–14. https://doi.org/10.1186/s40068-016-0078-x

Gashaw, T., Worqlul, A. W., Dile, Y. T., Addisu, S., Bantider, A., & Zeleke, G. (2020). Heliyon Evaluating potential impacts of land management practices on soil erosion in the Gilgel Abay watershed , upper Blue Nile basin. *Heliyon*, *6*(January), e04777. https://doi.org/10.1016/j.heliyon.2020.e04777

Gavlak, R., Horneck, R., & Miller, R. O. (2005). Potassium Fixation Test (Incubation Method). *Soil, Plant and Water Reference Methods for the Western Region*, *1*, 129–

134.

Gebeyehu, G., & Soromessa, T. (2018). Status of soil organic carbon and nitrogen stocks in Koga Watershed Area, Northwest Ethiopia. *Agriculture and Food Security*, *7*(1), 1–10. https://doi.org/10.1186/s40066-018-0162-8

Gee, & Bauder. (1986). Particle size analysis. Methods of soil analysis. *Am Soc Agron.*, *7*, 383–411. https://doi.org/10.1186/s40068-019-0149-x

Gelagay, H. S., & Minale, A. S. (2016). Soil loss estimation using GIS and Remote sensing techniques: A case of Koga watershed, Northwestern Ethiopia. *International Soil and Water Conservation Research*, *4*(2), 126–136. https://doi.org/10.1016/j.iswcr.2016.01.002

Genet, A. (2020). Population Growth and Land Use Land Cover Change Scenario in Ethiopia. *International Journal of Environmental Protection and Policy*, *8*(4), 77–85. https://doi.org/10.11648/j.ijepp.20200804.12

Gessesse, B., & Bewket, W. (2014). Drivers and Implications of Land Use and Land Cover Change in the Central Highlands of Ethiopia : Evidence from Remote Sensing and Socio-demographic Data Integration. *EJOSSAH*, *9*(2).

Gettelman, A., & Rood, R. B. (2016). Demystifying Climate Models: A Users Guide to Earth System Models. In *Earth Systems Data and Models* (Vol. 2).

Gezahegn, W. W., & Harka, A. E. (2020). E ff ect of Land Use and Land Cover Change on Soil Erosion in Erer Sub-Basin, Northeast Wabi Shebelle Basin, Ethiopia. *Land*, *9*(111), 6–25.

Gharaibeh, A., Shaamala, A., Obeidat, R., & Al-kofahi, S. (2020). Improving land-use change modeling by integrating ANN Improving land-use change modeling by integrating ANN with Cellular Automata-Markov Chain model. *Heliyon*, *6*(September), 1–18. https://doi.org/10.1016/j.heliyon.2020.e05092

Gidey, E., Dikinya, O., Sebego, R., Segosebe, E., & Zenebe, A. (2017). Cellular automata and Markov Chain (CA_Markov) model-based predictions of future land use and land cover scenarios (2015–2033) in Raya, northern Ethiopia. *Modeling Earth Systems and Environment*, *3*(4), 1245–1262. https://doi.org/10.1007/s40808-017-0397-6

Giorgi, F., & Gutowski, W. J. (2015). Regional Dynamical Downscaling and the CORDEX Initiative. *Annual Review of Environment and Resources*, *40*, 467–490. https://doi.org/10.1146/annurev-environ-102014-021217

Giorgi, F., & Gutowski, W. J. (2016). Coordinated Experiments for Projections of Regional Climate Change. *Current Climate Change Reports*, *2*(4), 202–210. https://doi.org/10.1007/s40641-016-0046-6

Girma, R., Fürst, C., & Moges, A. (2022). Land use land cover change modeling by integrating artificial neural network with cellular Automata-Markov chain model in Gidabo river basin, main Ethiopian rift. *Environmental Challenges*, *6*(December 2021), 100419. https://doi.org/10.1016/j.envc.2021.100419

Girma, R., & Gebre, E. (2020). Spatial modeling of erosion hotspots using GIS - RUSLE interface in Omo - Gibe river basin , Southern Ethiopia : implication for soil and water conservation planning. *Environmental Systems Research*. https://doi.org/10.1186/s40068-020-00180-7

Girmay, G., Moges, A., & Muluneh, A. (2020). Estimation of soil loss rate using the USLE model for Agewmariayam Watershed, northern Ethiopia. *Agriculture and Food Security*, *9*(1), 1–12. https://doi.org/10.1186/s40066-020-00262-w

Girmay, G., Moges, A., & Muluneh, A. (2021). Assessment of Current and Future Climate Change Impact on Soil Loss Rate of Assessment of Current and Future Climate Change Impact on Soil Loss Rate of Agewmariam Watershed , Northern Ethiopia. *Air, Soil and Water Research*, *14*(March), 1–11. https://doi.org/10.1177/1178622121995847

Gorfu, D., & Ahmed, E. (2011). *Crops and Agro-ecological Zones of Ethiopia*. 47. http://www.google.dk/url?sa=t&rct=j&q=&esrc=s&source=web&cd=1&ved=0CDQQFjAA&url=http://prrp-ethiopia.org/index.php/component/phocadownload/category/1-public-documents?download=51:crops-and-agro-ecological-zones-total-dereje-gorfu&ei=X91jUbLDFYH27AbBtYGgCg

Gupta, S., & Kumar, S. (2017). Simulating climate change impact on soil erosion using RUSLE model − A case study in a watershed of mid-Himalayan landscape. *Indian Academy of Sciences*. https://doi.org/10.1007/s12040-017-0823-1

Hamad, R., Balzter, H., & Kolo, K. (2018). Predicting land use/land cover changes using a CA-Markov model under two different scenarios. *Sustainability (Switzerland)*, *10*(10), 1–23. https://doi.org/10.3390/su10103421

Haregeweyn, N., Tsunekawa, A., Poesen, J., Tsubo, M., Meshesha, D. T., Fenta, A. A., Nyssen, J., & Adgo, E. (2017). Comprehensive assessment of soil erosion risk for better land use planning in river basins: Case study of the Upper Blue Nile River. *Science of the Total Environment*, *574*, 95–108. https://doi.org/10.1016/j.scitotenv.2016.09.019

Hassen, E. E., & Assen, M. (2017). Land use / cover dynamics and its drivers in Gelda catchment , Lake Tana watershed ,. *Environmental Systems Research*, *6*(4), 1–13. https://doi.org/10.1186/s40068-017-0081-x

Helden. (1987). *An assessment of woody biomass, community forests, land use and soil erosion in Ethiopia.*

Henricksen, B. L., Adiei-TwumMayer, D. C., Mayer, L., Pauw, E. de, R.A.Schipper, & Wicks, .A. (1988). Master land use plan Ethiopia. *FAO*.

Hurni, H. (1985). Erosion–productivity–conservation systems in Ethiopia. *IV International Conference on Soil Conservation November 3-9, 1985 Maracay, Venezuela*, *January 1985*, 654–674.

Hurni, H., Tato, K., & Zeleke, G. (2005). The Implications of Changes in Population , Land Use , and Land Management for Surface Runoff in the Upper Nile Basin Area of Ethiopia. *Mountain Research and Development*, *25*(2), 147–154.

Hyandye, C., & Martz, L. W. (2017). A Markovian and cellular automata land-use change predictive model of the Usangu Catchment. *International Journal of Remote Sensing*, *38*(1), 64–81. https://doi.org/10.1080/01431161.2016.1259675

Igwe, P. U., Onuigbo, A. ., Chinedu, O. ., Ezeaku, I. ., & Muoneke, M. . (2017). Soil Erosion: A Review of Models and Applications. *International Journal of Advanced Engineering Research and Science*, *4*(12), 138–150. https://doi.org/10.22161/ijaers.4.12.22

Issaka, S., & Ashraf, M. A. (2017). Impact of soil erosion and degradation on water quality: a review. *Geology, Ecology, and Landscapes*, *1*(1), 1–11. https://doi.org/10.1080/24749508.2017.1301053

Jacob, D. (2009). Regional Climate Models: Linking Global Climate Change to Local Impacts. In *Encyclopedia of Complexity and Systems Science Springer, New York, NY*. Nature Publishing Group UK. https://doi.org/https://doi.org/10.1007/978-0-387-30440-3

James, S., & Clayton, H. (1960). Double-Mass Curves. *WaterSupply Paper 1541B*, 66. http://dspace.udel.edu:8080/dspace/handle/19716/1592

Kafy, A. A., Naim, M. N. H., Subramanyam, G., Faisal, A. Al, Ahmed, N. U., Rakib, A. Al, Kona, M. A., & Sattar, G. S. (2021). Cellular Automata approach in dynamic modelling of land cover changes using RapidEye images in Dhaka, Bangladesh. *Environmental Challenges*, *4*(March). https://doi.org/10.1016/j.envc.2021.100084

Kaltenrieder, J. (2007). *Adaptation and Validation of the Universal Soil Loss Equation (USLE) for the Ethiopian-Eritrean Highlands. MSc Thesis*. 1–116.

Kavian, A., Hoseinpoor Sabet, S., Solaimani, K., & Jafari, B. (2017). Simulating the effects of land use changes on soil erosion using RUSLE model. *Geocarto International*, *32*(1), 97–111. https://doi.org/10.1080/10106049.2015.1130083

Khawaldah, H. A. (2016). A Prediction of Future Land Use / Land Cover in Amman Area Using GIS-Based Markov Model and Remote Sensing. *Journal of Geographic Information SystemSystem*, *8*, 412–427.

Kibret, S., Lautze, J., McCartney, M., Nhamo, L., & Wilson, G. G. (2016). Malaria and large dams in sub-Saharan Africa: Future impacts in a changing climate. *Malaria Journal*, *15*(1), 1–14. https://doi.org/10.1186/s12936-016-1498-9

Kogo, B. K., Kumar, L., & Koech, R. (2020). Impact of land use/cover changes on soil erosion in western kenya. *Sustainability (Switzerland)*, *12*(22), 1–17. https://doi.org/10.3390/su12229740

Koko, A. F., Yue, W., Abubakar, G. A., Hamed, R., & Alabsi, A. A. N. (2020). Monitoring and predicting spatio-temporal land use/land cover changes in Zaria City, Nigeria, through an integrated cellular automata and markov chain model (CA-Markov). *Sustainability (Switzerland)*, *12*(24), 1–21. https://doi.org/10.3390/su122410452

Kouli, M., Soupios, P., & Vallianatos, F. (2009). Soil erosion prediction using the Revised Universal Soil Loss Equation (RUSLE) in a GIS framework, Chania, Northwestern Crete, Greece. *Environmental Geology*, *57*(3), 483–497. https://doi.org/10.1007/s00254-008-1318-9

Laflen, Lane, & Foster. (1991). WEPP: a new generation of erosion prediction technology. *Soil Water Conserv*, *46*, 34–38.

Lal, R. (2014). Soil conservation and ecosystem services. *International Soil and Water Conservation Research*, *2*(3), 36–47. https://doi.org/10.1016/S2095-6339(15)30021-6

Lambin, E. F., Geist, H. J., & Lepers, E. (2003). DYNAMICS OF LAND- USE AND LAND- COVER CHANGE IN TROPICAL REGIONS. In *Annuual Reviews Environmetal Resource* (Issue 28, pp. 205–241). https://doi.org/10.1146/annurev.energy.28.050302.105459

Leta, M. K., Demissie, T. A., & Tränckner, J. (2021). Modeling and Prediction of Land Use Land Cover Change Dynamics Based on Land Change Modeler (LCM) in Nashe Watershed , Upper Blue Nile Basin , Ethiopia. *Sustainability*, *11*. https://doi.org/10.3390/SU13073740

Lillesand, T. M., Kiefer, R. W., & Chipman, J. W. (2015). *Remote sensing and image interpretation* (Seventh Ed). JohnWiley & Sons, Inc.

Lindbo, D., Havlin, J., Kozlowski, D., Robinson, C., L indbo, D. L., Kozlowski, D. A., & Robinson, C. (2012). *Know Soil, Know Life*. https://doi.org/10.2136/2012.knowsoil.c1

Liping, C., Yujun, S., & Saeed, S. (2018). Monitoring and predicting land use and land cover changes using remote sensing and GIS techniques—A case study of a hilly area, Jiangle, China. *PLoS ONE*, *13*(7), 1–23. https://doi.org/10.1371/journal.pone.0200493

Manyiwa, T., & Dikinya, O. (2013). Using universal soil loss equation and soil erodibility factor to assess soil erosion in Tshesebe village, north east Botswana. *African Journal of Agricultural Research*, *8*(30), 4170–4178. https://doi.org/10.5897/AJAR2013.7081

Maraun, D. (2016). Bias Correcting Climate Change Simulations - a Critical Review. *Current Climate Change Reports*, *2*(4), 211–220. https://doi.org/10.1007/s40641-016-0050-x

McIvor, I., Youjun, H., Daoping, L., Eyles, G., & Pu, Z. (2014). Agroforestry: Conservation Trees and Erosion Prevention. *Encyclopedia of Agriculture and Food Systems*, *1*, 208–221. https://doi.org/10.1016/B978-0-444-52512-3.00247-3

Mearns, L. O., & Hulme, M. (2001). Climate Scenario Development. *Climate Change 2001: The Physical Science Basis. Contribution of Working Group I to the Third Assessment Report of the Intergovernmental Panel on Climate Change*, *May 2014*, 739–768.

Mekonnen, F. (2014). *The history and future of banana in Arba Minch, Ethiopia*. Livestock and Irrigation Value Chains for Ethiopian Smallholders Project. https://doi.org/10.1007/978-3-030-33443-7_3

Mendez, M., Maathuis, B., Hein-Griggs, D., & Alvarado-Gamboa, L.-F. (2020).

Performance Evaluation of Bias Correction Methods for Climate Change Monthly Precipitation Projections over Costa Rica. *Water*, *12*(482). https://doi.org/10.3390/w12020482

Mengistu, D. A., & Salami, A. T. (2007). Application of remote sensing and GIS inland use/land cover mapping and change detection in a part of south western Nigeria. *African Journal of Environmental Science and Technology*, *1*(5), 99–109. http://www.academicjournals.org/AJEST

Mengistu, D. A., Waktola, D. K., & Woldetsadik, M. (2012). Detection and analysis of land-use and land-cover changes in the Midwest escarpment of the Ethiopian Rift Valley. *Journal of Land Use Science*, *7*(3), 239–260. https://doi.org/10.1080/1747423X.2011.562556

Meshesha, T. W., Tripathi, S. K., & Khare, D. (2016). Analyses of land use and land cover change dynamics using GIS and remote sensing during 1984 and 2015 in the Beressa Watershed Northern Central Highland of Ethiopia. *Modeling Earth Systems and Environment*, *2*(4). https://doi.org/10.1007/s40808-016-0233-4

Moges, D. M., & Bhat, H. G. (2017). Integration of geospatial technologies with RUSLE for analysis of land use / cover change impact on soil erosion : case study in Rib watershed , north - western highland Ethiopia. *Environmental Earth Sciences*, *76*, 1–14. https://doi.org/10.1007/s12665-017-7109-4

Moges, D. M., Kmoch, A., Bhat, H. G., & Uuemaa, E. (2020). Future soil loss in highland Ethiopia under changing climate and land use. *Springer-Verlag GmbH Germany*, *20*(32). https://doi.org/10.1007/s10113-020-01617-6

Moisa, M. B., Negash, D. A., Merga, B. B., & Gemeda, D. O. (2021). Impact of land-use and land-cover change on soil erosion using the RUSLE model and the geographic information system: a case of Temeji watershed, Western Ethiopia. *Journal of Water and Climate Change*, *00*(0), 1–17. https://doi.org/10.2166/wcc.2021.131

Molla, T., & Sisheber, B. (2017). Estimating soil erosion risk and evaluating erosion control measures for soil conservation planning at Koga watershed in the highlands of Ethiopia. *Solid Earth*, *8*(1), 13–25. https://doi.org/10.5194/se-8-13-2017

Moore, I. D., & Wilson, J. P. (1992). Length-slope factors for the revised universal soil loss equation: simplified method of estimation. *Journal of Soil & Water Conservation*, *47*(5), 423–428.

Morgan, & Nearing. (2011). *Universal Soil Loss Equation and Revised Universal Soil Loss Equation*.

MoWIE. (2002). Water Sector Development Program - Main report. In *Report: Vol. II* (Issue October).

Muke, M. (2019). Reported driving factors of land-use / cover changes and its mounting consequences in Ethiopia : A Review. *African Journal of Environmental Science and Technology*, *13*(7), 273–280. https://doi.org/10.5897/AJEST2019.2680

Mutayoba, E., & Kashaigili, J. J. (2017). Evaluation for the Performance of the CORDEX Regional Climate Models in Simulating Rainfall Characteristics over Mbarali River Catchment in the Rufiji Basin, Tanzania. *Journal of Geoscience and Environment Protection*, *05*(04), 139–151. https://doi.org/10.4236/gep.2017.54011

Nash, J. ., & Sutcliffe, J. . (1970). River Flow Forecasting through Conceptual Model. *Journal of Hydrology*, *10*, 282–290. https://doi.org/http://dx.doi.org/10.1016/0022-1694(70)90255-6

Nath, B., Wang, Z., Ge, Y., Islam, K., Singh, R. P., & Niu, Z. (2020). Land use and land cover change modeling and future potential landscape risk assessment using Markov-CA model and analytical hierarchy process. *ISPRS International Journal of Geo-Information*, *9*(2). https://doi.org/10.3390/ijgi9020134

Nearing, M., Pruski, F. F., & O'Neal, M. R. (2004). Expected climate change impacts on soil erosion rates: A review. *Journal of Soil and Water Conservation*, *59*(1), 43–50.

Negese, A. (2021). Impacts of Land Use and Land Cover Change on Soil Erosion and Hydrological Responses in Ethiopia. *Applied and Environmental Soil Science*, *2021*, 15–17. https://doi.org/10.1155/2021/6669438

Nelson, D. W., & Sommers, L. E. (1996). Total carbon, organic carbon, and organic matter. *Methods of Soil Analysis, Part 3: Chemical Methods*, *5*, 961–1010. https://doi.org/10.2136/sssabookser5.3.c34

Norovsuren, B., Tseveen, B., Batomunkuev, V., Renchin, T., Natsagdorj, E., Yangiv, A., & Mart, Z. (2019). Land cover classification using maximum likelihood method (2000 and 2019) at Khandgait valley in Mongolia. *IOP Conference Series: Earth and Environmental Science*, *381*(1). https://doi.org/10.1088/1755-1315/381/1/012054

Pal, S. C., & Chakrabortty, R. (2019). Modeling of water induced surface soil erosion and the potential risk zone prediction in a sub-tropical watershed of Eastern India. *Modeling Earth Systems and Environment*, *5*(2), 369–393. https://doi.org/10.1007/s40808-018-0540-z

Pandey, S., Kumar, P., Zlatic, M., Nautiyal, R., & Panwar, V. P. (2021). Recent advances in assessment of soil erosion vulnerability in a watershed. *International Soil and Water Conservation Research+++*. https://doi.org/https://doi.org/10.1016/j.iswcr.2021.03.001.

Pielke, R. A., Pitman, A., Niyogi, D., Mahmood, R., McAlpine, C., Hossain, F., Goldewijk, K. K., Nair, U., Betts, R., Fall, S., Reichstein, M., Kabat, P., & de Noblet, N. (2011). Land use/land cover changes and climate: Modeling analysis and observational evidence. *Wiley Interdisciplinary Reviews: Climate Change*, *2*(6), 828–850. https://doi.org/10.1002/wcc.144

Prasannakumar, V., Vijith, H., Abinod, S., & Geetha, N. (2012). Estimation of soil erosion risk within a small mountainous sub-watershed in Kerala, India, using Revised Universal Soil Loss Equation (RUSLE) and geo-information technology. *Geoscience Frontiers*, *3*(2), 209–215. https://doi.org/10.1016/j.gsf.2011.11.003

Randall, D. A., Wood, R. A., Bony, S., Colman, R., Fichefet, T., Fyfe, J., & Kattsov, V. (2007). Climate Models and Their Evaluation. In *Cambridge University Press, Cambridge, United Kingdom and New York, NY, USA* (Vol. 323, pp. 589–662). http://scholar.google.com/scholar?hl=en&btnG=Search&q=intitle:Climate+Models+and+Their+Evaluation#0

Rathjens, H., Bieger, K., Srinivasan, R., & Arnold, J. G. (2016). *CMhyd User Manual Documentation for preparing simulated climate change data for hydrologic impact studies*.

Regasa, M. S. R. M. N. and D. (2021). A Review on Land Use and Land Cover Change in Ethiopian Basins Motuma. *Land*, *10*(585), 1–18.

Renard, K. G., Foster, G. ., Weesies, G. ., McCool, D. K., & Yoder, D. C. (1997). Predicting Soil Erosion by Water. A Guide to Conservation Planning With the Revised Universal Soil Loss Equation (RUSLE). In *ASAE Publ.*

Routschek, A., Schmidt, J., Enke, W., & Deutschlaender, T. (2014). Future soil erosion risk — Results of GIS-based model simulations for a catchment in Saxony/Germany. *Geomorphology*, *206*(0169-555X), 299–306. https://doi.org///doi.org/10.1016/j.geomorph.2013.09.033.

Roy, S., Farzana, K., Papia, M., & Hasan, M. (2015). Monitoring and Prediction of Land Use / Land Cover Change using the Integration of Markov Chain Model and Cellular Automation in the Southeastern Tertiary Hilly Area of Bangladesh. *International Journal of Sciences: Basic and Applied Research*, *24*(4), 125–148.

Rwanga, S. S., & Ndambuki, J. M. (2017). Accuracy Assessment of Land Use/Land Cover Classification Using Remote Sensing and GIS. *International Journal of Geosciences*, *08*(04), 611–622. https://doi.org/10.4236/ijg.2017.84033

Sang, L., Zhang, C., Yang, J., Zhu, D., & Yun, W. (2011). Simulation of land use spatial pattern of towns and villages based on CA – Markov model. *Mathematical and Computer Modelling*, *54*(3–4), 938–943. https://doi.org/10.1016/j.mcm.2010.11.019

Sardari, M. R. A., Bazrafshan, O., Panagopoulos, T., & Sardooi, E. R. (2019). Modeling the impact of climate change and land use change scenarios on soil erosion at the minab dam watershed. *Sustainability (Switzerland)*, *11*(12). https://doi.org/10.3390/su10023353

Singh, A. (1989). Review Articlel: Digital change detection techniques using remotely-sensed data. *International Journal of Remote Sensing*, *10*(6), 989–1003. https://doi.org/10.1080/01431168908903939

Sisay, A. (2014). Landscape scale Soil Erosion Modeling and Risk Mapping of Mountainous areas in Eastern Escarpment of Wondo Genet Watershed, Ethiopia. *International Research Journal of Arts and Social Sciences*, *04*(06), 107–116. https://doi.org/10.14303/irjas.2014.040

Tan, Y., Guzman, S. M., Dong, Z., & Tan, L. (2020). Selection of E ff ective GCM Bias Correction Methods and Evaluation of Hydrological Response under Scenarios, Future Climate. *MDPI*, *8*(108), 1–21. https://doi.org/10.3390/cli8100108

Telkar, S. G., Singh, S. P. S., Dey, J. K., & Kant, K. (2015). Soil Erosion: Types and their mechanism soil erosion. *International Journal of Economic Plants*, *2*(4), 178–180. https://www.pphouse.org/ijep-article-details.php?art=47

Teutschbein, C., & Seibert, J. (2012). Bias correction of regional climate model simulations for hydrological climate-change impact studies: Review and evaluation of different methods. *Journal of Hydrology*, *456–457*, 12–29. https://doi.org/10.1016/j.jhydrol.2012.05.052

Trzaska, S., & Schnarr, E. (2014). A review of downscaling methods for climate change projections. In *United States Agency for International Development by Tetra Tech ARD* (Issue September).

Van Oost, K., Govers, G., & Desmet, P. (2000). Evaluating the effects of changes in landscape structure on soil erosion by water and tillage. *Landscape Ecology*, *15*(6), 577–589. https://doi.org/10.1023/A:1008198215674

Vittek, M., Brink, A., Donnay, F., Simonetti, D., & Desclée, B. (2013). Land cover change monitoring using landsat MSS/TM satellite image data over west Africa between 1975 and 1990. *Remote Sensing*, *6*(1), 658–676. https://doi.org/10.3390/rs6010658

Vuuren, D. P. Van, Edmonds, J., Kainuma, M., Riahi, K., Nakicenovic, N., Smith, S. J., & Rose, S. K. (2011). The representative concentration pathways : an overview. *Springer*, 5–31. https://doi.org/10.1007/s10584-011-0148-z

Walkley, A., & Black, I. A. (1934). An Examination of the Degtjareff Method for Determining Soil Organic Matter and a Proposed Modification of the Chromic Acid Titration Method. *Soil Science*, *37*, 29–38. https://doi.org/http://dx.doi.org/10.1097/00010694-193401000-00003

Wang, Z. Y., Lee, J. H. W., & Melching, C. S. (2015). River dynamics and integrated river management. In *River Dynamics and Integrated River Management*. https://doi.org/10.1007/978-3-642-25652-3

Wassie, S. B. (2020). Natural resource degradation tendencies in Ethiopia: a review. *Environmental Systems Research*, *9*(1), 1–29. https://doi.org/10.1186/s40068-020-00194-1

Wayne, G. P. (2003). *Representative Concentration Pathways*.

Wenner, C. G. (1983). Soil conservation in Kenya. In *Ambio* (Vol. 12, Issue 6). https://doi.org/10.1007/978-1-349-23206-2_6

Williams J.R. (1995). Chapter 25.The EPIC model. In V.P. Singh (ed.) Computer models of watershed hydrology. In *Water Resources Publications.*

Wischmeier, W. H., & Smith, D. D. (1978). *Predicting rainfall erosion losses- a guide to Conservation Planning. U.S Department of Agriculture, Agriculture Handbook* (Issue 537).

Woldemariam, G., Iguala, A., Tekalign, S., & Reddy, R. (2018). Spatial Modeling of Soil Erosion Risk and Its Implication for Conservation Planning: the Case of the Gobele Watershed, East Hararghe Zone, Ethiopia. *Land*, *7*(1), 25. https://doi.org/10.3390/land7010025

Woldesenbet, A. B., Wudmatas, S. D., & Denboba, M. A. (2020). Enset - based land use land cover change detection and its impact on soil erosion in Meki river watershed , Western Lake Ziway Sub - Basin , Central Rift Valley of Ethiopia. *Environmental Systems Research*. https://doi.org/10.1186/s40068-020-00198-x

WoldeYohannes, A., Cotter, M., Kelboro, G., & Dessalegn, W. (2018). Land use and land cover changes and their effects on the landscape of Abaya-Chamo basin, Southern Ethiopia. *Land*, *7*(1). https://doi.org/10.3390/land7010002

Wolka, K., Tadesse, H., Garedew, E., & Yimer, F. (2015). Soil erosion risk assessment in the Chaleleka wetland watershed, Central Rift Valley of Ethiopia. *Environmental Systems Research*, *4*(1), 1–12. https://doi.org/10.1186/s40068-015-0030-5

Worku, G., Teferi, E., Bantider, A., & Dile, Y. T. (2020). Statistical bias correction of regional climate model simulations for climate change projection in the Jemma sub-basin, upper Blue Nile Basin of Ethiopia. *Theoretical and Applied Climatology*, *139*(3–4), 1569–1588. https://doi.org/10.1007/s00704-019-03053-x

Worku, G., Teferi, E., Bantider, A., Dile, Y. T., & Taye, M. T. (2018). Evaluation of regional climate models performance in simulating rainfall climatology of Jemma sub-basin, Upper Blue Nile Basin, Ethiopia. *Dynamics of Atmospheres and Oceans*, *83*(June), 53–63. https://doi.org/10.1016/j.dynatmoce.2018.06.002

Wubie, M. A., Assen, M., & Nicolau, M. D. (2016). Patterns , causes and consequences of land use / cover dynamics in the Gumara watershed of lake Tana basin , Northwestern Ethiopia. *Environmental Systems Research*, 1–12. https://doi.org/10.1186/s40068-016-0058-1

Yadeta, L. T., Switoniak, M., Tessema, Y. M., & Gebregeorgis, E. G. (2020). *Soil Loss Estimation for Conservation Planning in the Welmel Watershed of the Genale Dawa*. 1–19.

Yesuph, A. Y., & Dagnew, A. B. (2019). Soil erosion mapping and severity analysis based on RUSLE model and local perception in the Beshillo Catchment of the Blue Nile Basin, Ethiopia. *Environmental Systems Research*, *8*(1), 1–22. https://doi.org/10.1186/s40068-019-0145-1

Yiferu, Y., Taddese, G., & Mebrate, T. (2018). Influence of soil erosion and conservation practices on soil physical properties in Ginaberet, Ethiopia. *Forestry Research and Engineering: International Journal*, *2*(5), 288–297. https://doi.org/10.15406/freij.2018.02.00062

Yirgu, T. (2018). Fruit Based Farming System and Threatened Landscape in the Wetlands of Abaya Chamo Basin, Southern Ethiopia. *International Journal of Social Research*, *2*(XX).

Zebire, D. A., Ayele, T., & Ayana, M. (2019). Characterizing soils and the enduring nature of land uses around the Lake Chamo Basin in South-West Ethiopia. *Journal of Ecology and Environment*, *43*(1), 1–32. https://doi.org/10.1186/s41610-019-0104-9

Zekarias, T., Govindu, V., Kebede, Y., & Gelaw, A. (2021). Degradation of wetlands and livelihood benefits of Lake Abaya-Chamo wetland, southern Ethiopia. *Current Research in Environmental Sustainability*, *3*, 100060. https://doi.org/10.1016/j.crsust.2021.100060

Zeleke, G. and, & Hurni, H. (2001). Landscape Dynamics and Soil Erosion Process Modeling in the North-Western Implications of Land Use and Land Cover Dynamics for Mountain Resource Degradation in the Northwestern Ethiopian Highlands. *Mountain Research and Development*, *21*(2), 184–191.

Zeleňáková, M., Harabinová, S., Mésároš, P., Abd-Elhamid, H., & Purcz, P. (2019). Modelling of erosion and transport processes. *Water (Switzerland)*, *11*(12), 1–12. https://doi.org/10.3390/w11122604

Zhong, B., Yang, A., Nie, A., Yao, Y., Zhang, H., Wu, S., & Liu, Q. (2015). Finer Resolution Land-Cover Mapping Using Multiple Classifiers and Multisource Remotely Sensed Data in the Heihe River Basin. *IEEE Journal of Selected Topics in Applied Earth Observations and Remote Sensing*, *8*(10), 4973–4992. https://doi.org/10.1109/JSTARS.2015.2461453

Zuazo, V. H. D., & Pleguezuelo, C. R. R. (2008). Soil-erosion and runoff prevention by plant covers. A review. *Agron Sustain Dev*, *28*(1), 65–86. https://doi.org/DOI: 10.1051/agro:2007062

7. APPENDICES

Appendix Table 1: Annual precipitation of 4 stations from 1987-2020

Year	Stations			
	Arbaminch	Gidole	Gato	Mirab Abay
1987	717.6	870.5	727.5	708.6
1988	**851.7**	**1138.6**	833.6	547.5
1989	945.7	1051.3	823.4	650.8
1990	996.4	720.8	812.2	**501.6**
1991	622.2	863.3	813.6	492.1
1992	776.9	867.2	**848.6**	393.9
1993	974.7	756.3	889.9	**817.0**
1994	874.6	771.0	817.5	659.6
1995	782.8	872.6	868.2	707.8
1996	932.5	1159.4	918	816.1
1997	810.5	*982.3*	835.7	1217.2
1998	856.8	687.4	**790.3**	952.8
1999	793.0	814.1	599.2	605.9
2000	780.9	**982.4**	762.2	779.4
2001	868.6	864.1	904.6	790.3
2002	1082.9	833.3	867.2	623.8
2003	814.2	**1206.2**	760.9	788.2
2004	881.1	709.6	897.2	796.7
2005	753.0	**1129.9**	986.6	844.6
2006	933.0	860.3	1159.7	979.1
2007	1128.4	**1384.3**	919.9	843.3
2008	1121.3	1504.7	906.9	594.0
2009	853.1	979.4	663.5	556.1
2010	639.5	1691.4	1128.3	1105.5
2011	1068.7	1633.2	**1003.7**	**937.8**
2012	**1079.7**	1447.8	1008.2	811.6
2013	1013.4	2996.3	880.2	735.8
2014	1061.1	**1730.9**	963.6	820.8
2015	866.2	1391.0	952.2	845.0
2016	1121.3	1765.9	720.9	**608.7**
2017	727.0	1802.5	**849.3**	767.2
2018	752.6	2340.2	588.4	912.8
2019	893.0	1251.0	855.6	762.8
2020	808.2	2627.1	762	988.1
Mean	**887.7**	**1255.5**	**856.4**	**763.6**

Source: (ENMA, 2021)

Appendix Table 2: Soil Sample location

SS. ID	Land use	Slope position	Soil color	X	Y
ID.1	Cultivation land	Upper	Brown	330207	645986
ID.2	Cultivation land	Middle	Brown	335506	655386
ID.3	Cultivation land	Lower	Brown	317969	668702
ID.4	Shrub land	Upper	Red	325420	653223
ID.5	Shrub land	Middle	Gray	325420	653223
ID.6	Shrub land	Lower	Gray	322272	665741
ID.7	Bare land	Upper	Brown	313901	666718
ID.8	Bare land	Middle	Gray	314781	664733
ID.9	Bare land	Lower	Gray	328784	649301
ID.10	Banana land	Upper	Black	336915	656830
ID.11	Banana land	Middle	Black	322569	654673
ID.12	Banana land	Lower	Black	321614	656434
ID.13	Grazing land	Upper	Gray	324086	653202
ID.14	Grazing land	Middle	Gray	327682	650840
ID.15	Grazing land	Lower	Gray	315555	671381
ID.16	Cultivation land	Upper	Gray	319340	665742
ID.17	Cultivation land	Middle	Gray	321177	669000
ID.18	Cultivation land	Lower	Gray	325708	669926
ID.19	Banana land	Upper	Black	332422	668669
ID.20	Banana land	Middle	Black	319259	672572
ID.21	Banana land	Lower	Black	316580	672076
ID.22	Forest land	Upper	Gray	329135	646681
ID.23	Forest land	Middle	Gray	330608	645609
ID.24	Forest land	Lower	Black	319731	662012
ID.25	Shrub land	Upper	Gray	319880	661538
ID.26	Shrub land	Middle	Gray	320664	660823
ID.27	Shrub land	Lower	Gray	320804	660004
ID.28	Forest land	Middle	Black	321385	659292
ID.29	Cultivation land	Middle	Gray	321632	656598
ID.30	Cultivation land	Lower	Black	318195	663395
ID.31	Grazing land	Upper	Red	317724	661946
ID.32	Grazing land	Middle	Red	328702	653054
ID.33	Grazing land	Lower	Gray	326782	653056
ID.34	Bare land	Upper	Red	326856	655003
ID.35	Bare land	Middle	Red	332712	655262
ID.36	Bare land	Lower	Gray	331798	656461
ID.37	Shrub land	Upper	Black	332751	656506
ID.38	Shrub land	Middle	Gray	333678	657902
ID.39	Shrub land	Lower	Gray	333561	658185

ID.40	Cultivation land	Upper	Gray	333603	658287
ID.41	Cultivation land	Middle	Gray	333528	658503
ID.42	Cultivation land	Lower	Gray	333764	658658
ID.43	Shrub land	Upper	Gray	333252	659055
ID.44	Shrub land	Middle	Red	332597	659756
ID.45	Shrub land	Lower	Red	332256	660243
ID.46	Bare land	Upper	Red	332049	661089
ID.47	Bare land	Middle	Gray	330778	662386
ID.48	Bare land	Lower	Red	329208	664305
ID.49	Banana land	Upper	Black	328346	664422
ID.50	Banana land	Middle	Black	330951	658253
ID.51	Banana land	Lower	Black	328649	656122
ID.52	Cultivation land	Upper	Gray	327463	659426
ID.53	Cultivation land	Middle	Gray	331028	659995
ID.54	Cultivation land	Lower	Gray	328583	660199
ID.55	Bare land	Upper	Red	333475	655361
ID.56	Bare land	Middle	Red	330878	654416
ID.57	Bare land	Lower	Gray	331898	656124
ID.58	Banana land	Upper	Gray	331608	660607
ID.59	Banana land	Middle	Black	329495	661745
ID.60	Banana land	Lower	Black	327328	659358
ID.61	Cultivation land	Upper	Gray	324214	656790
ID.62	Cultivation land	Middle	Red	323807	655036
ID.63	Cultivation land	Lower	Gray	327754	667884
ID.64	Shrub land	Upper	Red	323710	654806
ID.65	Shrub land	Middle	Gray	323453	654897
ID.66	Shrub land	Lower	Gray	322993	654919
ID.67	Cultivation land	Upper	Red	322825	655553
ID.68	Cultivation land	Middle	Red	322827	655866
ID.69	Cultivation land	Lower	Gray	322756	656462
ID.70	Grazing land	Upper	Gray	323204	654407
ID.71	Grazing land	Middle	Gray	317934	660544
ID.72	Grazing land	Lower	Gray	323221	659461
ID.73	Banana land	Upper	Black	315141	664984
ID.74	Banana land	Middle	Black	319730	666330
ID.75	Banana land	Lower	Black	320010	666116
ID.76	Cultivation land	Upper	Gray red	320496	666007
ID.77	Cultivation land	Middle	Black	320954	665719
ID.78	Cultivation land	Lower	Black	321285	666271
ID.79	Shrub land	Upper	Gray	317413	661990
ID.80	Shrub land	Middle	Gray	319346	662612

ID.81	Shrub land	Lower	Gray	320967	662748
ID.82	Bare land	Upper	Red	320151	652137
ID.83	Bare land	Middle	Red	327671	657576
ID.84	Bare land	Lower	Gray	327739	657773
ID.85	Banana land	Upper	Gray	328749	657494
ID.86	Banana land	Middle	Black	331457	659833
ID.87	Banana land	Lower	Black	331644	659715
ID.88	Cultivation land	Upper	Gray	327315	665001
ID.89	Cultivation land	Middle	Red	324112	652340
ID.90	Cultivation land	Lower	Gray	323383	653614
ID.91	Cultivation land	Upper	Gray	334619	652666
ID.92	Cultivation land	Middle	Gray	334071	652092
ID.93	Cultivation land	Lower	Gray	333347	651807
ID.94	Banana land	Upper	Black	333154	651190
ID.95	Banana land	Middle	Black	330004	652756
ID.96	Banana land	Lower	Black	331746	651330
ID.97	Forest land	Upper	Black	333922	652413
ID.98	Forest land	Middle	Red	334124	653012
ID.99	Forest land	Lower	Black	329996	652190
ID.100	Cultivation land	Upper	Red	328289	651642
ID.101	Cultivation land	Middle	Red	333547	652716
ID.102	Cultivation land	Lower	Gray	332849	655155

Appendix Table 3 : Laboratory result of soil samples for major soil properties affecting soil erodibility

SS. ID	%SAND	%Clay	%Silt	%OC	Fcsand	fcl_si	Forg	fhisand	K_Factor
ID.1	28	32	40	1.64	0.204	0.838	0.778	1.000	0.133
ID.2	18	38	44	1.44	0.223	0.830	0.801	1.000	0.148
ID.3	32	40	28	3.90	0.201	0.766	0.750	1.000	0.115
ID.4	20	34	46	1.91	0.219	0.847	0.762	1.000	0.141
ID.5	66	20	14	0.90	0.200	0.766	0.919	0.976	0.137
ID.6	22	56	22	1.95	0.204	0.684	0.760	1.000	0.106
ID.7	8	74	18	1.91	0.256	0.613	0.762	1.000	0.120
ID.8	42	32	26	2.30	0.200	0.786	0.753	1.000	0.118
ID.9	14	28	58	2.11	0.267	0.889	0.756	1.000	0.179
ID.10	28	28	44	2.50	0.205	0.863	0.752	1.000	0.133
ID.11	30	52	18	2.11	0.201	0.665	0.756	1.000	0.101
ID.12	26	42	32	0.78	0.203	0.778	0.943	1.000	0.149
ID.13	24	52	24	1.48	0.203	0.708	0.796	1.000	0.114

ID.14	22	38	40	1.64	0.210	0.818	0.778	1.000	0.134
ID.15	4	68	28	2.34	0.344	0.691	0.753	1.000	0.179
ID.16	14	48	38	3.43	0.233	0.783	0.750	1.000	0.137
ID.17	2	66	32	1.52	0.412	0.715	0.791	1.000	0.233
ID.18	28	28	44	2.03	0.205	0.863	0.758	1.000	0.134
ID.19	22	36	42	1.95	0.211	0.831	0.760	1.000	0.134
ID.20	20	42	38	3.08	0.213	0.800	0.750	1.000	0.128
ID.21	12	54	34	3.51	0.240	0.752	0.750	1.000	0.135
ID.22	46	24	30	1.72	0.200	0.838	0.772	1.000	0.129
ID.23	12	32	56	1.64	0.278	0.873	0.778	1.000	0.189
ID.24	27	28	45	1.54	0.207	0.865	0.789	1.000	0.141
ID.25	36	33	31	1.74	0.201	0.805	0.770	1.000	0.124
ID.26	19	42	39	3.26	0.215	0.803	0.750	1.000	0.130
ID.27	12	46	42	1.91	0.251	0.801	0.762	1.000	0.153
ID.28	56	20	24	0.90	0.200	0.834	0.919	0.997	0.153
ID.29	21	47	32	2.95	0.208	0.763	0.750	1.000	0.119
ID.30	28	52	20	2.91	0.201	0.681	0.750	1.000	0.103
ID.31	37	39	24	3.30	0.200	0.749	0.750	1.000	0.112
ID.32	63	23	14	1.21	0.200	0.747	0.846	0.987	0.125
ID.33	53	20	27	2.60	0.200	0.847	0.751	0.998	0.127
ID.34	46	32	22	3.32	0.200	0.764	0.750	1.000	0.115
ID.35	53	30	17	0.99	0.200	0.737	0.898	0.998	0.132
ID.36	38	32	30	2.48	0.200	0.804	0.752	1.000	0.121
ID.37	51	28	21	1.64	0.200	0.776	0.778	0.999	0.121
ID.38	65	15	20	2.61	0.200	0.845	0.751	0.981	0.125
ID.39	29	46	25	2.43	0.201	0.731	0.752	1.000	0.111
ID.40	19	60	21	1.32	0.206	0.667	0.822	1.000	0.113
ID.41	33	19	48	2.03	0.204	0.905	0.758	1.000	0.140
ID.42	34	38	28	2.20	0.201	0.773	0.755	1.000	0.117
ID.43	49	17	34	3.08	0.200	0.885	0.750	0.999	0.133
ID.44	31	54	35	2.81	0.202	0.756	0.751	1.000	0.114
ID.45	55	37	21	3.52	0.200	0.737	0.750	0.997	0.110
ID.46	26	32	44	2.64	0.207	0.849	0.751	1.000	0.132
ID.47	22	32	46	1.30	0.214	0.853	0.826	1.000	0.151
ID.48	11	28	61	3.81	0.300	0.893	0.750	1.000	0.201
ID.49	31	32	37	2.60	0.202	0.829	0.751	1.000	0.126
ID.50	30	27	43	1.91	0.204	0.864	0.762	1.000	0.134
ID.51	44	33	23	1.78	0.200	0.766	0.768	1.000	0.118
ID.52	46	45	9	1.48	0.200	0.584	0.796	1.000	0.093
ID.53	36	12	52	1.64	0.204	0.940	0.778	1.000	0.149
ID.54	23	47	30	1.34	0.205	0.754	0.818	1.000	0.126

ID.55	33	49	18	3.11	0.200	0.674	0.750	1.000	0.101
ID.56	23	13	64	1.52	0.236	0.946	0.791	1.000	0.177
ID.57	28	17	55	2.03	0.212	0.922	0.758	1.000	0.148
ID.58	44	47	9	2.95	0.200	0.578	0.750	1.000	0.087
ID.59	47	24	29	3.08	0.200	0.835	0.750	1.000	0.125
ID.60	29	54	17	1.15	0.201	0.651	0.858	1.000	0.112
ID.61	28	22	50	2.34	0.208	0.896	0.753	1.000	0.141
ID.62	37	12	51	2.75	0.203	0.939	0.751	1.000	0.143
ID.63	54	43	3	1.24	0.200	0.441	0.839	0.998	0.074
ID.64	22	20	58	2.33	0.228	0.915	0.753	1.000	0.157
ID.65	36	32	32	2.76	0.201	0.812	0.751	1.000	0.122
ID.66	47	30	23	2.20	0.200	0.778	0.755	1.000	0.117
ID.67	43	32	25	0.86	0.200	0.781	0.927	1.000	0.145
ID.68	24	28	48	2.71	0.212	0.871	0.751	1.000	0.139
ID.69	56	15	29	3.43	0.200	0.882	0.750	0.997	0.132
ID.70	34	46	20	0.56	0.200	0.699	0.975	1.000	0.136
ID.71	25	60	15	2.65	0.201	0.617	0.751	1.000	0.093
ID.72	43	19	38	2.72	0.200	0.885	0.751	1.000	0.133
ID.73	44	38	18	2.32	0.200	0.711	0.753	1.000	0.107
ID.74	49	17	34	1.27	0.200	0.885	0.832	0.999	0.147
ID.75	34	54	12	2.13	0.200	0.600	0.756	1.000	0.091
ID.76	24	37	39	3.76	0.207	0.819	0.750	1.000	0.127
ID.77	34	32	34	2.24	0.201	0.820	0.754	1.000	0.124
ID.78	36	32	32	2.77	0.201	0.812	0.751	1.000	0.122
ID.79	11	28	61	2.78	0.300	0.893	0.751	1.000	0.201
ID.80	44	32	24	1.95	0.200	0.776	0.760	1.000	0.118
ID.81	30	46	24	1.48	0.201	0.725	0.796	1.000	0.116
ID.82	41	35	24	1.87	0.200	0.764	0.763	1.000	0.117
ID.83	46	33	21	1.27	0.200	0.753	0.832	1.000	0.125
ID.84	36	38	26	2.65	0.200	0.763	0.751	1.000	0.115
ID.85	23	46	31	1.24	0.205	0.761	0.838	1.000	0.131
ID.86	33	47	20	0.13	0.200	0.696	0.998	1.000	0.139
ID.87	23	44	33	2.14	0.206	0.776	0.755	1.000	0.121
ID.88	28	38	34	2.16	0.203	0.798	0.755	1.000	0.122
ID.89	44	40	16	3.15	0.200	0.687	0.750	1.000	0.103
ID.90	47	36	17	1.53	0.200	0.711	0.790	1.000	0.112
ID.91	29	33	38	3.17	0.203	0.829	0.750	1.000	0.126
ID.92	44	31	25	2.89	0.200	0.785	0.750	1.000	0.118
ID.93	73	16	11	0.90	0.200	0.764	0.919	0.915	0.128
ID.94	31	14	55	2.68	0.208	0.934	0.751	1.000	0.146
ID.95	25	56	19	0.98	0.202	0.662	0.899	1.000	0.120

ID.96	27	56	17	3.22	0.201	0.646	0.750	1.000	0.097
ID.97	25	49	26	1.55	0.203	0.728	0.788	1.000	0.116
ID.98	18	62	20	2.87	0.208	0.655	0.750	1.000	0.102
ID.99	22	55	23	3.16	0.204	0.693	0.750	1.000	0.106
ID.100	26	47	27	0.23	0.202	0.739	0.996	1.000	0.149
ID.101	27	46	27	2.97	0.202	0.742	0.750	1.000	0.112
ID.102	21	36	43	1.99	0.232	0.821	0.752	0.993	0.153

Source: (Own data, 2021)

Appendix Table 4: Cramer's V and P-value for each of the explanatory variables

Driver Variables	**Cramer's V**	**Cramer's P**
Elevation	0.2734	0.00
Aspect	0.4010	0.00
Population Density	0.1903	0.00
Distance to Road	0.2601	0.00
Slope	0.4172	0.00
Distance to Stream	0.4630	0.00

Appendix Table 5: Forcing all independent variables except one to be constant

Model	**Accuracy (%)**	**Skill measure**
With all variables	86.47	0.7294
All constant but var. 1	50.00	0.0000
All constant but var. 2	50.03	0.0005
All constant but var. 3	50.00	0.0000
All constant but var. 4	49.97	0. 05425
All constant but var. 5	50.00	0.0000
All constant but var. 6	86.70	0.7339

Appendix Table 6: Backwards stepwise constant forcing

Model	Variables included	Accuracy (%)	Skill measure
With all variables	All variables	86.47	0.7294
Step 1: var. [3] constant	[1,2,4,5,6]	86.72	0.7344
Step 2: var. [3,1] constant	[2,4,5,6]	86.72	0.7344
Step 3: var. [3,1,2] constant	[4,5,6]	86.72	0.7344
Step 4: var. [3,1,2,5] constant	[4,6]	86.72	0.7344
Step 5: var. [3,1,2,5,4] constant	[6]	86.70	0.7339

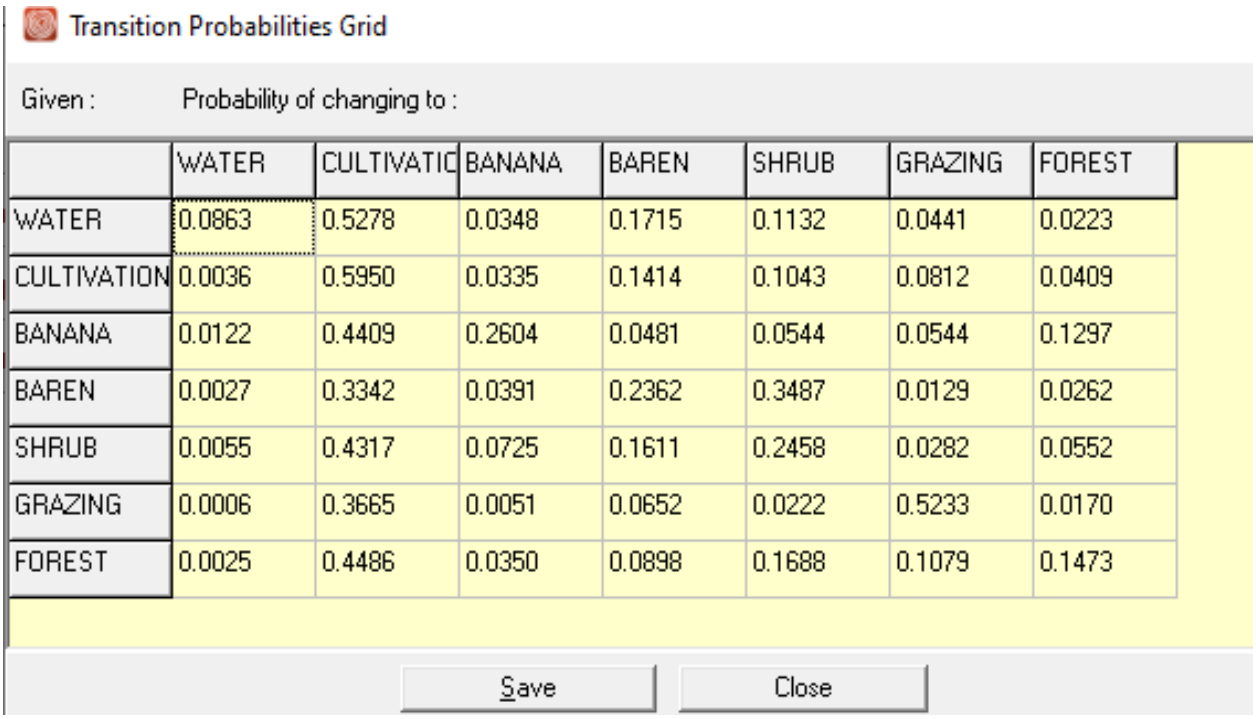

Appendix Figure 1: Transition matrix of Markov prediction 2050 based on 2020LULC map

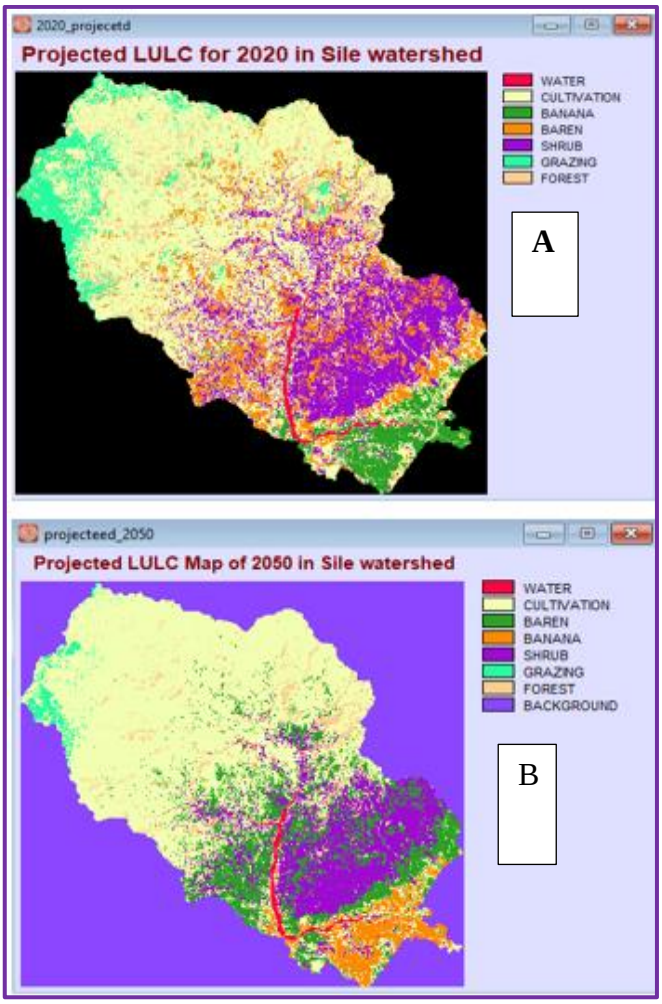

Appendix Figure 2: Projected LULC of 2020 (A) and Projected LULC for 2050 (B) in Sile watershed

Appendix Figure 3. Pictorial representation of field and laboratory activities